

POLITECNICO DI TORINO

MASTER OF SCIENCE THESIS

LES and RANS simulations of flow and combustion in
NG/HCNG engines



Author:

Silvestru CHIRICHES

Supervisors:

Daniela MISUL

Mirko BARATTA

A Thesis in the Field of Mechanical Engineering

for the Degree of Master of Science

in the

Department of Mechanical and Aerospace Engineering

April 10, 2019

Alla famiglia, agli amici

ABSTRACT

LES and RANS simulations of flow and combustion in NG/HCNG engines

The main objective of this thesis project is to give a contribution to the definition of the optimal CFD simulation methodology for NG engine investigation, so as to support the design process of innovative engines featuring a low environmental impact. The first part of this study presents the effect of hydrogen addition and EGR dilution on two different SI engines with different turbulence characteristics. The focus of the research has been to analyze the effect of different fuels and mixture composition by comparing experiments and corresponding numerical models. Natural gas has been a focus of research as an alternative fuel due to its chemistry which helps in reducing the CO₂ emissions and its high knock tolerance. The slow laminar burning velocity of methane has been an associated drawback which can be overcome by addition of hydrogen in various fractions. This theory is supported by experiments performed on low a turbulence engine. Experimental results show that for stoichiometric condition, hydrogen addition to CNG has been beneficial in terms of bsfc and unburned hydrocarbon emissions [1] and increases the EGR tolerance of the engine by 33% by adding 15 % H₂ (% vol). The results are confirmed by numerical results. Addition to this, the increase of turbulence in local flow field leads to greater flame wrinkling of the flame front and thus increases the turbulent burning rate. This combined effect of hydrogen and high turbulence leads to faster overall combustion and thus increases the EGR tolerance. The effect of hydrogen addition and EGR on combustion regime has been studied and is explained with the help of 3D results. In the second part of this thesis, LES simulations were studied, with reference to an injection event in a direct injection NG engine. The goal was to assess strengths and weaknesses of RANS and LES approaches by applying them to the same fluid-dynamic problem, at the same operation points. The effect of changing the turbulence model was then studied with the help of 3D results.

Acknowledgements

I would like to thank my supervisors Prof. Daniela Misul and Prof. Mirko Baratta for giving me the opportunity to join their team and for allowing me to expand my knowledge of the engine world by working on their projects. Also, I would like to thank them for their guidance and help in the work and preparation for this thesis; most importantly I am grateful for their help and interest for my future.

Also, a big thank you goes to the PhD Student Prashant Goel, my direct supervisor, my friend. His patience and knowledge helped me get through all the difficult times. He is a truly inspiring person, a good leader.

The biggest thanks go to them, my family. Without their sacrifices and support I know that I wouldn't be where I am today.

Lastly but not least, I would like to thank all my friends and all those special people that listened to me, guided me or simply have been there for me when I needed it. All my accomplishments are as much theirs as they are mine.

TABLE OF CONTENTS

1	INTRODUCTION	1
2	Direct Injection Methane engines.....	2
2.1	H2 addition.....	2
3	Borghi Plot.....	5
4	Computational Fluid Dynamics (CFD).....	7
4.1	Navier-Stokes equations	8
4.1.1	Mass conservation equation	9
4.1.2	Momentum conservation equation	10
4.1.3	Energy conservation equation	11
4.2	Discretization methods	12
4.2.1	Finite volume method.....	13
5	Turbulence modelling	17
5.1	Large Eddy Simulation- LES	19
5.2	RANS Turbulence Model	23
5.2.1	Governing equations in RANS	23
5.2.2	Eddy viscosity models	25
5.3	Laminar Flame Speed	28
5.3.1	LFS	29
5.4	Ignition and combustion modelling	34
5.4.1	Ignition model: ISSIM	34
5.4.2	Combustion Modelling.....	36
5.4.3	ECFM Combustion Model	42
6	Mesh Generation in CONVERGE	46
6.1	Fixed Embedding.....	46
6.2	Adaptive Mesh Refinement (AMR)	47
7	RANS Simulations setup, procedure and results.....	49
7.1	Validation of the models.....	49
8	Results.....	55
8.1	2000x6 bar CNG EGR0%- Turbulence Effect	55
8.1.1	Tumble Analysis.....	59
8.2	2000x6 bar CNG EGR20%- EGR Effect.....	66
8.3	HCNG- Effect of Hydrogen Addition.....	70

8.4	2000x6 bar HCNG15 EGR0%- Effect of Hydrogen Addition	71
8.5	2000x6 bar HCNG15 EGR10%.....	72
8.5.1	Combined effects of Hydrogen and EGR.....	72
8.6	2000x6 bar HCNG25- Limit of Hydrogen addition.....	74
8.6.1	CNG vs HCNG25 EGR20% Polito Engine	75
8.6.2	HCNG25 EGR0% & EGR25% GasOn vs Polito	76
8.7	Conclusion	80
8.8	Future works	80
9	LES Simulation setup, procedure and results.....	82
9.1	Case setup	82
9.2	Procedure	84
9.3	Results and discussion.....	84
9.4	Conclusion	88
10	Figures Index	90
11	Tables Index.....	92
12	Bibliography.....	93

1 INTRODUCTION

In recent years, there has been an increasing demand for improved, advanced internal combustion engines in terms of exhaust emissions and engine efficiency. This fact suggests a need for more accurate predictions of thermal conditions and fluid motion inside the cylinder, as a better prediction would help to control the level of emissions of motor vehicles.

As the objectives of standards are pointed mainly towards emissions reduction, companies are forced to invest into developing innovative engine concepts. Direct injection spark ignition engine has a large potential to reduce emissions and specific fuel consumption. In part load they can be operated in stratified charge mode which combines the advantages of reduced pumping losses and lean combustion.

However, especially in the case of engines operating with an air guided concept, they are very sensitive to cycle-to-cycle variations of the flow and mixing field. These fluctuations result in variations of the indicated mean effective pressure, hence work output. In the worst case these CCV's can result in combustion failures leading to a total loss of the energy trapped in the cylinder and to the ejection of unburned hydrocarbons into the environment.

Consequently, a greater understanding of the in-cylinder flow, spray injection, fuel–air mixing and combustion is needed in order to control and optimize this crucial process. For this purpose, 3D CFD simulations can be of great help. Having a clear image of the gas flow inside the cylinder, even if it is a quasi-realistic view, it is possible to determine what parameters could be changed or what methods can be improved in order to have the best replica of the conditions inside the cylinder throughout all the cycles.

Another method to face the difficult task of emissions reduction can be paying attention to: the type of fuel that is used in the engine, reaching a high efficiency combustion, use of exhaust after-treatment or use of low-carbon fuels.

Compressed natural gas (CNG) is one such low-carbon fuel; having a high hydrogen-to-carbon ratio, this fuel has a high potential for efficient combustion. Use of CNG as a fuel in an ICE can result in up to 25% reduction in CO₂ emissions compared with Gasoline. Currently, efforts are directed towards the development of CNG-only engines[2].

Natural gas vehicles are a potential alternative to gasoline vehicles in the short term as they are less polluting and fuel is widely available.

Natural gas (NG) is a mixture of different gases. Composition of natural gas may differ depending on its origin. The main component of natural gas is methane in a fraction of about 99% of the total volume. Even if methane is always the main component of natural gas, the total composition is never constant. NG can have traces non-methane hydrocarbons such as ethane, propane and butane and in some cases, traces of higher hydrocarbons as well as inert gases like nitrogen, helium, carbon dioxide, hydrogen sulphide and sometimes water.

As a fuel, natural gas has optimal characteristics. Of all fossil fuels it is the cleanest and its reserves the biggest as it is easy to find in many parts of the world. It is easy to transport and store, available on demand and cheaper than gasoline and diesel.

2 Direct Injection Methane engines

CNG vehicles using port fuel injection (PFI) already exist. However, the use of such engines on a large scale is limited by an intrinsic fault: these engines do not perform very well at lower part-load because the developed torque is too low when compared to Gasoline or Diesel ICEs.

At low-loads these engines are characterized by a low volumetric efficiency, which is caused by the fact that a gas is injected in the intake manifold (for a gasoline PFI engine for example, fuel is injected in a liquid form and as it evaporates it subtracts heat from the environment, cooling the air thus allowing a greater quantity of air to enter). The injected gas occupies the space in the duct thus reducing the quantity of air intake.

Another problem for a PFI engine is the possibility of methane slip to the exhaust port during the valves overlap.

These limitations can be overcome by direct gas injection. Moreover, due to high knock resistance of CNG as a fuel, the direct-injected (DI) ICE can be operated at high compression ratio potentially increasing thermal efficiency compared to conventional spark-ignition (SI) ICEs. Although a DI seems to have many advantages, such engines are not yet widely used due to their difficulties encountered during their design. A gaseous fuel injection process may appear simpler than a liquid fuel injection; a gas injection involves a single-phase flow as opposed to liquid injection where there is a dispersion of a liquid phase in a gas phase. However, injection of a gas with high pressure ratios create some problems in the flow. Effects of compressibility become dominant resulting in supersonic flow with shocks and discontinuities thus becoming challenging in predicting the flow.

Measuring the flow field close to a small injector can be difficult during experiments. Having a highly dynamic flow field in the area close to the injector and even inside the cylinder and measuring the interaction between the injected gas and the flow field inside the cylinder can be extremely difficult and requires very specific and often costly equipment.

In such cases, predictive simulation can be of great help for the design and development process.

Problems that arise during simulations of the gas injection processes are due to difficult and very expensive numerical processes. Reasons for this are very small gas passages of the order of micrometres, high Mach number flow, and compressible turbulence. The small length scales accompanied by large velocity scales increase the computational wall time required for the same simulation run-time. Additionally, large differences between in-nozzle and in-cylinder length and velocity scales make the simultaneous simulation of both regions computationally expensive [2].

2.1 H2 addition

Natural gas has been a focus of research as an alternative fuel to diesel or gasoline, due to its simple chemistry which helps in reducing the CO₂ emission, but for also its high knock tolerance.

Most of the energy used in the world is supplied by fossil fuels. Burning of the fossil fuels generates waste materials, mainly emissions to the atmosphere in the form of combustion fuel gases and dust,

as well as some ash and/or clinker. These waste materials have hazardous effects on the environment, some of them locally, others with more widespread or even global impact.

Hydrogen is a potential alternative to gasoline in the future. It is considered a near perfect energy storage medium, as it can be created from fossil [3] or non-fossil sources [4]. Its use in conventional combustion engines has generally shown decreased pollutant emissions [5] and [6] primarily due to the lean-burn characteristics of hydrogen and a reduction of carbon in the fuel. Also, in today's world, where the effects of global warming are a serious problem, the basic advantage of hydrogen combustion is that the greenhouse gas carbon dioxide (CO₂) is not formed at all[7].

However, even if the benefits seem to be interesting, hydrogen is currently under-used if compared to hydrocarbon fuels due, in part, to a much smaller distribution infrastructure. Current use of hydrogen in transportation is probably limited to the role of a fuel additive rather than a fuel itself.

Mixtures of hydrogen and natural gas are considered as very promising solutions as alternative fuels thanks to their lower pollutant emissions; nevertheless, a drawback to this solution is the on-board storage which results in a limited vehicle autonomy.

A study about the consequences of using mixtures of H₂ and CNG on BSFC, NO_x, HC, BSCO and BMEP has been carried out by [7].

In general, HC, CO₂, and CO emissions decrease with increasing H₂, but NO_x emissions generally increase due to higher temperature developed during H₂ burning. However, if a catalytic converter is used, NO_x emission values can be decreased to extremely low levels in accordance with the limits imposed by the ever more stringent new legislations. Consequently, equivalence zero emission vehicles (EZEV) standards may be reached if the latter solution can be successfully applied. Efficiency values vary with increasing H₂ amount but also spark timing, compression ratio, equivalence ratio, etc. Under certain conditions, efficiency values can be increased. In terms of BSFC, emissions and BTE, a mixture of low hydrogen percentage is suitable for using and benefits are reached.

It is known that the slow laminar burning velocity of methane has been an associated drawback, especially at low-load operating points; however, this drawback can be overcome by addition of hydrogen in various fractions. This hypothesis is supported by experiments which were performed on a low turbulence engine.

These experiments were conducted in Politecnico di Torino on an engine for stoichiometric conditions. Hydrogen addition to CNG has been beneficial in terms of bsfc and unburned hydrocarbon emissions [1] and increases the EGR tolerance of the engine by 33% by adding 15 % H₂ (% vol) as predicted by numerical results.

One of the reasons why hydrogen addition comes with benefits for the combustion is because it provides a large number of H and OH radicals, both of them being helpful for the increase in combustion reactions.

Hydrogen is an excellent additive to methane or gasoline due to its unique characteristics. Based on examination of the properties of the fuel when compared to methane and gasoline, it has been seen that hydrogen is able to burn ultra-lean at an equivalence ratio of 0.1. In comparison, methane and gasoline are capable of burning at equivalence ratios no lower than of 0.53 and 0.70, respectively [8]. Some key properties are shown in the Table 1:

	Hydrogen [H ₂]	Methane [CH ₄]	Gasoline [C ₈ H ₁₈]
Equivalence ratio lower limit in NTP air	0.1	0.53	0.7
Mass lower heating value [kJ/kg]	119930	50020	44500
Density of gas at NTP [kg/m ³]	0.083764	0.65119	4.4
Molar carbon to hydrogen ratio	0	0.25	0.44
Flame temperature in air [K]	2318	2148	2470
Burning speed in NTP air [cm/s]	265-325	37-45	37-43

Table 1- Hydrogen properties as a fuel with respect to Methane and gasoline [8]

3 Borghi Plot

In order to understand the combustion dynamics, but also to distinguish between stable and unstable combustion, a very useful tool can be the Borghi Plot.

First, some flame characteristics are shown:

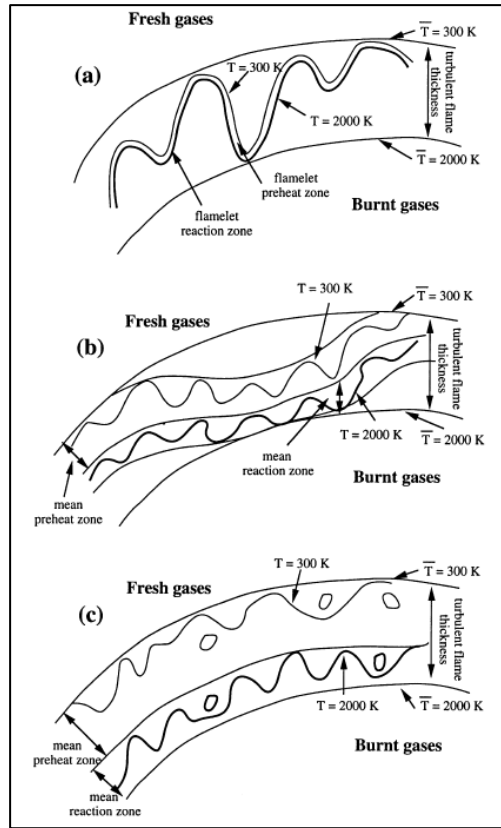


Figure 1- Turbulent premixed combustion regimes

a) flamelet (thin wrinkled flame); b) thickened wrinkled flame regime; c) thickened flame regime [9]

The objective is to analyze the premixed turbulent combustion regimes by comparing turbulence and chemical characteristic length and time scales. This diagram can be of help when analysing and studying combustion models and also analysing results from existing models.

A very important number when analysing premixed combustion is the Karlovitz number:

$$Ka = \frac{\tau_c}{\tau_k} = \frac{\delta_l u_k}{l_k S_L}$$

Where τ_c is the chemical time scale (the time needed for the flame to advance over a distance equal to its own thickness), τ_k is the turbulence time scale (turning time of the eddies), δ_l is the flame thickness, l_k is the turbulence length scale, u_k is the turbulence velocity (turbulence fluctuations) and finally S_L is the flame velocity (laminar flame speed).

Consequently, the next turbulence regimes have been proposed, based on the Karlovitz number (with reference to Figure 2:

- $Ka < 1$: *Flamelet regime* or *thin wrinkled flame regime*. This regime can be divided in two parts:
 1. $\frac{u'}{s_L} < 1$ *wrinkled flame*. Turbulent structures are not able to interact with the flame and wrinkle it, thus the flame propagation is predominant.
 2. $\frac{u'}{s_L} > 1$ *corrugated flames*. Turbulent structures are able to disturb the propagation and wrinkle excessively the flame.
- $1 < Ka < 100$: *Thickened wrinkled flame regime* (or *thin reaction zone*). Turbulent structures are able to disturb and thicken the flame preheat zone, but they are not able to modify the reaction zone.
- $Ka > 100$: *Thickened flame regime* (well stirred reactor). Both preheat and reaction zones are affected by the turbulence movements.

All these regimes are shown in a log-log diagram $(\frac{u'}{s_L}; \frac{l_t}{\delta_l})$ called *Borghi Plot*:

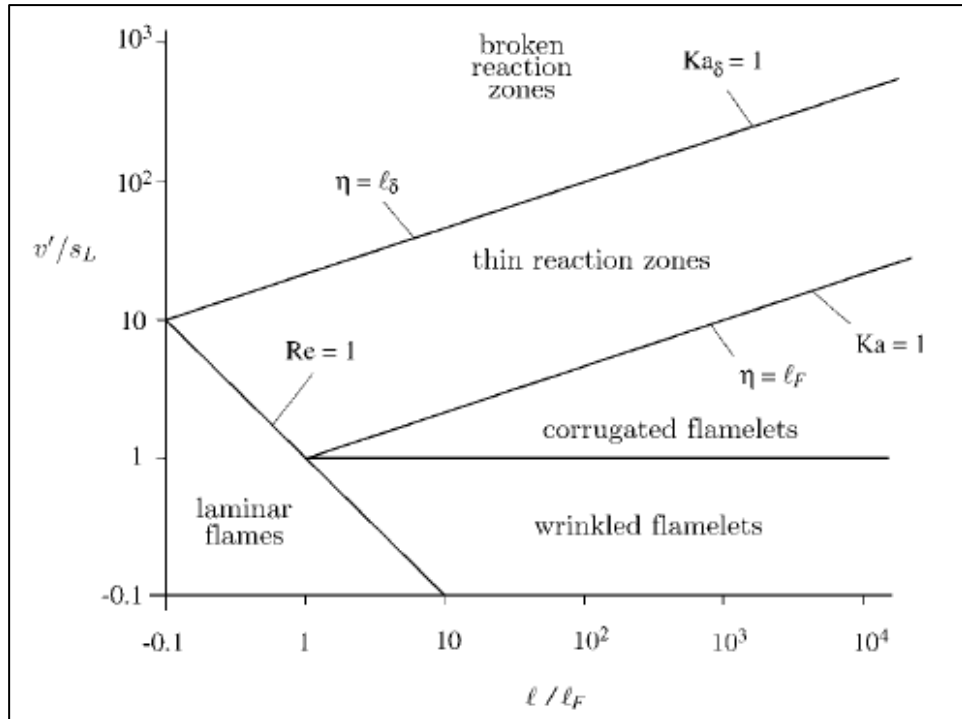


Figure 2- Logarithmic Borghi plot [10]

3.1.1.1 Notes and comments

The analysis based on dimensionless numbers leads to an approximate classification of combustion regimes and consequently, turbulent combustion models can be chosen accordingly. Such analysis must be used with care as it is only qualitative. A better explanation is given in [11].

4 Computational Fluid Dynamics (CFD)

Computational Fluid Dynamics (or CFD) is a method which uses algorithms and a numerical analysis to solve and analyze fluid flows and all the related issues and characteristics with the use of computers.

It is a method mainly used for industrial applications, which have to deal with fluid flows interactions (interactions between a fluid and a mechanical part or simply aerodynamic interactions between fluids).

In recent years 3D CFD simulations proved to be an efficient way of solving and predicting fluid motion, especially when applied to internal combustion engines.

In the early stages of an engine development, CFD can become a powerful tool if used properly. A 3D CFD simulation has the ability to capture key properties of the fluid (pressure, temperature, fluid dynamics characteristics) during the main phases of an engine operating points. These abilities have led the main companies in the sector into investing more time and resources for the development and use of software and qualified personnel.

These types of simulations are performed by softwares which are programmed into solving Navier-Stokes' equations in the virtual domain of the engine. A more detailed explanation about the methodology used by the softwares will be given in the next chapters of the thesis.

The base steps for setting up and use of a 3D CFD simulation of an engine are relatively simple:

- Create 3D model of the engine/cylinder plus intake and exhaust ducts
- Create the best possible mesh for the 3D model in agreement with the type of simulation that has to be performed
- Choose the best mathematical models for all the events that will take place in the engine (combustion, wall models/heat exchange, chemistry dynamics)
- Set up all the boundary conditions for the fluid and also the engine
- Choose the best mathematical methods (discretisation of the equations, solving algorithms, wanted accuracy degree) accordingly with the type of simulation that has to be performed

Once the simulation has been completed, even if incorrectly, results will be available. The important thing is to be able to have a critical view upon these results and, if the job at hand requires it, to know which of the previous steps have to be modified in order to obtain an accurate model.

Once a good model has been set up (verified with experimental results), simulations can be performed on the model, the results can be analysed and changes can be made on the model of the engine that has to be engineered. This allows to perform tests that were not performed on the engine. The obtained results give an idea of the best results and/or compromises that could be obtained on the actual engine.

Although this may seem a long procedure, once the model has been verified, simulations will give sufficiently accurate results on the macro-performances of the engine with a decrease in costs for the development of the engine.

As the development of a new engine can last up to 5 years, CFD simulations can be used to shorten this period, if made properly.

The purpose of the 3D CFD simulations, at an academic level, is to give an insight of the macro-phenomena, which are happening in a cylinder during the strokes, in a quasi-realistic way.

It is obvious that, being the software based on mathematic models, errors will be present in each resolution of the equations. In this way, the results from every simulation will be affected by numerical errors that do not depend on model itself, but they are related to the mathematical models.

Softwares that are used for 3D simulations give a great liberty into changing many of the parameters needed for the engine to run, such as spark advance, lift profiles of the valves, lift profiles for the injectors, boundary conditions, Exhaust Gas Recirculation (EGR), fuel composition and even the use of multiple fuels inside the chamber; each one of these parameters have to be set accordingly with the type of simulation that has to be run.

In addition to the speed and reduced cost of CFD methods, compared to experimental procedures in most engineering applications, they also offer a more complete set of information. They usually provide all relevant flow information throughout the domain of interest. Experimental methods are mostly limited

to measurements of some flow quantities at certain locations accessible by the measuring equipment.

To solve a fluid flow, it is convenient to study the flow within a certain region of space that normally is called a Control Volume. The usual approach is to deal primarily with two quantities: mass and momentum conservation.

The conservation law relates the rate of change of a certain quantity within a particular control volume.

Although these two conservation equations are enough to solve the fluid flow, and they seem to be quite simple, their resolution is more complex than it appears.

As showed in[12] these equations are non-linear, coupled, and difficult to solve. It is difficult to prove by the existing mathematical tools that a unique solution exists for particular boundary conditions.

4.1 Navier-Stokes equations

In this section the governing equations of CFD will be discussed. These equations are conservation laws, which mean that they can be given either in an integral form or in a differential one.

$$\frac{\partial}{\partial t} \int \rho \Phi d\Omega + \int \rho \Phi \mathbf{u} \cdot \mathbf{n} dS = \int s d\Omega$$

$$\frac{\partial}{\partial t} (\rho \Phi) + \nabla \cdot (\rho \Phi \mathbf{u}) = s$$

Where ϕ can be any conserved intensive quantity, \mathbf{u} is the velocity vector and \mathbf{s} a sink/source term. A conservation law can be derived either following the Lagrangian approach also known as the control mass approach, either by following the Eulerian approach, also known as the control volume approach.

In fluid mechanics, it is convenient to use the Eulerian approach; following a fluid particle along its path can be difficult. Instead, fixing a control volume and writing the quantity balance equation across, it simplifies the work, without any apparent disadvantages.

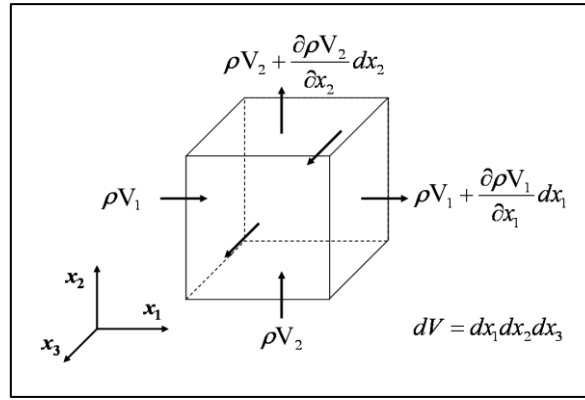


Figure 3- Finite volume method- Mass Conservation

Fluid flow equations are essentially differential equations which represent the correlation between the flow variables and their evolution in time and in space. These equations are complemented by algebraic relations such as the equation of state for compressible flow. The basic physical laws of motion that govern solids are valid also for gasses and liquids. The greatest difference between solids and fluids is that fluids distort continuously without limit. For example, while for a solid, when a force is applied, it distorts; if the force stops, the solid will tend to return to its original form and position. For a fluid, the same thing does not happen; if a force is applied, layers of fluid particles will move relatively to each other. As the force stops, particles will not return to their original position.

This means that during an analysis, such properties have to be accounted for.

Another important fact that has to be accounted for is that a fluid responds to forces in the same way as a solid. If a force is applied, the fluid will experience Newton's second law, resulting in an acceleration.

The forces that a fluid can experience are:

- Pressure forces
- Body forces (gravity and electromagnetism)
- Forces due to rotation
- Viscous forces
- Friction forces

It is useful now to analyze the three main equations which stand at the base of every CFD code.

4.1.1 Mass conservation equation

Also known as the continuity equation, it is written analysing which quantities are entering a certain control volume (CV) and which ones exit instead. For a certain control volume, the equation can be written as:

$$\frac{\partial}{\partial t} \int_{\Omega} \rho d\Omega + \int_{S=\partial\Omega} \rho \mathbf{u} \cdot \mathbf{n} dS = 0$$

In this equation we have Ω as control volume, $S=\partial\Omega$ as boundary of the control volume. The first term is the variation in time of the mass in the control volume. The second term is the velocity

transported mass, addressed as the transported term. The equation is equal to zero because the assumption is that the total mass in the CV is conserved. Also, this equation is written in integral form, whereas the differential form can be written by mean of the Gauss theorem. It means that the transport term should be written as a volume integral rather than a surface integral. Since the CV does not change over time and the two integrals are referred to the same CV, the derivative and integral operators can be swapped, turning the same equation into its differential form:

$$\frac{\partial \rho}{\partial t} + \nabla \cdot (\rho u) = 0$$

4.1.2 Momentum conservation equation

It is a vectoral quantity defined as the product between velocity and density. As for the mass conservation, the momentum conservation can be written in an integral form:

$$\frac{\partial}{\partial t} \int_{\Omega} \rho u d\Omega + \int_{S=\partial\Omega} \rho u \times u \cdot n dS = \sum_i f_i$$

- The first term is the rate of change of the momentum in the CV
- The second term is a tensor which represents the momentum transported by the velocity
- The term on the right represents the sum of all the external forces acting in the control volume

The term on the right is a complex term. It represents the sum of the forces, hence a sum of vectors. As always, forces can be divided into two categories: body forces, like gravitational forces, Coriolis forces, electromagnetic forces etc; the second category consists in the sum of surface forces such as pressure and external forces.

Problems arise when considering the forces. If the forces acting on the fluid in control volume are not function of the system variables (ρ , \mathbf{u}), they do not allow closure for the equations, so the flow cannot be resolved. In this case, to be able to have a closure, actions need to be taken. It is possible to make assumptions in order to correlate the terms as function of system variables. The downside of the assumptions is that, by doing so, errors are introduced.

The most common assumption used is that of Newtonian fluids, which means assuming that the fluids obey to Newton's law of viscosity (fluids whose viscosity tensor is never constant). Having the stress tensor σ of surface forces, it can be written as a sum of various tensors:

- Normal stresses
- Pressure tensor
- Shear tensor

The latter is expressed as function of velocity:

$$\sigma = -pI + \mu \left[\nabla u + (\nabla u)^T - \frac{2}{3} (\nabla \cdot u) \cdot I \right]$$

Introducing this term, the equation of momentum conservation becomes:

$$\frac{\partial}{\partial t} \int_{\Omega} \rho u d\Omega + \int_{S=\partial\Omega} \rho u \times u \cdot n dS = \int_{S=\partial\Omega} \sigma \cdot n dS + \int_{\Omega} \rho b d\Omega$$

Where this equation keeps track of the body forces within the **b** term. Also, by applying Gauss' theorem, this equation can be written in differential form:

$$\frac{\partial(\rho u)}{\partial t} + \nabla \cdot (\rho u \times u) = \nabla \cdot \sigma + \rho b$$

4.1.3 Energy conservation equation

The balance of scalars gives the equation:

$$e_{tot} = e_i + e_k = e_i + \frac{1}{2} u \cdot u$$

Where the first term is the total energy, e_i is the internal energy and e_k is the kinetic energy. In the differential form this equation can be written as:

$$\frac{\partial}{\partial t} \left(e_i + \frac{1}{2} u \cdot u \right) + \nabla \cdot \left[\rho \left(e_i + \frac{1}{2} u \cdot u \right) u \right] = -\nabla \cdot q - \nabla \cdot (\sigma \cdot u) + \rho b \cdot u$$

Using the momentum equation and applying the total derivative, the last equation becomes:

$$\rho \frac{De_i}{Dt} = -\nabla \cdot q - p \nabla \cdot u - \tau : (\nabla u)$$

In this equation it can be seen a new term, τ , which represents the viscous part of the stress tensor.

The equation can be simplified if the effect of viscous heating and compressibility is neglected, turning the equation in what is known to be called as *Heat Equation*:

$$\rho c_p \frac{\partial T}{\partial t} + \rho c_p u \cdot \nabla T = \nabla \cdot (k \nabla T)$$

It is convenient to write all of these equations in the same differential form in order to have a clear and complete view:

Continuity equation:

$$\frac{\partial \rho}{\partial t} + \nabla \cdot (\rho u) = 0$$

Momentum equation in the three dimensions:

$$\rho \left(\frac{\partial u}{\partial t} + u \frac{\partial u}{\partial x} + v \frac{\partial u}{\partial y} + w \frac{\partial u}{\partial z} \right) = -\frac{\partial p}{\partial x} + \mu \left(\frac{\partial^2 u}{\partial x^2} + \frac{\partial^2 u}{\partial y^2} + \frac{\partial^2 u}{\partial z^2} \right) + F_x$$

$$\rho \left(\frac{\partial v}{\partial t} + u \frac{\partial v}{\partial x} + v \frac{\partial v}{\partial y} + w \frac{\partial v}{\partial z} \right) = -\frac{\partial p}{\partial y} + \mu \left(\frac{\partial^2 v}{\partial x^2} + \frac{\partial^2 v}{\partial y^2} + \frac{\partial^2 v}{\partial z^2} \right) + F_y$$

$$\rho \left(\frac{\partial w}{\partial t} + u \frac{\partial w}{\partial x} + v \frac{\partial w}{\partial y} + w \frac{\partial w}{\partial z} \right) = -\frac{\partial p}{\partial z} + \mu \left(\frac{\partial^2 w}{\partial x^2} + \frac{\partial^2 w}{\partial y^2} + \frac{\partial^2 w}{\partial z^2} \right) + F_z$$

Energy equation:

$$\rho c_p \left(\frac{\partial T}{\partial t} + u \frac{\partial T}{\partial x} + v \frac{\partial T}{\partial y} + w \frac{\partial T}{\partial z} \right) = \Phi + \frac{\partial}{\partial x} \left(\frac{\partial T}{\partial x} \right) + \frac{\partial}{\partial y} \left(\frac{\partial T}{\partial y} \right) + \frac{\partial}{\partial z} \left(\frac{\partial T}{\partial z} \right) + \left(u \frac{\partial p}{\partial x} + v \frac{\partial p}{\partial y} + w \frac{\partial p}{\partial z} \right)$$

It has been proven that Navier-Stokes equations are able to describe a Newtonian flow accurately enough.

If one assumes some properties constant, such as viscosity and specific heat, the previously written system of equations contains six unknowns; with only five equations available, a sixth equations needs to be introduced in order to be able to close the system. It is common to use a constitutive relation for the pressure; in particular, for an ideal gas, one can use the universal law for ideal gasses: $p = \rho RT$.

Even so, directly solving these equations is possible only for fully developed flows in simple geometries like in pipes, between parallel plates etc. These flows are important for understanding the fundamentals of fluid dynamics, but they do not find an important use in practical situations. The ‘turbulence problem’ has proven to be very difficult, with no prospects of a new, simple analytic theory. The objective is to use the ever-more powerful digital computers to complete the calculation of relevant properties of turbulent flows.

One of the properties of turbulent flows that make it difficult to develop a compliant theory or model is the velocity field $\mathbf{U}(\mathbf{x}, \mathbf{t})$. This property is three-dimensional, time-dependent, and random [13].

4.2 Discretization methods

Choosing a discretization method is an important step in every numerical method. A discretization method is a method of approximating the differential equations by a system of algebraic equations for the studied variables at a certain location and time.

There are many approaches, but the most important ones are:

- Finite volume (FV)
- Finite difference (FD)
- Finite element (FE)

There are other methods available, but for the case in point, it is not useful nominating them.

Each type of method should give the same results at any points, if the grid is fine enough. Depending on the problem to be solved, some methods are more suitable than others. The choice is up to the developer[12].

4.2.1 Finite volume method

It is the main method used when 3D CFD simulations have to be performed.

In the finite volume method, the physical domain is divided into a series of small control volumes and choosing, for each one of the volumes, a significant point, called Node. An advantage of this method is that it conserves the transported quantities for both regularly and irregularly shaped cells. When applying the finite volume method, the next steps should be followed as explained next:

- The integral form of the conservation equation must be taken into consideration. It is also equivalent using another approach: integrating the differential equations in the CV, obtaining the integrals of a generic variable in the CV and on each of the control volume's surfaces.
- Approximation of each of the integrals by means of numerical integration. For CV method, it is usual to use simple methods (the product of a value in a certain point by the value of the surface or the volume). The precision of this method is not controlled by the numerical integration; it is instead dictated by the number of control volumes in which the total space is divided. More cells mean more accurate results.
- Writing the values of the variable at the borders of the CV in relation to the value of the variable at the node. This particular step is defined by the method of spatial discretization used.
- Choosing the time step at which the value of the chosen variable is defined in the nodes adjacent to the node where the integration is applied. By doing so, the time-step discretization method is defined [14].

In order to understand the inputs for finite volume, consider the simple three cell computational domain shown in the figure:

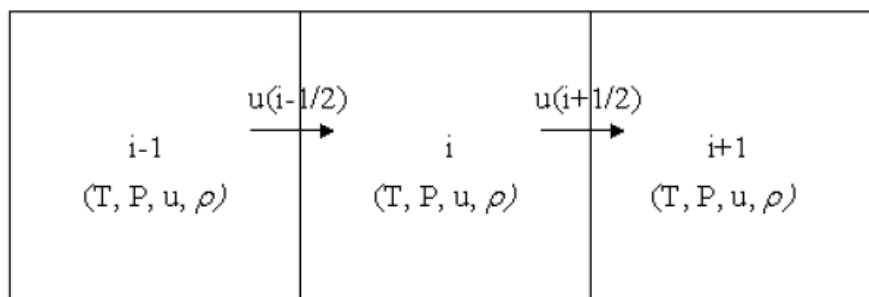


Figure 4- Finite volume scheme [14]

For an easy understanding, the simple transport equation can be used:

$$\frac{\partial \Phi}{\partial t} + \frac{\partial u\Phi}{\partial x} = 0$$

It is convenient to write it in an integral form:

$$\frac{d}{dt} \int_V \Omega dV + \int_S u \cdot n \Phi dS = 0$$

Where V is the cell volume, ϕ is the flux of a certain quantity, S is the surface of the volume, \mathbf{n} is the surface normal. As pointed out earlier, the finite volume method solves easier the integral form of the conservation equations rather than the differential form. This integral form is solved by summing the fluxes on each face of the cell.

Thus, in order to solve the equation, the velocity and ϕ must be interpolated to the cell surface. One method used by the CFD softwares is to average the two values of adjacent cells and to place them at the surface, which gives a surface ϕ given as:

$$\phi_{i+1/2} = \frac{1}{2} \phi_i + \frac{1}{2} \phi_{i+1}$$

And for the other cell:

$$\phi_{i-1/2} = \frac{1}{2} \phi_i + \frac{1}{2} \phi_{i-1}$$

If that was the average method, there is another method that can be used in order to obtain the cell surface value: The Upwind Method[15]. It results in:

$$\phi_{i+1/2} = \phi_i$$

And for the other cell:

$$\phi_{i-1/2} = \phi_i$$

4.2.1.1 Implementation of Boundary Conditions

Each CV provides one algebraic equation. Volume integrals are calculated in the same way for every CV, but fluxes through CV faces coinciding with the domain boundary require special treatment. These boundary fluxes must either be known, or be expressed as a combination of interior values and boundary data. Since they do not give additional equations, they should not introduce additional unknowns. Since there are no nodes outside the boundary, these approximations must be based on one-sided differences or extrapolations.

Usually, convective fluxes are prescribed at the inflow boundary. Convective fluxes are zero at impermeable walls and symmetry planes, and are usually assumed to be independent of the coordinate normal to an outflow boundary; in this case, upwind approximations can be used. Diffusive fluxes are sometimes specified at a wall e.g. specified heat flux (including the special case of an adiabatic surface with zero heat flux) or boundary values of variables are prescribed. In such a case the diffusive fluxes are evaluated using one-sided approximations for normal gradients. If the gradient itself is specified, it is used to calculate the flux, and an approximation for the flux in terms of nodal values can be used to calculate the boundary value of the variable [12].

4.2.1.2 PISO algorithm

The pressure-velocity coupling in CONVERGE is achieved using a modified Pressure Implicit with Splitting of Operators (PISO). The PISO algorithm as implemented in CONVERGE starts with a predictor step where the momentum equation is solved. After the predictor, a pressure equation is derived and solved, which leads to a correction, which is applied to the momentum equation. This process of correcting the momentum equation and re-solving can be repeated as many times as necessary to achieve the desired accuracy. After the momentum predictor and first corrector step have been completed, the other transport equations are solved in series.

The PISO method was chosen for use in CONVERGE for various reasons. With only minor variations, this method can be used for solving either compressible or incompressible flows. In addition, the predictor-corrector concept allows for a semi-implicit treatment of sources and sinks: the sources and sinks can be updated at each corrector step. A more detailed explanation can be found in [15].

4.2.1.3 Solution procedure

In order to correctly configure the simulation parameters, it is extremely important to understand the order in which the transport equations are solved. It is useful to have a scheme which summarizes the order in which the steps are taken in order to solve the equations:

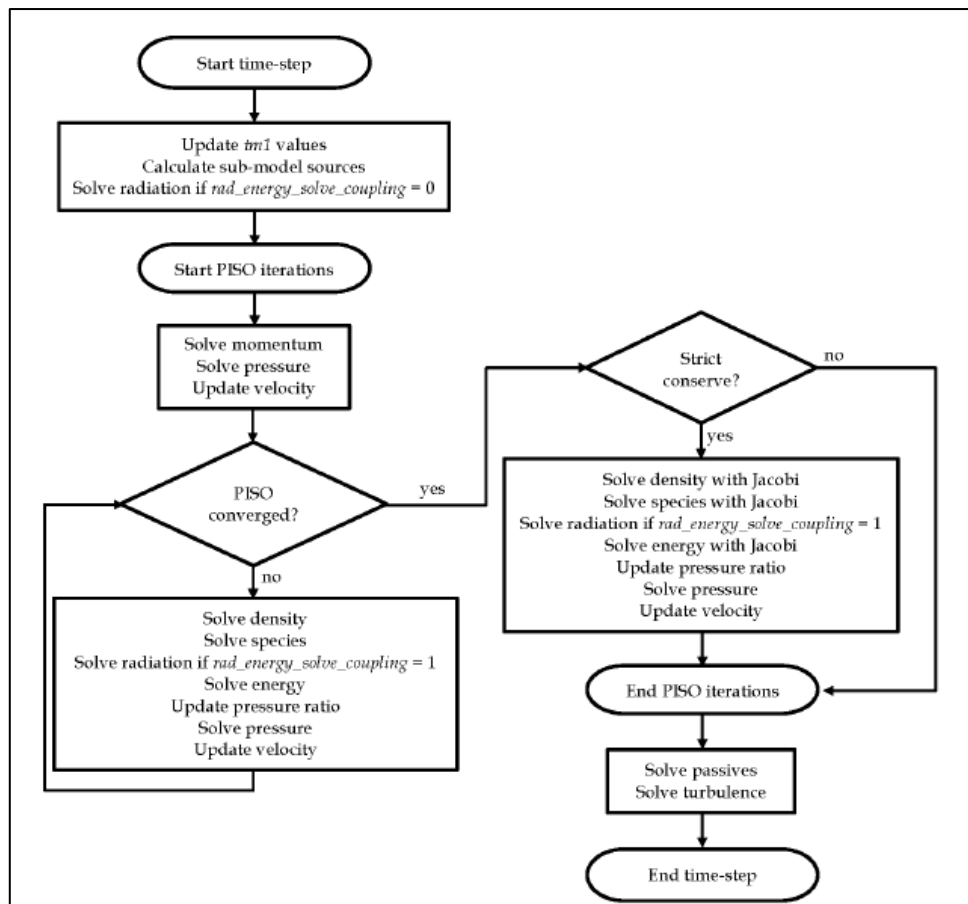


Figure 5-Solution procedure + PISO algorithm [15]

A short description is needed in order to understand the algorithm, referring to the previous figure (and considering that CONVERGE is the CFD simulation software used in this thesis).

At the start of each time-step, the previous values (the time-step minus 1) are stored for all transported quantities. Next, explicit sources are calculated for each submodel that is currently activated and radiation is solved if energy and radiation are decoupled. At the beginning of the PISO loop (the first PISO iteration), CONVERGE solves for momentum and pressure, which sets the velocity for the other transport equations. After each PISO iteration, it is necessary to check for PISO loop convergence. For compressible cases, CONVERGE considers the PISO loop to be converged if

$$\Delta\rho < tol_piso$$

where $\Delta\rho$ is the density correction error. For incompressible cases, CONVERGE considers the PISO loop to be converged if

$$\Delta P < tol_piso$$

where ΔP is the pressure correction error.

All the values of the factors used in this particular part have to be chosen accordingly with the level of accuracy that is wanted from the simulation.

It is also convenient to have a better look at the algorithm in question.

5 Turbulence modelling

Most flows encountered in engineering applications (especially in the engines sector) are of the turbulent type. These flows require a special treatment and are characterized by the following properties:

- Turbulent flows are highly unsteady. A plot of the velocity as a function of time at most points in the flow would appear random to an observer unfamiliar with these flows. The word 'chaotic' could be used but it has been given a more appropriate definition in recent years: stochastic flow.
- They are three-dimensional. The time-averaged velocity may be a function of only two coordinates, but the instantaneous field fluctuates rapidly in all three spatial dimensions.
- They contain a great deal of vorticity. Indeed, vortex stretching is one of the principal mechanisms by which the intensity of turbulence is increased
- Turbulence increases the rate at which conserved quantities are stirred. Stirring is a process in which parcels of fluid with differing concentrations of at least one of the conserved properties are brought into contact. The actual mixing is accomplished by diffusion. Nonetheless, this process is often called turbulent diffusion.
- By means of the processes just mentioned, turbulence brings fluids of differing momentum content into contact. The reduction of the velocity gradients due to the action of viscosity reduces the kinetic energy of the flow; in other words, mixing is a dissipative process. The lost energy is irreversibly converted into internal energy of the fluid.
- It has been shown in recent years that turbulent flows contain coherent structures-repeatable and essentially deterministic events that are responsible for a large part of the mixing. However, the random component of turbulent flows causes these events to differ from each other in size, strength, and time interval between occurrences, making study of them very difficult.
- Turbulent flows fluctuate on a broad range of length and time scales. This property makes direct numerical simulation of turbulent flows very difficult.

Engineers need to be able to understand and predict these effects in order to achieve good designs. In some cases, it is possible to control the turbulence, at least in part.

The effects produced by turbulence may or may not be desirable, depending on the application. Intense mixing is useful when chemical mixing or heat transfer are needed; both of these may be increased by orders of magnitude by turbulence. On the other hand, increased mixing of momentum results in increased frictional forces, thus increasing the power required to pump a fluid or to propel a vehicle; again, an increase by an order of magnitude is not unusual.

To optimize a design, it is usually necessary to understand the source of the undesired effects; this requires detailed measurements that are costly and time-consuming.

Some types of measurements, for example, the fluctuating pressure within a flow, are almost impossible to make at the present time. Others cannot be made with the required precision. As a result, numerical methods have an important role to play.

According to the paper of Bardina et al. (1980) [16] there are six main categories of the main approaches to predict turbulent flows:

- The first involves the use of correlations such as ones that give the friction factor as a function of the Reynolds number or the Nusselt number of heat transfer as a function of the Reynolds and Prandtl numbers. This method, which is usually taught in introductory

courses, is very useful but is limited to simple types of flows, ones that can be characterized by just a few parameters.

- The second uses integral equations which can be derived from the equations of motion by integrating over one or more coordinates. Usually this reduces the problem to one or more ordinary differential equations which are easily solved.
- The third is based on equations obtained by averaging the equations of motion over time (if the flow is statistically steady), over a coordinate in which the mean flow does not vary, or over an ensemble of realizations (an imagined set of flows in which all controllable factors are kept fixed). This approach is called one-point closure and leads to a set of partial differential equations called the Reynolds-averaged Navier-Stokes (*or RANS*) equations. As we shall see later, these equations do not form a closed set so this method requires the introduction of approximations (turbulence models).
- The fourth type of method is called *two-point closure*. It uses equations for the correlation of the velocity components at two spatial points or, more often, the Fourier transform of these equations. These methods are only used for homogeneous turbulence; hence, they are of little importance.
- The fifth is *large eddy simulation (LES)* and solves for the largest scale motions of the flow while approximating or modeling only the small-scale motions. It can be regarded as a kind of compromise between one-point closure methods and direct numerical simulation.
- Finally, there is *direct numerical simulation (DNS)* in which the Navier-Stokes equations are solved directly, without resorting to modelling, for all of the motions in a turbulent flow. It is the most accurate and complete method, but obviously the most computationally expensive one.

All of the methods described in this chapter require the solution of some form of the conservation equations for mass, momentum, energy, or chemical species. The major difficulty is that turbulent flows contain variations on a much wider range of length and time scales than laminar flows. So, even though they are similar to the laminar flow equations, the equations describing turbulent flows are usually much more difficult and expensive to solve.

It is important to understand the formation of eddies of different length scales in a turbulent flow. Following the explanation of [10], a description about the phenomena will be given.

In every turbulent flow, the main thing to be noted is the simultaneous presence of multiple eddies; each one of them is characterized by different length scales. The formation of such eddies can be easily explained with the help of the next figure. If a turbulent jet enters from a nozzle in an ambient characterized by (still) quiescent surroundings, the large difference in velocity of the two fluids generates a shear layer instability; further down from the nozzle a transition zone is formed where the jet destroys itself becoming this way a turbulent flow.

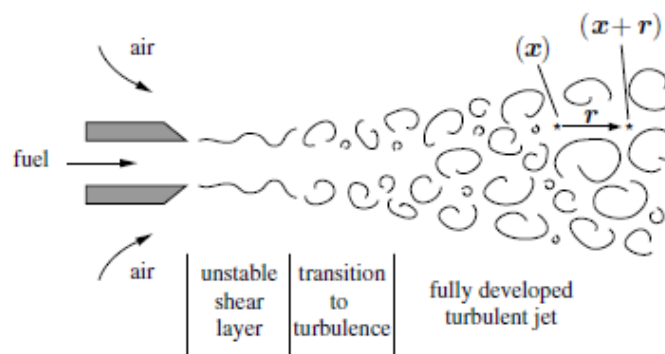


Figure 6- Eddy formation from a jet [10]

In order to characterize the distribution of eddy length scales at any position within the jet, one measures at point \mathbf{x} and time t the axial velocity $u(\mathbf{x}, t)$, and simultaneously at a second point $(\mathbf{x} + \mathbf{r}, t)$ with distance \mathbf{r} apart from the first one, the velocity $u(\mathbf{x} + \mathbf{r}, t)$.

The velocities at the two points are correlated by the definition of the average:

$$R(x, r, t) = \overline{u'(x, t)u'(x + r, t)}$$

If the definition is referred to a homogeneous isotropic turbulence,

During this thesis only RANS and LES methods have been used, thus they will be studied carefully. For the other methods, a complete description can be found in [12].

5.1 Large Eddy Simulation- LES

It is important to know that every turbulent flow contains a very wide range of length and time scales. It is an important characteristic when dealing with modelling; the resolving of these scales has a great influence on the accuracy of the model and most importantly on the computational time.

It can be easier to understand the significance of scales in the next two figures: on the left side the range of eddy sizes can be seen. On the right side it is shown the time history of a typical velocity component in the flow.

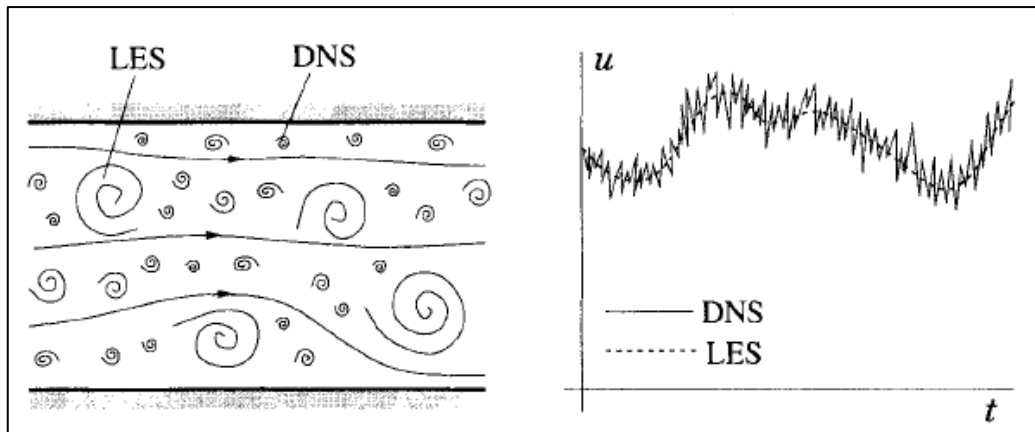


Figure 7- Schematization and differences between LES and DNS simulations [12]

The large eddies usually contain the most amount of energy out of all the flow. Their size and strength make them the most effective transporters of the conservative properties of the flow. In contrast, the smaller eddies have a much less relevant role in the transport of the conserved properties.

It is obvious that having a simulation which takes into account only the bigger eddies has more sense with respect to one which solves all the eddies. This is called the Large Eddies Simulation (LES) approach.

In every LES simulation, four conceptual steps can be found:

- i. The velocity field $U(x, t)$ is filtered into two parts: a sum of filtered (resolved) component $\overline{U}(x, t)$ and a residual (or unresolved or sub-grid scale) component $u'(x, t)$. The resolved component represents the motion of the large eddies.

- ii. The equations needed for the evolution of the resolved part of the velocity field are derived from the Navier-Stokes equations. In this step a residual form emerges, which represents the momentum equation containing the residual stress tensor (or SGS).
- iii. Closure is then obtained by introducing a model for the resolution of the stress tensor. There can be many models for the SGS; a very common one could be an eddy-viscosity model.
- iv. The resolved filtered equations are numerically solved for $\bar{U}(x, t)$, operation that gives an approximation of the large-scale eddies in the total flow.

LES simulations are three-dimensional, time dependent and expensive but much less costly than DNS of the same flow. It is the type of simulation preferred instead of DNS when Reynolds number is too high (computational time increases as the cube of the Reynolds number) or when the geometry to be simulated is too complex.

For the understanding of the method, it is important to define the quantities that have to be computed precisely.

From the definition of LES, it is important to use a velocity field that only contains the large scales components of the total velocity field. In the work of [17] it is shown how to filter a velocity field; the resolved scale field, the one that has to be simulated, is defined as a local average of the complete field.

It is simpler to use one-dimensional notation, which can be easily generalized to the three-dimensional field. The filtered velocity (introduced by [17]) is defined as follows:

$$\bar{u}_i(x) = \int G(x, x') u_i(x') dx$$

Where G is a localized function. Filter kernels which have been applied in LES include a Gaussian, a box filter (a simple local average) and a cutoff (a filter which eliminates all Fourier coefficients belonging to wavenumbers above a cutoff). It is obvious that a length scale Δ has to be defined for every filter. Then, eddies' length scales have to be compared to Δ ; if the eddies' length scale is bigger than Δ , it is considered a Large Eddy; otherwise, it is considered a Small Eddy and it becomes part of the group of eddies that must be modeled.

Navier-Stokes equations are filtered, and, for incompressible flow (constant density), the following equations are obtained:

$$\frac{\partial(\rho \bar{u}_i)}{\partial t} + \frac{\partial(\rho \bar{u}_i \bar{u}_j)}{\partial x_j} = -\frac{\partial \bar{p}}{\partial x_i} + \frac{\partial}{\partial x_j} \left[\mu \left(\frac{\partial \bar{u}_i}{\partial x_j} + \frac{\partial \bar{u}_j}{\partial x_i} \right) \right]$$

Because the continuity equation is linear, filtering does not affect it:

$$\frac{\partial(\rho \bar{u}_i)}{\partial x_i} = 0$$

For LES modeling, it is important to know that, since

$$\overline{u_i u_j} \neq \bar{u}_i \bar{u}_j$$

And the quantity on the left is difficult to compute, it can be easier to model the difference between the sides, resulting in:

$$\tau_{ij}^s = -\rho(\overline{u_i u_j} - \overline{u_i} \overline{u_j})$$

This new term, for LES modeling, is called a *subgrid-scale Reynolds stress*. It is important not to think at the word *stress* as a physical nature; it has been called because of how it is treated. It is in fact the contribution on the momentum flux given by the small and unresolved scales.

Also, the name subgrid can be misleading. It has nothing to do with the grid size other than the condition necessary that $\Delta > h$, being h the grid size. Sub grid scales (also known as SGS) are models used to approximate SGS Reynolds-stress.

The important thing about the subgrid-scale Reynolds stress is that it contains local averages of the small-scale field. Ergo, models need to contain informations about local velocity field or local averages based on the local history of the fluid.

5.1.1.1 Smagorinsky and Related models

One of the most used and the earliest sub grid scale model is the one proposed by Smagorinsky (a detailed description of the method can be found in [18]).

Smagorinsky model is based on the fact that SGS Reynolds stress' principal effects are dissipation and increased transport. These phenomena are due to viscosity in laminar flows, so it comes easy in mind to assume that the model could be:

$$\tau_{ij}^s - \frac{1}{3}\tau_{kk}^s\delta_{ij} = \mu_t \left(\frac{\partial \overline{u_i}}{\partial x_j} + \frac{\partial \overline{u_j}}{\partial x_i} \right) = 2\mu_t \overline{S_{ij}}$$

Where μ_t is the eddy viscosity and $\overline{S_{ij}}$ is the strain rate of the resolved field. Instead, the eddy viscosity can be derived as follows:

$$\mu_t = C_s^2 \rho \Delta^2 |\overline{S}|$$

Where C_s is a parameter that still has to be derived and it could change its value depending on the application; delta is the filter length scale and $|\overline{S}| = (\overline{S_{ij}} \overline{S_{ij}})^{1/2}$.

This model, even if successful (or better said, very used), has its own problems. Depending on the problem to be simulated, the values of the coefficients must be changed using empirical formulas and approximations; these changes obviously introduce errors that should be kept in mind.

A way to solve some of the problems can be introducing the van Driest damping model. In the work of [19] and [20], this method is explained.

Even so, other problems arise, as explained in [12]. If the objective is to simulate more complex geometries with higher Reynolds number flows, it can be essential to use more detailed and accurate models. Also, because, as shown in DNS studies, Smagorinsky models are quite poor into describing the details of SGS's.

5.1.1.2 *The dynamic model*

The research for new SGS models is motivated by the shortcomings that arise from the use of the simple Smagorinsky model.

One of the main problems with the Smagorinsky model is that the value for the coefficient C_s must change depending on the application and on the flow regime. For example, in a zero laminar flow, $C_s = 0$, in other applications its usual value is $C_s = 0.15$ while in near wall applications for high-Reynolds-number turbulence-free flows that value must be changed using empirical models.

The dynamic model takes into account all these considerations and provides a methodology for calculating the appropriate value for the C_s coefficient depending on the case taken into account.

A complete explanation of the method along with the other methods (which exert from the work of this thesis) available in literature can be found in the work of [13].

5.1.1.3 *Near wall treatments*

For LES applications where Near wall resolution is applied, some conditions must be applied to the filtered velocity field: no-slip and impermeability boundary conditions.

If the simple Smagorinsky method is applied, due to the constant value of C_s , incorrect values for the length scale, viscosity and SGS are yield. To overcome this problem, a method can be that of applying the von Driest damping function. An even better solution could be abandoning the use of simple Smagorinsky and using instead the more complete dynamic model.

By using the dynamic model, correct near-wall scaling can be obtained and also good results in the resolution of the flow.

If the accuracy in the near-wall region is not required, but the goal is to save computational time (especially for very high Reynolds numbers), a solution can be not to resolve the viscous wall region. Following this path, the effects of unresolved motions are modelled through the use of simple boundary conditions very similar to the wall functions used in RANS applications. This method implies that these boundary conditions must be applied at the wall or at the first grid node next to the wall.

For a better understanding of the LES-NWM a good reference is [13].

5.2 RANS Turbulence Model

As usual engineering problems often require only the simplest of the solutions in fluid flow problems, just a few quantitative properties of the flow are usually solved, such as:

- Average forces on a body
- Distribution of forces on a body
- Degree of mixing of two or more fluids
- Quantity of a certain substance that has reacted
- Basic properties of a fluid such as temperature, pressure, density etc.

Using other methods like LES or DNS can be a waste of time. Such methods should be used only if the problem at hand is complex and require accurate results, if the objective is to validate a model or if a great amount of computational resources is available, which is not usually the case.

Osborne Reynolds proposed the Reynolds-Averaged-Navier-Stokes (RANS) method over a century ago.

In this method, all the unsteadiness that is part of the turbulence is averaged out. Averaging out the non-linearity in the Navier Stokes equations comes with difficulties. Terms must be modeled and errors occur while introducing these models. As turbulence is a very complex phenomena, averaging important parts of its composition means that the Reynolds-average model will not be able to represent correctly all turbulent flows; these turbulence models should not be regarded as scientific laws, rather they should be considered as engineering approximations.

5.2.1 Governing equations in RANS

Every variable in a statistical steady flow can be described as a sum of a time-averaged quantity and a variation about that value:

$$\Phi(x_i, t) = \bar{\Phi}(x_i) + \Phi'(x_i, t)$$

Where:

$$\bar{\Phi}(x_i) = \lim_{T \rightarrow \infty} \frac{1}{T} \int_0^T \Phi(x_i, t) dt$$

In this equation, t is the time and T is the averaging interval. If T is big enough with respect to the time scale of the fluctuations, $\bar{\Phi}$ doesn't depend on the time at which the averaging started.

If an unsteady flow is considered, time averaging has no effect and ensemble averaging must be taken into consideration. It is illustrated as follows:

$$\bar{\Phi}(x_i, t) = \lim_{N \rightarrow \infty} \frac{1}{N} \sum_{n=1}^N \Phi(x_i, t)$$

In this equation N is the number of members of the ensemble; if this number is high enough, the effect of the fluctuations can be eliminated, which is the objective of this method. Any flow can be averaged by following this method.

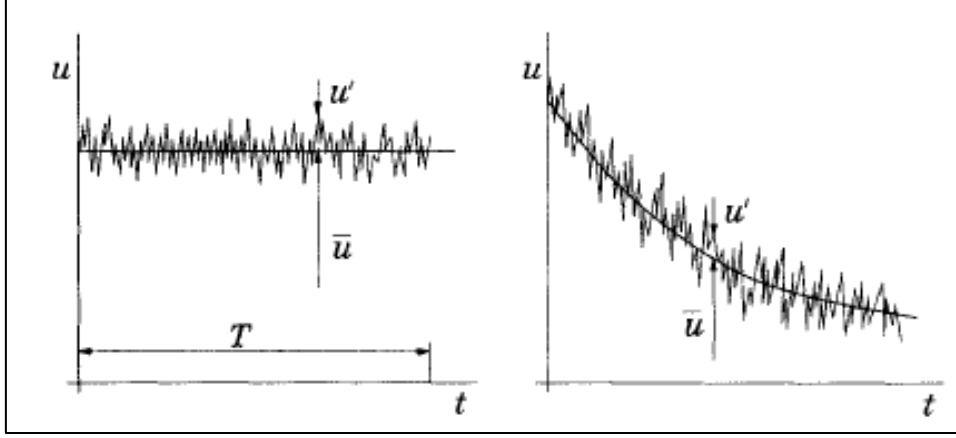


Figure 8- Time averaging of a flow

statistically steady flow (left); ensemble averaging for an unsteady flow (right) [12]

By applying the average method to Navier-Stokes equations, Reynolds-averaged Navier-Stokes (RANS) equations are yielded.

It is known that averaging a linear term from conservation equations gives the same term for the averaged quantity. In exchange, averaging a quadratic non-linear term, other two terms are obtained:

$$\overline{u_i \Phi} = \overline{(\bar{u}_i + u'_i)(\bar{\Phi} + \Phi')} = \bar{u}_i \bar{\Phi} + \overline{u'_i \Phi'}$$

By averaging conservation equations, the resulting equations contain some terms called Reynolds stresses and others called turbulent scalar fluxes. The difficulty stands in the fact that these terms cannot be expressed as function of mean quantities. If continuity and momentum equations are averaged, for incompressible flows for example, they can be written as:

$$\begin{aligned} \frac{\partial(\rho \bar{u}_i)}{\partial x_i} &= 0 \\ \frac{\partial(\rho \bar{u}_i)}{\partial t} + \frac{\partial(\rho \bar{u}_i \bar{u}_j + \rho \overline{u'_i u'_j})}{\partial x_j} &= -\frac{\partial \bar{p}}{\partial x_i} + \frac{\partial \bar{\tau}_{ij}}{\partial x_j} \end{aligned}$$

Where the $\bar{\tau}_{ij}$ is the mean viscous stress tensor component:

$$\bar{\tau}_{ij} = \mu \left(\frac{\partial \bar{u}_i}{\partial x_j} + \frac{\partial \bar{u}_j}{\partial x_i} \right)$$

After averaging the NS equations, the turbulent scalar flux and Reynold stresses are introduced, which means that more unknowns are also introduced; there are more variables than equations, which means that the conservations equations are not closed. To be able to close these equations, it is necessary to express the turbulent scalar flux and Reynold stresses in terms of mean quantities.

It becomes mandatory to introduce approximations called turbulence models in order to be able to close the equations.

5.2.2 Eddy viscosity models

To be able to understand the turbulence models, one could note that the energy dissipation and transport of mass, momentum and energy in a normal direction with respect to the streamlines are done by the viscosity; easily, it comes to mind that turbulence effects can be seen as an increase in the viscosity. In this way, an eddy-viscosity model for the Reynolds stress can be written:

$$-\rho \overline{u'_i u'_j} = \mu_t \left(\frac{\partial \overline{u}_i}{\partial x_j} + \frac{\partial \overline{u}_j}{\partial x_i} \right) - \frac{2}{3} \rho \delta_{ij} k$$

This model is not correct in detail but it is easy to implement and if applied correctly, can provide good results in many applications.

As already said, turbulence is quite difficult to describe; in a simple description, one can say that turbulence can be characterized by only two parameters: its kinetic energy k or a velocity q , and a length scale L .

Difficulties arise when, in three dimensional flows, turbulence quantities must be described. A logical choice can be to derive these quantities from differential equations; one for velocity scale and one for length scale. An equation for the k term, the velocity scale can be easily derived [21]:

$$\frac{\partial(\rho k)}{\partial t} + \frac{\partial(\rho \overline{u}_j k)}{\partial x_j} = \frac{\partial}{\partial x_j} \left(\mu \frac{\partial k}{\partial x_j} \right) - \frac{\partial}{\partial x_j} \left(\frac{\rho}{2} \overline{u'_j u'_i u'_i} + \overline{p' u'_j} \right) - \rho \overline{u'_i u'_j} \frac{\partial \overline{u}_i}{\partial x_j} - \mu \frac{\partial^2 \overline{u'_i}}{\partial x_k^2}$$

For a clear description of this equation[12].

To determine the length scale, another equation is necessary. A commonly used equation is based on the fact that dissipation is needed in energy equation and also in those turbulent flows where the production and destruction of turbulence are in a quasi-equilibrium state. A way to correlate dissipation ε , kinetic energy k and length scale is:

$$\varepsilon \approx \frac{k^{3/2}}{L}$$

The base idea for this equation is based on the energy cascade hypothesis described earlier.

A more complete definition of the dissipation written in a differential form is:

$$\varepsilon = \nu \left[\left(\frac{\partial u'}{\partial x} \right)^2 + \left(\frac{\partial u'}{\partial y} \right)^2 + \left(\frac{\partial u'}{\partial z} \right)^2 + \left(\frac{\partial v'}{\partial x} \right)^2 + \left(\frac{\partial v'}{\partial y} \right)^2 + \left(\frac{\partial v'}{\partial z} \right)^2 + \left(\frac{\partial w'}{\partial x} \right)^2 + \left(\frac{\partial w'}{\partial y} \right)^2 + \left(\frac{\partial w'}{\partial z} \right)^2 \right]$$

Where (u', v', w') is the fluctuating velocity vector. The kinetic energy is zero for laminar flow and can be as large as 5 % of the kinetic energy of the mean flow in a highly turbulent case.

The models use turbulent diffusion and turbulent conductivity terms to account for the presence of turbulence in mass transport and energy transport. The turbulent diffusion and conductivity terms are given by:

$$D_t = \left(\frac{1}{S_{ct}} \right) \mu_t$$

$$K_t = \left(\frac{1}{P_{rt}} \right) \mu_t c_p$$

where S_{ct} is the turbulent Schmidt number, P_{rt} is the turbulent Prandtl number, D_t is the turbulent diffusion, and K_t is the turbulent conductivity.

An equation for the energy dissipation at the smallest eddies is:

$$\frac{\partial(\rho\varepsilon)}{\partial t} + \frac{\partial(\rho u_j \varepsilon)}{\partial x_j} = C_{\varepsilon 1} P_k \frac{\varepsilon}{k} - \rho C_{\varepsilon 2} \frac{\varepsilon^2}{k} + \frac{\partial}{\partial x_j} \left(\frac{\mu_t}{\sigma_\varepsilon} \frac{\partial \varepsilon}{\partial x_j} \right)$$

Where the entire equation can be seen as a model itself. In this model, eddy-viscosity is:

$$\mu_t = \rho C_\mu \sqrt{k} L = \rho C_\mu \frac{k^2}{\varepsilon}$$

These last equations are the base for the most widely used k- ε closure model. This model needs a series of constant values in order to be applicable:

$$C_\mu = 0.09 \quad C_{\varepsilon 1} = 1.44 \quad C_{\varepsilon 2} = 1.92 \quad \sigma_k = 1 \quad \sigma_\varepsilon = 1.3$$

This model is the easiest that can be applied in a computer code. That is because RANS equations have the same form as the much simpler laminar equations. The main difference is that in RANS two new differential equation need to be solved in order to close the resolution of the model. As the time scales that are associated with the turbulence are much shorter than those of the mean flow, the equations and the k-epsilon model become much stiffer than the equations of laminar flows. Some difficulties arise in the discretization and resolution of these equations, other than the fact that the stiffness has to be taken into account. A good description of the resolution method is given in [12].

A similar method to the k-epsilon method is the RNG k-epsilon model.

5.2.2.1 RNG k-epsilon model

The equation of energy dissipation at the smallest eddies can be written as:

$$\frac{\partial \rho \varepsilon}{\partial t} + \frac{\partial \rho u_i \varepsilon}{\partial x_i} = \frac{\partial}{\partial x_i} \left(\frac{\mu}{Pr_k} \frac{\partial \varepsilon}{\partial x_j} \right) + c_{\varepsilon 3} \rho \varepsilon \frac{\partial u_i}{\partial x_i} + \left(c_{\varepsilon 1} \frac{\partial u_i}{\partial x_j} \tau_{ij} - c_{\varepsilon 2} \rho \varepsilon + c_s S_s \right) \frac{\varepsilon}{k} + S - \rho R$$

where S is the user-supplied source term and S_s is the source term that represents interactions with discrete phase (spray). Note that these two terms are distinct. The $c_{\varepsilon 1}$ terms are model constants that account for compression and expansion. The R term is zero in the classical k-epsilon model but for the RNG model it is:

$$R = \frac{C_\mu \eta^3 \left(1 - \frac{\eta}{\eta_0}\right) \varepsilon^2}{(1 + \beta \eta^3) k}$$

In the Rapid Distortion RNG k-epsilon model the equation of energy transport/dissipation becomes:

$$\begin{aligned} \frac{\partial \rho \varepsilon}{\partial t} + \frac{\partial \rho u_i \varepsilon}{\partial x_i} = & \frac{\partial}{\partial x_i} \left(\frac{\mu}{Pr_k} \frac{\partial \varepsilon}{\partial x_j} \right) - \left[\frac{2}{3} c_{\varepsilon 1} - c_{\varepsilon 3} + \frac{2}{3} c_\mu c_\eta \frac{k}{\varepsilon} \frac{\partial u_k}{\partial x_k} \right] \rho \varepsilon \frac{u_i}{x_i} \\ & + \left(c_{\varepsilon 1} - c_\eta \frac{\partial u_i}{\partial x_j} \tau_{ij}^* - c_{\varepsilon 2} \rho \varepsilon + c_s S_s \right) \frac{\varepsilon}{k} \end{aligned}$$

Where:

$$\begin{aligned} c_\eta &= \frac{\eta \left(1 - \frac{\eta}{\eta_0}\right)}{(1 + \beta \eta^3)} \\ \tau_{ik}^* &= \tau_{ij} - \frac{1}{3} \delta_{ij} \tau_{kk} = 2\mu_T \left(S_{ij} - \frac{1}{3} \delta_{ij} \frac{\partial u_k}{\partial x_k} \right) \end{aligned}$$

The S_s term takes into account the turbulence with the discrete phase. It is defined as:

$$S_s = - \frac{\sum_P N_P (F'_{drag,i} u'_i)_P}{V}$$

where the summation is over all parcels in the cell, N_P is the number of drops in a parcel, V is the cell volume, u'_i is the fluctuating component of the gas-phase velocity and the last term is the drag force on a drop:

$$F'_{drag,i} = \frac{F_{drag,i}}{u_i + u'_i - v_i}$$

CONVERGE CFD uses the RNG k-epsilon method (Re-Normalized Group), a method proposed by [22]. It is a method whose aim is simply to consider more than one eddy length scale contributing to the turbulence diffusion.

5.3 Laminar Flame Speed

Combustion of fuel air mixture inside the engine cylinder is one of the main processes that controls efficiency and emissions. The combustion process is a fast-exothermic gas phase reaction. The area inside the mixture where products convert to reactants is called reaction zone.

The burning velocity is called laminar burning velocity. It is a property of the fuel (thermo chemical property) which depends on:

- Fuel-to-air ratio ϕ
- Temperature in the unburnt mixture
- Pressure

The introduction of laminar flame speed in the whole combustion environment means that LFS is considered as an additional property in the fluid-dynamical system.

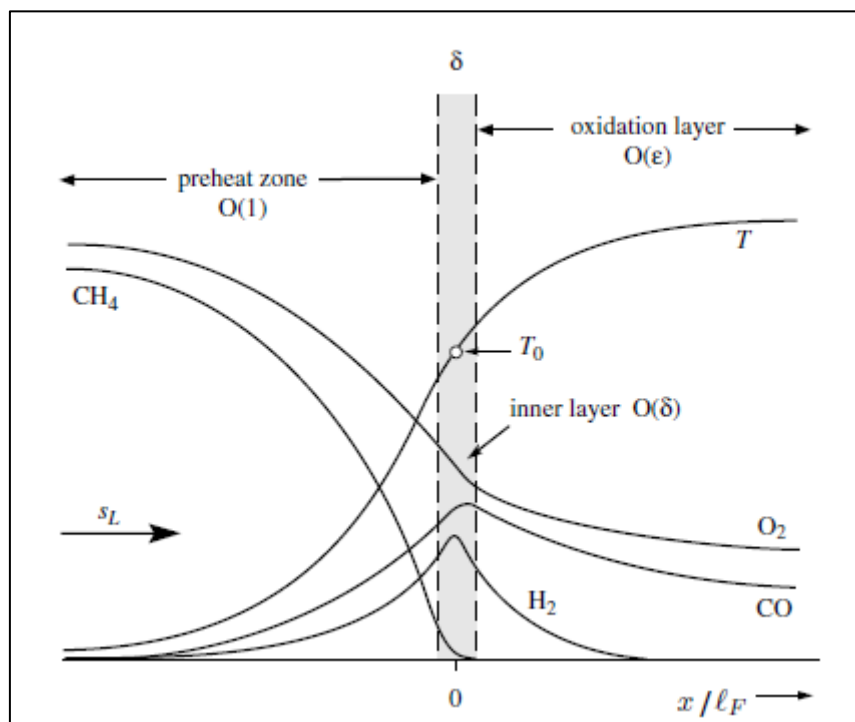


Figure 9- Flame structure, chemical reactants and products of combustion [10]

The flame propagation is determined by a series of characteristics dictated by the strong coupling between chemical reaction, transport processes of mass diffusion and heat conduction and fluid motion, all of these playing a very important role.

If combustion of pure methane is analysed, the Figure 9 shows that the flame structure contains multiple zones:

- Chemically inert preheat zone
- Multiple reaction layers (δ and ϵ). The δ layer is the most important one; in the latter the fuel is consumed and the radicals are consumed by chain-breaking reactions. This layer is the one responsible for keeping the flame alive. Also, this layer is the most sensible one to the turbulence; if eddies of the Kolmogorov length scale penetrate into the layer, the layer will be disrupted. The reason why this happens is because of heat conduction and diffusion: this phenomenon will enhance the transport of radicals out of the layer, thus breaking the flame. Since the Kolmogorov length scale is the smallest scale that could affect the reaction layer, the latter should be thinner than the dimension of the scale η (Kolmogorov).

Having to simulate the combustion, a model for this process has to be developed. The characteristics of flame propagation has to be developed in order to match the realistic phenomena. To understand the combustion simulation (which is turbulent in nature), we will first introduce the laminar flames fundamentals. Then we will relate laminar flame speed with turbulent flame speeds and then to combustion process.

5.3.1 LFS

The laminar flame speed is a property that every flammable mixture possesses. It can be defined as the speed at which the un-stretched laminar flame will propagate through a quiescent mixture of reactants. LFS is given by:

$$S_L = \frac{dm_b/dt}{A_f \rho_u}$$

In this formula, dm_b/dt is the mass burning rate in time. It depends on a series of terms like pressure, turbulence, spark advance, flame surface and temperature. Every premixed fuel has a different LFS, even if tested in the same conditions. Another important term that has to be taken into consideration when determining the LFS is the gas dilution with EGR.

If LFS is addressed from the stoichiometric point of view, there are many fuels which have a maximum burning speed if the mixture is slightly in the rich zone, as shown in the Figure 10:

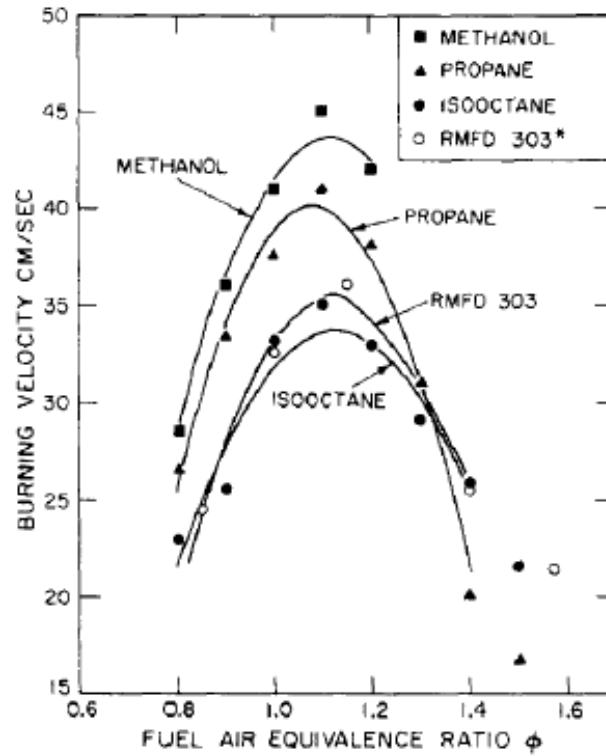


Figure 10- Burning velocities

Dependence on air-to-fuel ratio determined from the vapor pressure of the fuel [23]

If higher pressures and temperatures are developed, as often happens, new formulas must be developed. As discussed in:[23] a new formula can be used:

$$S_L = S_{L,0} \left(\frac{T_u}{T_0} \right)^\alpha \left(\frac{P}{P_0} \right)^\beta$$

The fact that a velocity scale is considered gives birth to a need to introduce a length scale. Length scale in the laminar flame can be defined as:

$$l_F = \frac{(\lambda/c_p)_0}{(\rho S_L^0)_u}$$

The λ and c_p are considered at the inner layer temperature T_0 and instead λ and S_L^0 are considered in the unburned layer.

There are multiple ways to study the phenomena occurring during the flame propagation. The Bunsen burner has been analysed.

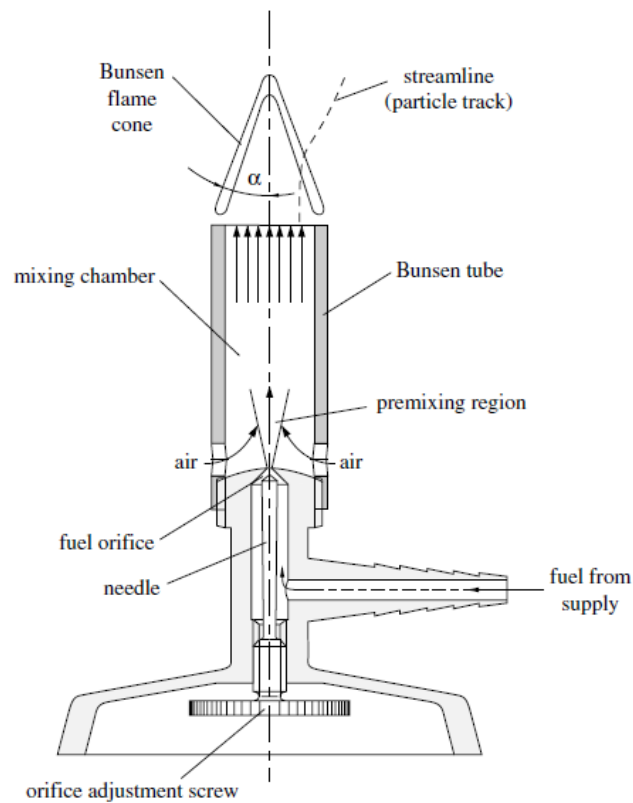


Figure 11- Bunsen Burner scheme [10]

Fuel is pumped from the fuel supply and the quantity can be adjusted with the orifice adjustment screw. It then enters the premixing area where air enters from the 2 side orifices. The fuel and air must be able to mix homogeneously in order to have a fully premixed mixture before reaching the flame.

The Bunsen burner is able to develop laminar or turbulent flames; the passage from laminar to turbulent is dictated by the velocity of the flow or by a turbulence grid placed at the end of the mixing chamber. It can happen that the burning velocity (turbulent S_T or laminar S_L) is smaller than the velocity of the flow exiting the chamber; if that happens, a flame cone will be generated.

It is possible to analyze these velocities as shown in the next figure:

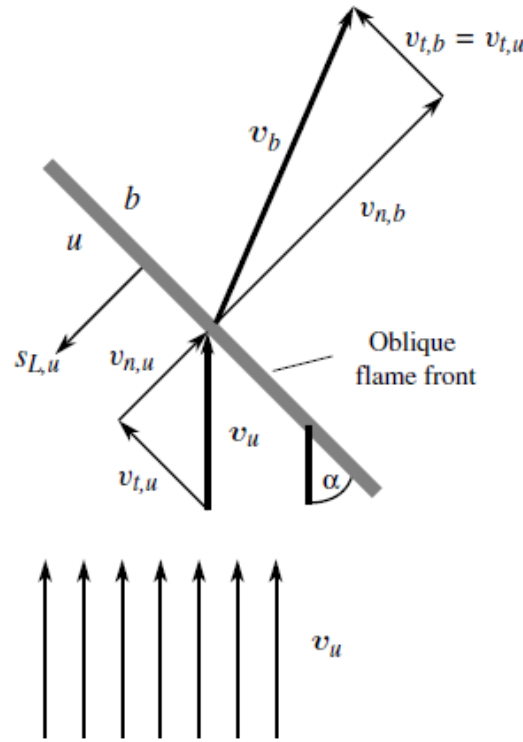


Figure 12- Velocity vectors

Analysis of the vectors exiting from the Bunsen burner [10]

By studying this figure and applying the equation of continuity we obtain:

$$(\rho v_n)_u = (\rho v_n)_b$$

And having the density that decreases:

$$v_{n,b} = v_{n,u} \frac{\rho_u}{\rho_b}$$

And since the tangential velocity is not affected by the expansion of the gasses, it does not change between burnt and unburnt gasses.

If the vectors addition is executed, the v_b vector is deflected, having a different direction with respect to the flow.

The flow considered in this case is stationary thus the burning velocity with respect to the unburnt mixture must be equal to the flow velocity of the unburnt mixture normal to the front. We can distinguish the two burning velocities: laminar and turbulent respectively:

$$S_{L,u}^0 = v_{n,u}$$

$$S_{T,u}^0 = \overline{v_{n,u}}$$

And from the last equation it results that the turbulent burning velocity is an averaged quantity. By taking into consideration the angle α of the cone in the figure, the normal velocity can be calculated:

$$v_{n,u} = |v_u| \sin \alpha$$

Having calculated all these variables, it is possible to determine the burning velocity experimentally by measuring the flow velocity and the cone angle.

The equations written until now are just empirical, and they give only a general rule for a given fuel-air mixture. In said equations, the effects of burnt gas on the LFS is not taken into account. Also, the equations are not defined specifically for methane-air mixtures.

To have a realistic prediction of laminar flame speed, generally two methods are used:

1. Power Laws (Gulder)

This method is proposed by Gulder [24] and it relay on:

$$S_{L-ref} = \omega \Phi^\eta \exp[-\xi(\Phi - 1.075)^2]$$

Where ω , ξ and η are constants which depend on the fuel and oxidizer utilized for the simulation.

$Tu-ref$	P_{ref}	ω	ξ	η	γ	β
298 K	1013525 Pa	0.4220	5.18	0.150	2	-0.5

Table 2- Gulder Method- Constants

Once the flame speed has been calculated for the reference case, this has to been corrected for the actual conditions of temperature and pressure by using:

$$S_L = S_{L-ref} \left(\frac{T_u}{T_{u-ref}} \right)^\gamma \left(\frac{P}{P_{ref}} \right)^\beta (1 - 2.1Y_{dil})$$

Where are taken into consideration unburned gas conditions and reference conditions. Also, Y_{dil} is the fraction of diluted species in the mixture. Instead the temperature and pressure exponents, respectively γ and β are defined as:

$$\gamma = \gamma_{ref} - 0.8(\Phi - 1)$$

$$\beta = \beta_{ref} - 0.22(\Phi - 1)$$

2. Kinetic mechanism

This mechanism shows a step by step description of reaction mechanism which happen at a molecular level during a combustion. It is able to descript the transition state of molecules, the breaking and re-bonding of bonds at each given time step. For each species, the reaction rate can be expressed as:

$$k_k = A_k T^{n_k} \exp\left(-\frac{E_k}{RT}\right)$$

Where k_k is rate coefficient, A_k is the frequency factor, n_k is the pre-exponential temperature exponent and E_k is the activation energy of reaction k.

The upside of kinetic mechanisms is that they can be defined for different fuel compositions, different number of species defined and the sub-reactions defined for each one of the species.

A complete disclosure on kinematic mechanisms can be found in [25]

For predicting the laminar flame speed, based on the work of [26] an LFS table was used.

For the work of this thesis, tables obtain by [26] were used by CONVERGE CFD software based on a user defined function (UDF).

The LFS tables were obtained through the GRI Mech 3.0 with the DARS software. These tables were specifically designed for:

- Pure methane
- Methane plus hydrogen in 10%, 15%, 25% volume
- EGR dilution of 10%, 20%, 25%

5.4 Ignition and combustion modelling

5.4.1 Ignition model: ISSIM

For the work of this thesis, CONVERGE CFD software used the ignition model ISSIM (Imposed Stretch Spark Ignition Model). This model is based on another model, the ATKIM model. This has a scheme showed in the next figure:

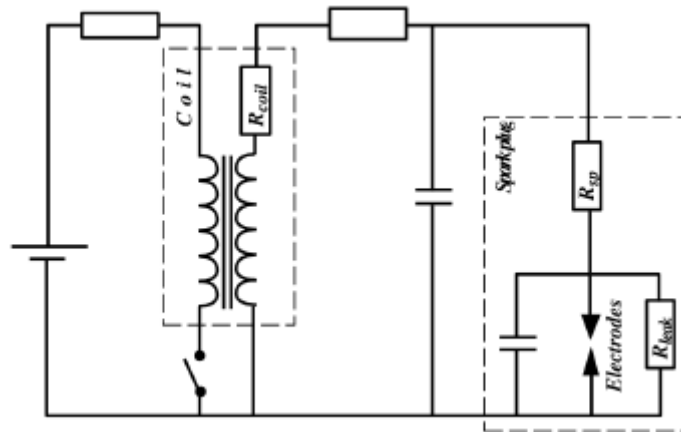


Figure 13- ATKIM inductive scheme

Scheme of the spark plug's electrical circuit [27]

The ATKIM and also the ISSIM model have the same governing equations for the scheme and the initialization of the spark:

$$E_{mag,prime} = \frac{1}{2} L_p i_p^2$$

Where: L_p is the primary inductance of the circuit. Of this $E_{mag,prime}$ only about 60% of the energy is utilized during the spark discharge.

The life of the spark is generally divided into three phases. The breakdown and arc phases, which last typically less than a microsecond, are taken into account by considering an instantaneous energy deposit in the gas, E_{bd} which is given by:

$$E_{bd} = \frac{V_{bd}^2}{C_{bd}^2 d_{ie}}$$

Where V_{bd}^2 is the breakdown voltage, C_{bd} is a constant and d_{ie} is the distance between the two electrodes. Then there is the glow phase which lasts a few milliseconds usually. The current discharged by the spark plug is defined by:

$$i_s = \sqrt{\frac{2E_s}{L_s}}$$

The current is calculated from the energy E_s and the inductance L_s which are defined by the user. On the secondary circuit then another energy will result:

$$\frac{\partial E_s(t)}{\partial t} = -R_s i_s^2(t) - V_{ie} i_s(t)$$

And the glow phase survives as long as the value of E_s is positive.

As the spark voltage reaches the breakdown voltage, the gas starts to break down and the conductive phase begins. Once the conductive phase has begun, the gas starts to receive energy from the spark kernel. The energy received must be greater than a critical value in order to have a proper ignition of the gasses. This happens when $E_{ign} > E_{crit}$, where:

$$E_{ign} = 0.6E_{bd} + \int_{t_{spk}}^t V_{gc} i_s dt$$

$$E_{crit} = 4 \frac{\gamma}{1 - \gamma} l_{spk} p \pi \delta_L^2$$

$$V_{gc} = 40.46 l_{spk} i_s^{-0.32} p^{0.51}$$

Where p is the pressure, l_{spk} is the spark length, δ_L is the flame thickness and γ is the gas heat capacity ratio.

When ignition begins, a mass of burning gases m_{bg}^{ign} is deposited near the spark. The target burned gas volume fraction is given by:

$$\overline{c_{ign}}(x, t_{ign}) = c_0 \exp\left(-\left(\frac{|x - x_{spk}|}{0.5d_{ie}}\right)^2\right)$$

Where x represents the coordinates for each cell, x_{spk} gives the spark location and c_0 is a constant that guarantees that the targeted mass of burned fraction is equal to the mass of burning gasses near the spark plug.

Once the ignition occurred, an ignition flame density must be defined (FSD). When the ignition occurs, the assumption is that the initial kernel is a sphere with a radius:

$$r_b^{ign} = \left(\frac{3}{4\pi} \int \overline{c_{ign}} dV\right)$$

And the FSD can be:

$$\Sigma_{ign} = C_{surf} \frac{3\overline{c}}{r_b^{ign}}$$

Where C_{surf} is a value that takes into account the initial non sphericity of the kernel. Once the kernel is created, its radius increases according to the law:

$$\frac{dr_b}{dt} = (1 + \tau)\mathcal{E}S_L$$

Where the term \mathcal{E} is the turbulent wrinkling factor, one of the main calibration factors taken into consideration when the model is created. Also, τ is the expansion ratio defined as $\frac{\rho_u}{\rho_b} - 1$. In conclusion, the ISSIM model takes into consideration the deformation of the gasses surface due to combustion (convection and turbulence), in contrast with the AKTIM model from which is created.

5.4.2 Combustion Modelling

In the previous chapters laminar flames have been introduced and discussed broadly. In this chapter the turbulence flame models will be introduced and then the premixed turbulence combustion.

Combustion requires that fuel and oxidizer are mixed at the molecular level. How this takes place in turbulence combustion depends on the turbulent mixing process thus on the entire turbulent motion present in the cylinder prior to the combustion.

Premixing is only possible at sufficiently low temperatures where the chain-branching mechanism that drives the reaction chain in hydrogen and hydrocarbon oxidation is unable to compete with the effect of three-body chain-breaking reactions. Under such low temperature conditions combustion reactions are said to be “frozen.”

The general view is that once a range of different size eddies have developed, strain and stress will increase and thereby steepen the concentration gradients at the interface between reactants, which in turn enhances their molecular inter-diffusion. Molecular mixing of fuel and oxidizer, as a prerequisite of combustion, takes place at the interface between small eddies.

Once fuel and oxidizer have homogeneously been mixed and a heat source has been supplied, it becomes possible for a flame front to start and advance through the mixture.

Some criteria have to be met in order to allow the flame to advance: the fuel-to-air ratio must lie between the flammability limits; these range typically from approximately $\phi = 0.5$ to $\phi = 1.5$ for a Methane-air mixture, where ϕ is the fuel-air-equivalence ratio.

Combustion is an intrinsically complex process involving a large range of chemical time and length scales. Some of the chemical phenomena controlling flames takes place in short times over thin layers and are associated with very large mass fractions, temperatures and density gradients the full description of chemical mechanisms in laminar flames may require hundreds of species and thousands of reactions leading to considerable numerical difficulties.

Also, turbulence (as a separate phenomenon) has to be considered when referring to a turbulent premixed combustion, as in the case of the simulations studied in this thesis.

Turbulent combustion is a result from the interaction between chemical reactions and turbulence. When flame interacts with a turbulent flow, turbulence is modified by combustion and because of the large changes in kinematic viscosity associated with temperature changes. This mechanism may generate turbulence called “flame generated turbulence” or damp it. On the other hand, turbulence alters the flame structure, which may enhance the chemical reaction but also, in extreme cases, completely inhibit it, leading to flame quenching.

In other words, there will be a mutual interaction between flame front and turbulence and each of the two phenomena alters the other in a positive or negative way. A schematic vision can be seen in the Figure 14:

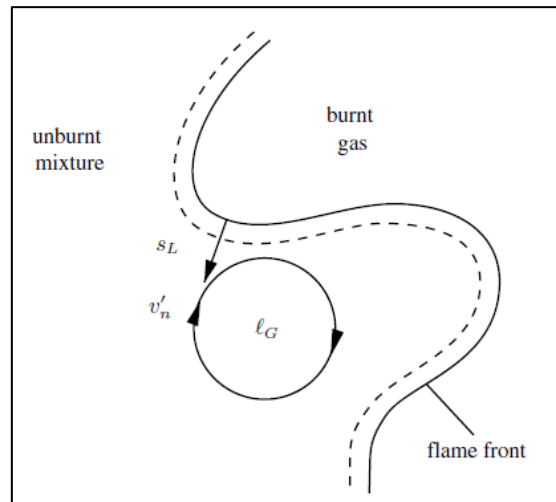


Figure 14- Flame Front description

Interaction between eddies and flame front [10]

The figure is useful because it allows understand which of the eddies are able to affect the flame front, thus the combustion. To be able to understand if an eddy is able to interact directly with the flame front, we impose that the turnover velocity v'_n is equal to the flame speed S_L . Consequently, the length scale of the eddy is determined as:

$$l_G = \frac{S_L^3}{\varepsilon}$$

It results that only the eddies with a characteristic length scale equal to l_G , meaning a turnover velocity equal to S_L are able to affect the flame front. Instead, the eddies with a turnover velocity greater than the burning velocity are not able to enter the flame front and they are only able to disturb the flame front by corrugating it.

Smaller eddies with a length scale $l_n < l_G$ and with a turnover velocity smaller than the flame front are not able to disturb the advancing of the flame in any way.

A logarithmic graph is available to understand, for each burning velocity, the length scale that corresponds to it.

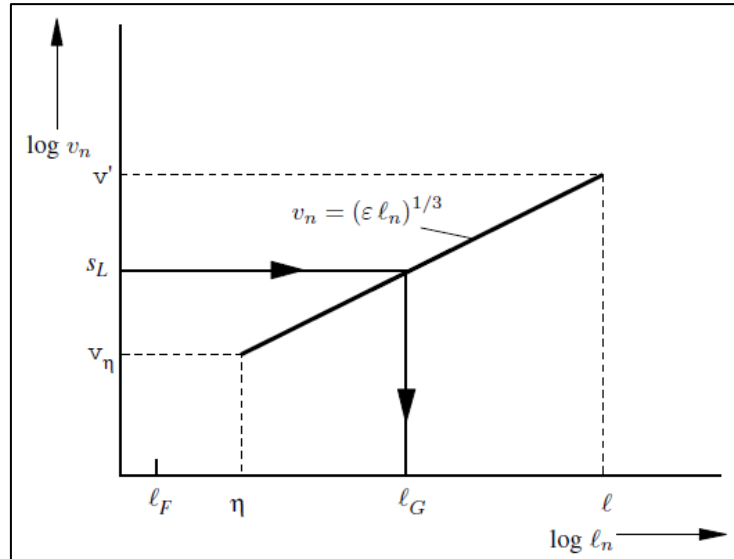


Figure 15- Length scales of eddies with respect to burning velocities [10]

If one enters from the vertical axis, by choosing a burning velocity, the corresponding length scale can be obtained.

More explanation on the various length scales can be found in [10].

Another important parameter to be taken into account when explaining combustion is the quenching time. It has been shown by Peters [28] that if t_q is of the same timescale as the time scale t_F , the flame can be extinguished.

Researches from [10] show that there is a certain length scale called $l_m = (\epsilon t_q^3)^{1/2}$; this can be seen as a mixing length scale. It means that it is small enough to penetrate the reaction front; eddies that have this dimension and a turnover time equal to the time needed to diffuse scalars over a distance same as diffusion thickness. These eddies have the capability of transporting fluids from the reaction front into the reaction zone in front of the flame.

This effect is therefore undesired as it comes with a cooling effect of the flame; moreover, it thickens the flame and slows the overall combustion process.

This effect can be seen in the Figure 16:

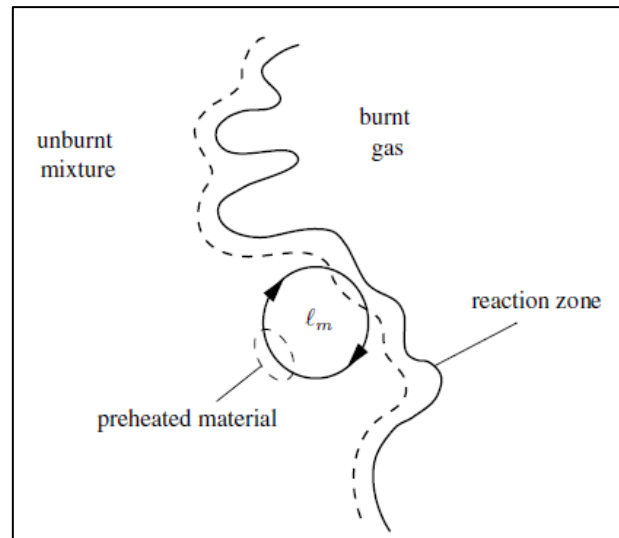


Figure 16- Destructive interaction between eddies and flame front [10]

There are eddies with length scales bigger than l_m that are able to transport even more mass therefore corrugating ever more the flame structure.

5.4.2.1 1D Turbulent premixed flames

It is known that changing the turbulence level before starting combustion in a combustion chamber may change the time needed for the complete combustion due to the turbulent flame speed. The combustion rate is maximum when the reactants are mixed in stoichiometric or slightly rich proportions and increases when the flow becomes turbulent.

An empirical definition about the relation between laminar and turbulent combustion was given by Abdel-Gayed, Gulder et al:

$$\frac{S_T}{S_L} \cong 1 + \frac{u'}{S_L}$$

Whereas the u' is the root mean square of the velocity fluctuations (or the rms of TKE), more commonly known as an indication of the turbulence. The relation shows that premixed combustion is actually enhanced by the presence of turbulence.

Experiments show that for very large turbulent burning speeds, the S_T becomes almost independent of the laminar flame speed S_L .

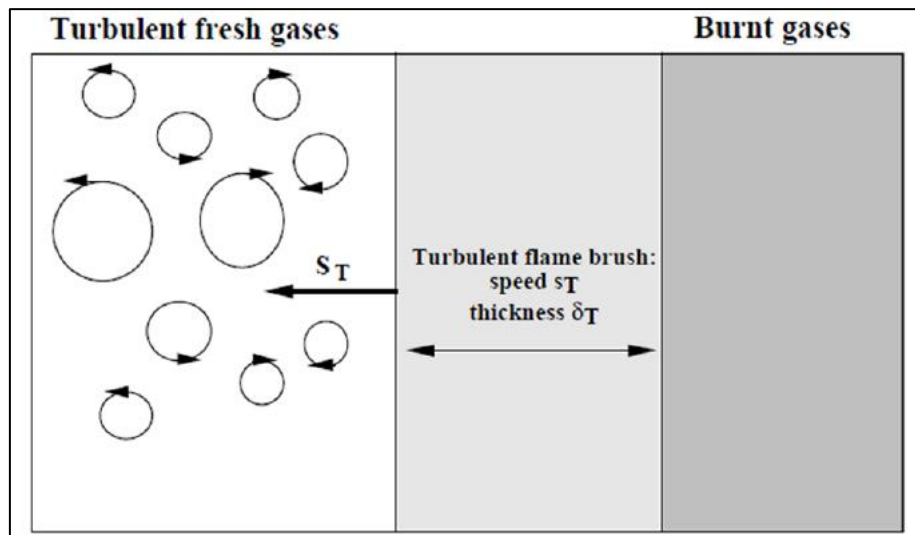


Figure 17- Representation of a turbulent flame advance [29]

The Figure 17 shows the advancing of a turbulent flame with a turbulent velocity. Experimentally though, it has been shown that mean turbulent flame brush thickness δ_T is always larger than the laminar flame thickness δ_L .

In the 1D turbulent premixed flames model, the mean reaction rate based on the series expansion of the Arrhenius law cannot be retained because of the large number of closure problems (unclosed quantities like species concentration and temperature fluctuations) and of large truncated errors due to high non linearities.

For these reasons, many combustion models have been developed and proposed in order to take into account the difficulties that turbulent premixed combustion brings.

Since in the case of combustion in an engine a premixed turbulent flame is present, the combustion model has to be able to compute the reactions in order to have a precise model. Other than that, it is known how the combustion time changes when a turbulent flame is involved:

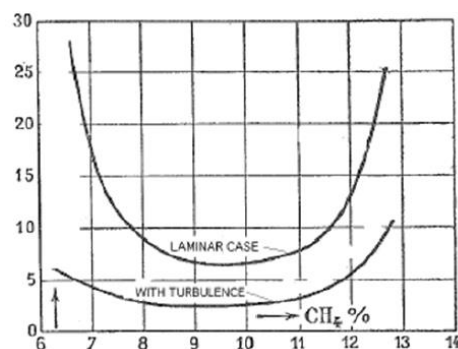


Figure 18- Burning speeds in a laminar and turbulent combustion

Difference between laminar and turbulent burning speeds (on y-axis there is burning speed and on x-axis methane percentage in a mixture) [30]

Typically, a combustion model has to be able to solve the premixed combustion as illustrated in the next figure:

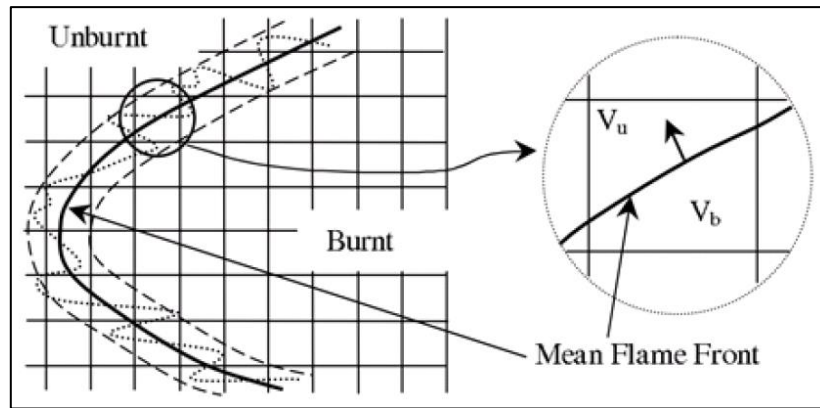


Figure 19- Flame front advance in the computational domain [15]

The combustion system model contains two stable states: the unburnt (index u) and the burned gas state (index b) as shown above in the Figure 19. In premixed combustion, both states concurrently exist in the system. They are spatially separated by the flame front, where the transition from one to the other takes place [15].

5.4.2.2 Flamelet assumption

The combustion in our models is happening in such a way that the flamelet assumption can be used. This theory affirms that the whole environment can be seen as two major areas: burnt and unburnt gasses. These two areas are divided by what can be called flamelets. They are elements of the flame; each flamelet behaves as it would be a laminar flame.

An important assumption is that burnt and unburnt gasses are separated by a continuous region where the combustion chemical reactions take place.

In this region a laminar flame structure may be present but, at the same time, it can be thickened by the phenomena described above.

The combustion can be divided into combustion regimes [10]. As explained above, combustion can be slowed or even stopped by various events: external perturbations, heat losses, excessive stretch of the flame front which can decrease the chemical reactions to a stop, interruptions of the flame front.

Otherwise, if the combustion continues and a turbulent premixed flame exists, the flame zone exists and it is active. This is the zone called “flamelet regime”.

A simple definition of the turbulent premixed reacting flow in the flamelet regime can be given as follows:

- If a point A in the unburned gasses can be connected to a point B in the burned gasses by a straight line and the said line passes at least once the active flame front, then it means that the flow is in a flamelet regime Figure 20:

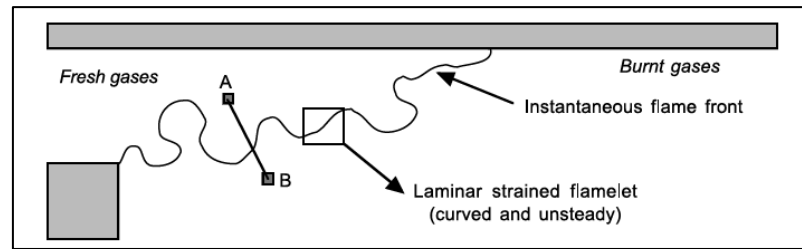


Figure 20- Flamelet regime assumption scheme [29]

The danger with this assumption is that, if turbulence intervenes and modifies the flame structure, combustion stops in the vicinity of this point and fresh reactants diffuse into the products without burning. In this situation, the description of the reacting flow becomes much more complex and standard flamelet approaches are no longer valid.

Therefore, quenching in a turbulent premixed flame determines the limit between two fundamentally different behaviours (i.e. flamelets or no flamelets). Flame elements are usually assumed to quench in turbulent flows if their condition is traced to a condition similar to laminar stagnation point flames.

The parameter that is able to tell apart from turbulent flamelets and laminar stagnation point flames is flame stretch. This assumption is justified, once again, from asymptotic theories which show that, under certain assumptions (mainly low levels of stretch), the whole flame structure and many important flame parameters, such as displacement and consumption speeds, depend and are governed only by stretch.

5.4.3 ECFM Combustion Model

In the work of this thesis, the ECFM combustion model has been used. It is an extension of the Coherent Flame Model developed by Marble and Broadwell [31]. The ECFM is used to accurately model the combustion process, in particular for spark-ignited engines. It is a flamelet-based model and, to be able to calculate the flame density, ECFM uses the fuel/air equivalence ratio in the fresh gasses, their composition (even if residual gasses are present) and also the temperature in the immediate vicinity of the flame. The obtained result of the flame density is then used to describe the large-scale stratification of the fractions of burned/unburned gasses.

This model does not only model the combustion in SI engines but also in Auto Ignition applications; moreover, it is able to model pollutant formation even for highly stratified cases.

In order to account for both mixing processes and for the Flame Diffusion (DF), each computational cell is subdivided in 3 zones: a pure fuel zone, a pure air zone (plus possible EGR) and a mixed zone.

This structure allows to take in account the three main combustion modes (Auto Ignition, Propagation Flame and Diffusive Flame). To determine the flame surface density, the ECFM uses the fuel/air equivalence ratio in fresh gases, the composition (including residual gases), and the temperature near the flame. The resulting flame surface density is used to describe large scale burned/unburned stratification. A scheme of the computational cell can be seen in Figures (21, 22)

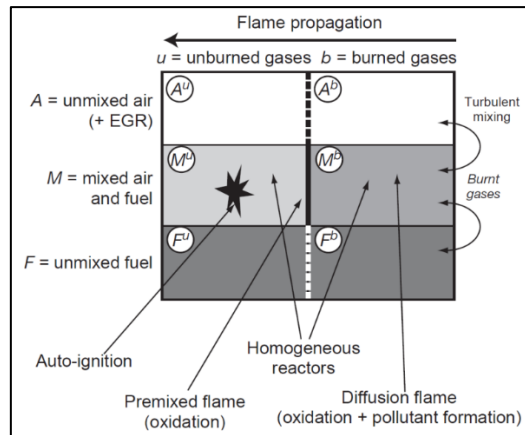


Figure 21- Computational cell of ECFM Combustion model [15]

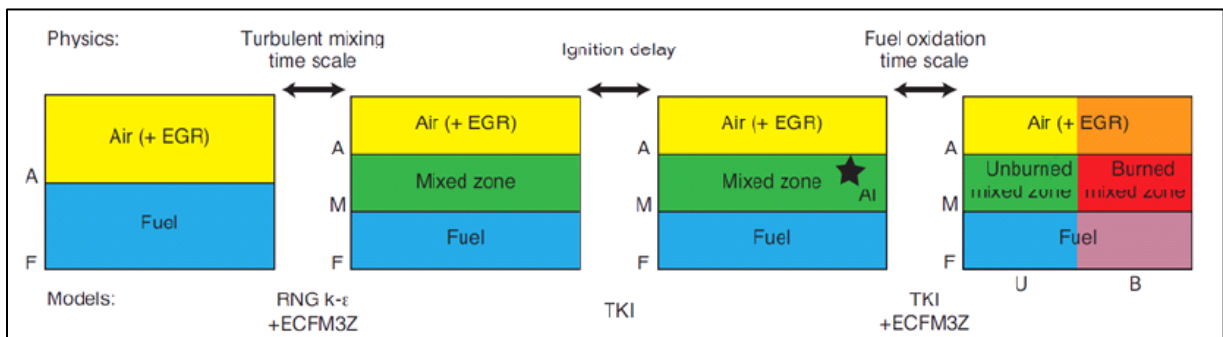


Figure 22- Computational cell of ECFM Combustion model [15]

As said before, the high levels of turbulence inside a combustion chamber cannot be ignored and thus, one must take them into account when treating with combustion models. A proper turbulent combustion description cannot be based on a simple mathematical expansion around mean values. Therefore, reaction rate closures are generally developed from physical analysis, comparing chemical and turbulent time scales.

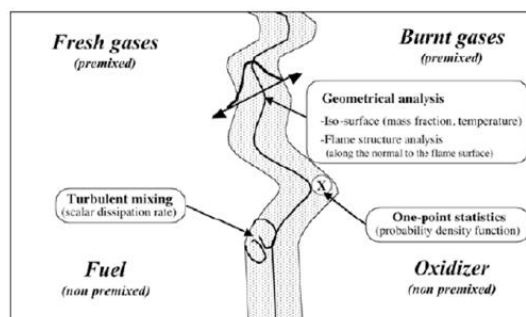


Figure 23- Modelling of turbulent combustion

Approaches for geometrical analysis, mixing description or pure statistical approach (probability density function formalism) [11]

5.4.3.1 Turbulent flamespeed calculations

During simulations, tracking the turbulent flame front requires that one knows the values of turbulent flamespeed S_T . In the RANS turbulent model, the turbulent velocity is calculated as follows:

$$S_T = S_L + u' \left\{ -\frac{a_4 b_3^2}{2b_1} Da + \left[\left(\frac{a_4 b_3^2}{2b_1} Da \right)^2 + a_4 b_3^2 Da \right]^{1/2} \right\}$$

Where u' is the rms of turbulent fluctuating velocity; S_L is the laminar flame speed; a_4 , b_1 , b_3 are model constants; Da is the Damkohler number that can be expressed as:

$$Da = \frac{S_L l_t}{u' l_F}$$

And l_F is the flame thickness expressed as:

$$l_F = \frac{(\lambda/c_p)_o}{(S_L \rho)_u}$$

And l_T is the turbulent length scale expressed as:

$$l_T = \frac{c_\mu^3 k^3 / 2}{4 \varepsilon}$$

And λ is the conductivity; the index o indicates a cell value and the index u indicates the unburnt region value.

5.4.3.2 Flame propagation tracking

Once the combustion has started and it is being modeled, the flame surface density has to be modeled and tracked:

$$\frac{\partial \Sigma}{\partial t} + \frac{\partial u_i \Sigma}{\partial x_i} = \frac{\partial}{\partial x_i} \left(\frac{\mu}{Sc} \frac{\partial (\Sigma / \bar{\rho})}{\partial x_i} \right) + (P_1 + P_2 + P_3) \Sigma - D + P_k$$

Where μ is the laminar viscosity, Sc is the Schmidt number, P_1 is the flame surface production by turbulent stretch, $P_2 = \frac{2}{3} \frac{\partial \tilde{u}_i}{\partial x_i}$ is a factor that models the effects of the thermal expansion and curvature;

$P_3 = \frac{2}{3} \bar{S}_L \frac{1-\tilde{c}}{\tilde{c}} \Sigma$ is the flame density production by mean flow dilation, $D = \beta \bar{S}_L \frac{\Sigma^2}{1-\tilde{c}}$ is a term that takes into account the destruction due to consumption, P_K is the source that initiated the flame (such as the spark plug), \tilde{c} is the mass progress variable.

5.4.3.3 Turbulent stretch model

In the end, there is another model, the ITNFS (Intermittent Turbulent Net Flame Stretch); it takes into account how the intermittent turbulence affects the distribution of stretch along the flame front.

This model is a library of the net flame stretch constructed which uses a curve fitting method to be able to implement the effects. The turbulent stretch K_t is given as:

$$\frac{K_t}{\varepsilon/k} = ITNFS_{factor} f\left(\frac{u'}{S_L}; \frac{L}{l_F}\right)$$

Where k is the turbulent kinetic energy and L is the integral length scale.

6 Mesh Generation in CONVERGE

In every CFD calculation a proper choice of the grid is crucial. This choice will affect both the accuracy and the reliability but also the duration needed to complete a simulation. The finer the grid, the more the accuracy and the resolution of the results will increase; the drawback of high accuracy is the high computational cost so the time (strictly linked to the cost) of a simulation. Usually the best solution is a trade-off between the two issues.

Because of these issues, a good understanding of the system under observation is needed; this allows for a proper system optimization.

The critical point of the geometry in terms of requirements must be found in order to set a refinement of the mesh only in that particular region. These points could be regions where bottle-necks are present, for example deviation of the flow, or where some particular phenomena of the system happen, such as injection or ignition in an internal combustion engine.

In these particular cases, a finer grid could be applied in order to get accurate results, while for computational time saving a coarse grid could be applied in the rest of the geometry during events that don't require particular attention. The grid could also be adjusted with a finer or a coarser one according to the evolution in time of the simulation. If the simulation is not steady state a finer mesh may be used when the rate of variation of thermo-physical quantity is higher while a coarser one is to be preferred during non-critical simulation times. Proper algorithms are implemented in the CONVERGE software to take in account this problem.

There are some algorithms that can be applied in some cases, during particularly sensitive events of the simulation.

6.1 Fixed Embedding

This algorithm is used to refine the grid only in specific locations (but for different periods of time imposed by the user) in the domain where a finer resolution is critical to the accuracy and precision of the solution during specific periods of time which are known even before the simulation has started. For example, when simulating sprays, you can add an area of fixed embedding by the nozzle to resolve the complex flow behaviour. Fixed embedding allows the rest of the grid to remain coarse to minimize simulation time [15].

The fixed embedding as well as other algorithms for mesh refining are based on the following formula:

$$dx = \frac{dx_{base}}{2^{es}}$$

Where dx will be the final value of the cell size, dx_{base} is the base dimension given during the case setup, $es=embedding\ scale$ is the scale to be applied to the base dimension.

CONVERGE software works with the so called two-to-one connectivity between cells, this means that every side of a cell can confine with, at maximum, two sides per each dimension, so a face of a structured cell can touch at maximum four faces of other four cells. This is done for improving the discretization of the physical model. This limitation translates in the fact that each cell,

characterized by a certain value of the grid scaling parameter, can be adjacent only to cells with grid scaling equal or modified by one unity.

For the fixed embedding different approaches can be taken:

- Boundary embedding
- Sphere embedding
- Cylinder embedding
- Injector/nozzle embedding
- Box embedding
- Region embedding

6.2 Adaptive Mesh Refinement (AMR)

Adaptive Mesh Refinement (AMR) is a tool that is supposed to be used to automatically refine the grid based on fluctuating and moving conditions such as temperature, velocity, species concentration etc. This option is useful for using a highly refined grid to accurately simulate complex phenomena such as flame propagation or high velocity flow without unnecessarily slowing the simulation with a globally refined grid.

Ideally, a good AMR algorithm will add higher grid resolution (embedding) where the flow field is most under-resolved or where the sub-grid field is the largest (i.e., where the curvature [gradient] of a specified field variable is the highest or anyway where it exceeds a value imposed by the user) [15].

For a scalar, the sub-grid field is defined as:

$$\phi' = \phi - \bar{\phi}$$

Where ϕ is the actual field, $\bar{\phi}$ is the resolved field and finally ϕ' is the sub-grid field. The latter can be expressed as an infinite series and it is given by:

$$\phi' = -\alpha_{[k]} \frac{\partial^2 \bar{\phi}}{\partial^2 x_k} + \frac{1}{2!} \alpha_{[k]} \alpha_{[l]} \frac{\partial^4 \bar{\phi}}{\partial^2 x_k \partial^2 x_l} - \alpha_{[k]} \alpha_{[l]} \alpha_{[m]} \frac{\partial^6 \bar{\phi}}{3! \partial^2 x_k \partial^2 x_l \partial^2 x_m} + \dots$$

But since the entire summation is not possible, only the first term is taken into consideration. CONVERGE gives an example of how the AMR works for an injection case:

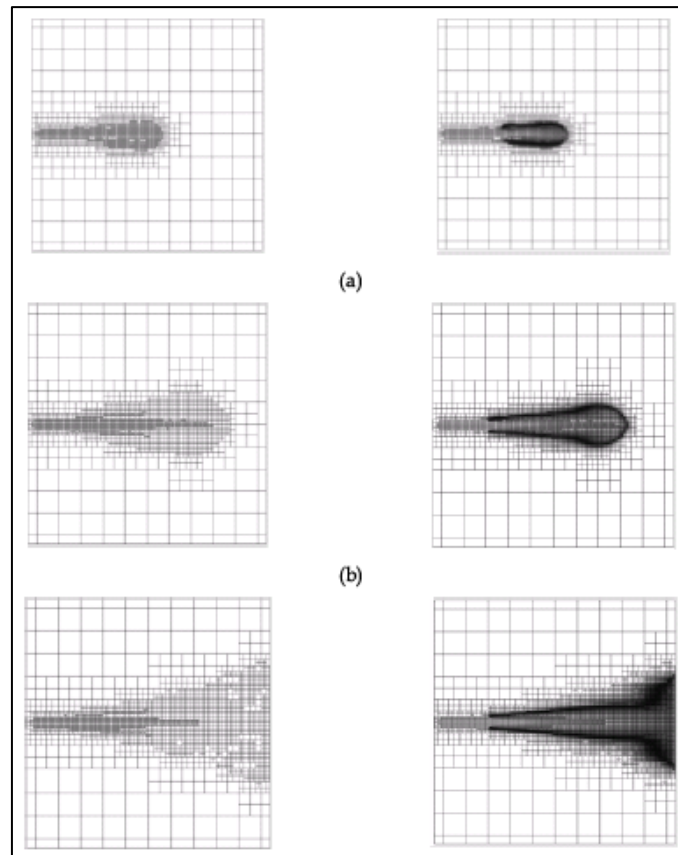


Figure 24-AMR application in CONVERGE

Evolution of a combustor spray bomb. The grid was generated by AMR in a sequence of time steps after the start of the simulation. Right column- Grid only. Left column Grid and temperature values (Black means $T=2800\text{ K cca}$) [15]

7 RANS Simulations setup, procedure and results

In order to be able to use a 3D CFD simulation, the simulation model has to be first calibrated with respect to the experimental results available on the research engine that will also be used for the simulations.

7.1 Validation of the models

Both Polito (Engine 1) and GasOn (Engine 2) models were validated in the DENERG labs before the work of this thesis [32]. The methodology is next shown:

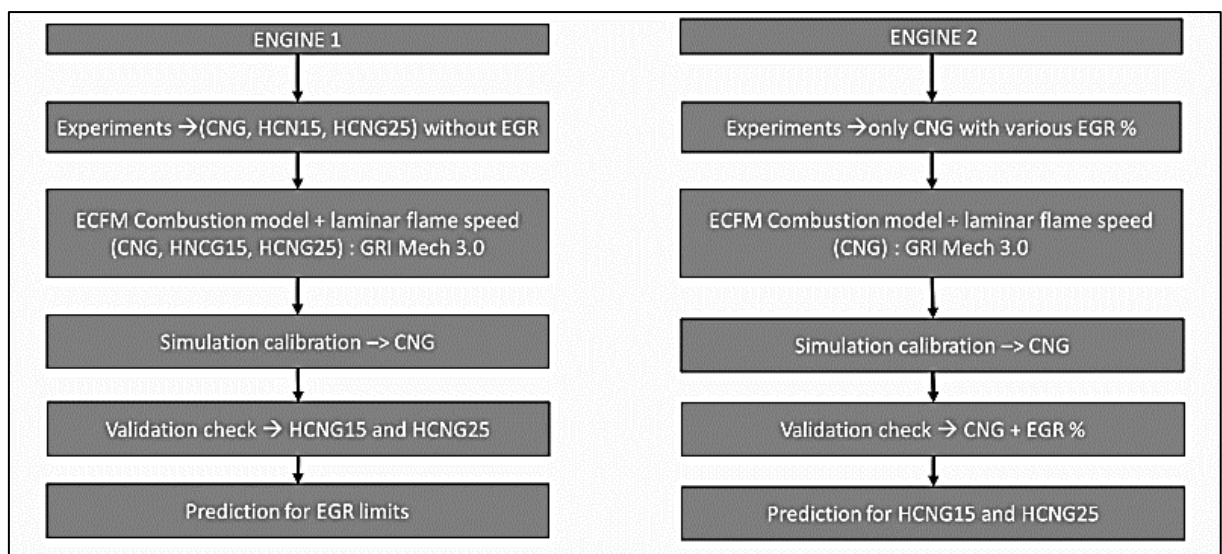


Figure 25- Calibration methodologies for both Polito (Engine 1) and GasOn (engine 2)

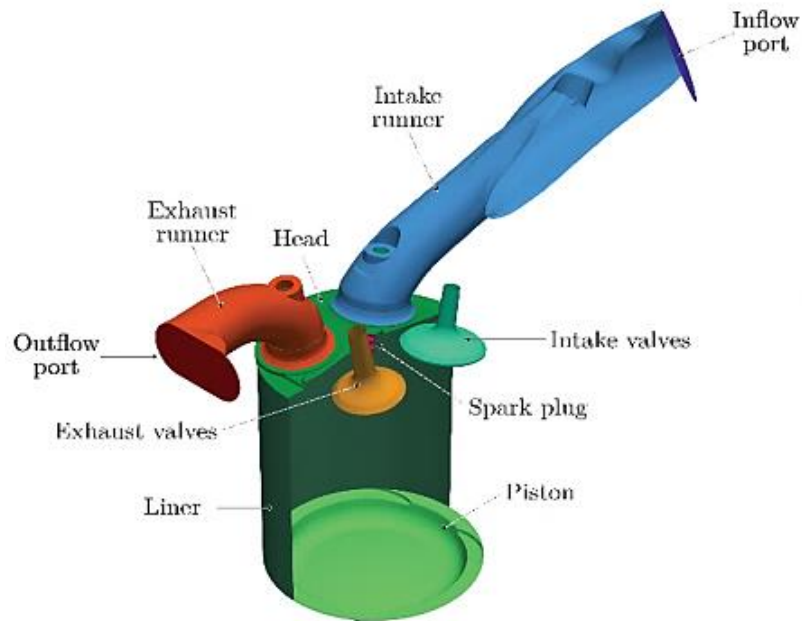


Figure 26- Polito Engine

<u>Mesh Characteristics</u>	
Base Grid [mm]	4*4*4
Fixed Embedding (cylinder)	scale=1
Fixed Embedding (Spark Plug)	scale=5
AMR- Velocity	sub-grid criterion= 1m/s scale=3
AMR- Temperature	sub-grid criterion= 5 K Scale=5
<u>Numerical setup</u>	
Flow	Compressible
Gas Simulation	Redlich Kwong model
Numerical Method	Implicit Method
Turbulence model	RNG k- ϵ
Combustion Model	ECFM
Heat transfer Model	Angelberger
<u>Engine Characteristics</u>	
Cylinder displacement	342 cm ³
Bore / Stroke	72 mm / 84 mm
Compression Ratio	9.8:1

Valves per cylinder	4
Combustion chamber	Pent-roof
Intake valve	Opening duration = 250CAD / maximum lift = 7.5mm
Exhaust valve	Opening duration = 244 CAD / maximum lift = 7 mm
Injection system	Port Fuel injection
Turbocharger	Wastegate-controlled, fixed geometry turbine

Table 3- Polito Engine characteristics

Meshing parameters, Geometric characteristics, Engine characteristics, Modelling parameters

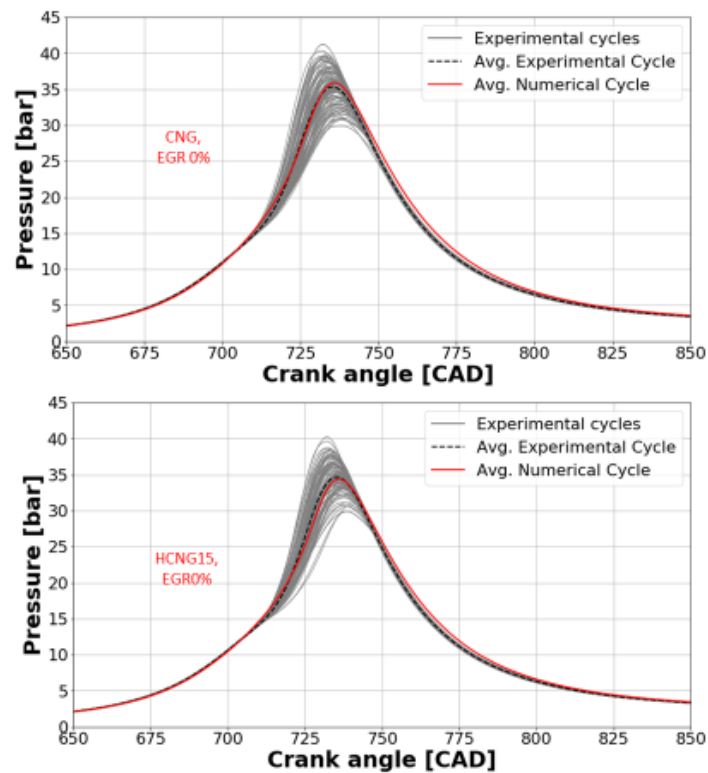


Figure 27- Polito Engine Calibration

Results with respect to experimental data

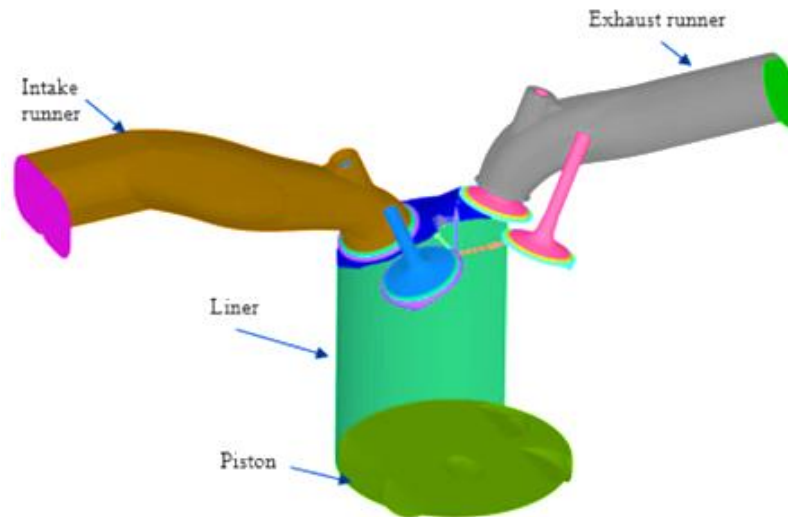


Figure 28- GasOn engine

<u>Mesh Characteristics</u>	
Base Grid [mm]	4*4*4
Fixed Embedding (cylinder)	scale=2
Fixed Embedding (Spark Plug)	scale=5
AMR- Velocity	sub-grid criterion= 1m/s scale=3
AMR- Temperature	sub-grid criterion= 2.5 K Scale=3
<u>Numerical setup</u>	
Flow	Compressible
Gas Simulation	Redlich Kwong model
Numerical Method	Implicit Method
Turbulence model	RNG k-ε
Combustion Model	ECFM
Heat transfer Model	Angelberger
<u>Engine Characteristics</u>	
Cylinder displacement	405 cm ³
Bore / Stroke	80 mm / 80.5 mm
Compression Ratio	13.4:1

Valves per cylinder	4
Combustion chamber	Pent-roof
Intake valve	Opening duration = 169CAD / maximum lift = 8.5mm
Exhaust valve	Opening duration = 200 CAD / maximum lift = 8.5 mm
Injection system	Direct injection/ Port-Fuel
Piston	Central shallow bowl

Table 4- GasOn Engine Characteristics

Meshing parameters, Geometric characteristics, Engine characteristics, Modelling parameters

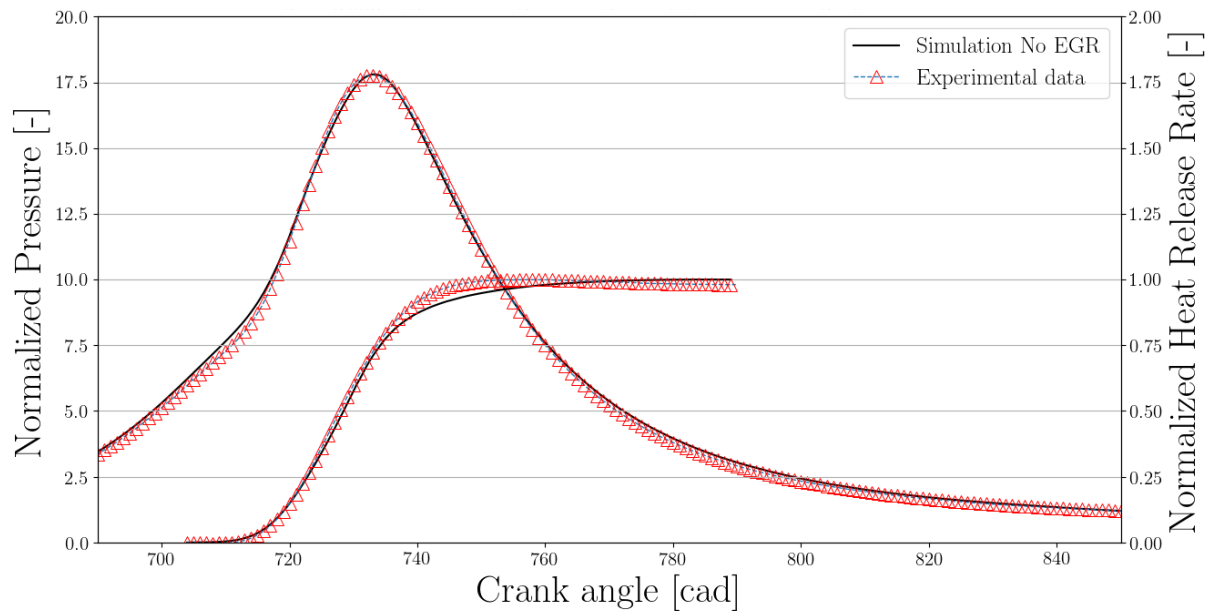


Figure 29- GasOn Engine Calibration Results

Having calibrated the models, they give the possibility to predict and simulate conditions that are not have been performed during the experiments; for example, it is possible to predict and analyse effects of EGR, effect of change in fuel composition, effect of slight change in the engine geometry, or effects of all of these parameters combined.

Polito engine was a project developed in DENERG at Politecnico di Torino a few years ago. Its objective was to investigate combustion behaviour of methane plus the addition of hydrogen. Afterwards, EGR dilution was added in order to try and reach the EGR limit while still having a stable combustion.

Instead, the GasOn engine is part of an EU founded project in which a DI, SI methane engine is studied. For this thesis, a deviation of this engine has been used, meaning that the injector was not used, and the DI engine has been transformed into a homogeneous charge engine.

Simulations had to be performed on the so-called GasOn engine in a previously established operating point: 2000x6 bar. The reason why this operating point has been chosen is because a comparison between GasOn and Polito engine is wanted.

For a simulation to be considered valid two key goals were set: IMEP of each cycle had to reach cca 6 bar and MFB50 of fuel had to be in a range of $+2^\circ$ or -2° around 728° of the crank angle.

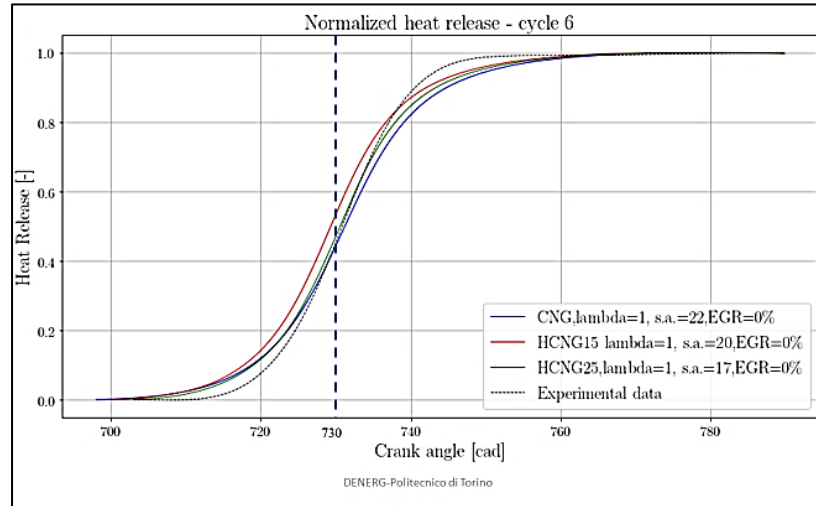


Figure 30- Normalized heat release rate for Polito engine: Validation of MFB50 with respect to experimental data

If these conditions were to be met, the simulation was considered valid. Moreover, for each simulation the first complete cycle was not considered; the objective of eliminating the first cycle is to eliminate the influence of the initial conditions imposed at the beginning of every simulations. These initial conditions were based on the experimental data available for each engine, but they introduce errors, mainly in the first cycle.

On the GasOn engine the following simulations were performed:

Fuel	CH ₄	CH ₄ EGR10%	CH ₄ EGR20%	HCNG15	HCNG15 EGR10%	HCNG25 EGR0%	HCNG25 EGR25%
Spark advance	17°	20°	27°	15°	17°	14°	29°

Table 5- Details on GasOn simulations

The purpose of such simulations is to demonstrate that an engine with higher turbulence and compression ratio (GasOn), in the same operating conditions as a low turbulence and lower compression ratio engine (Polito), has a faster combustion, leading to a higher limit of EGR dilution while maintaining a stable combustion.

8 Results

8.1 2000x6 bar CNG EGR0%- Turbulence Effect

In the first comparison between the two engines, combustion of pure methane is analyzed. The differences between the combustion in the two engines is then due only to the difference of tumble (turbulence) inside the cylinder.

A greater tumble motion for GasOn engine results in a faster combustion, as combustion is directly proportional to the turbulence inside the cylinder for a Spark Ignition engine.

In the next figures, comparisons between turbulence related characteristics will be shown, in order to understand the differences between GasOn and Polito engines.

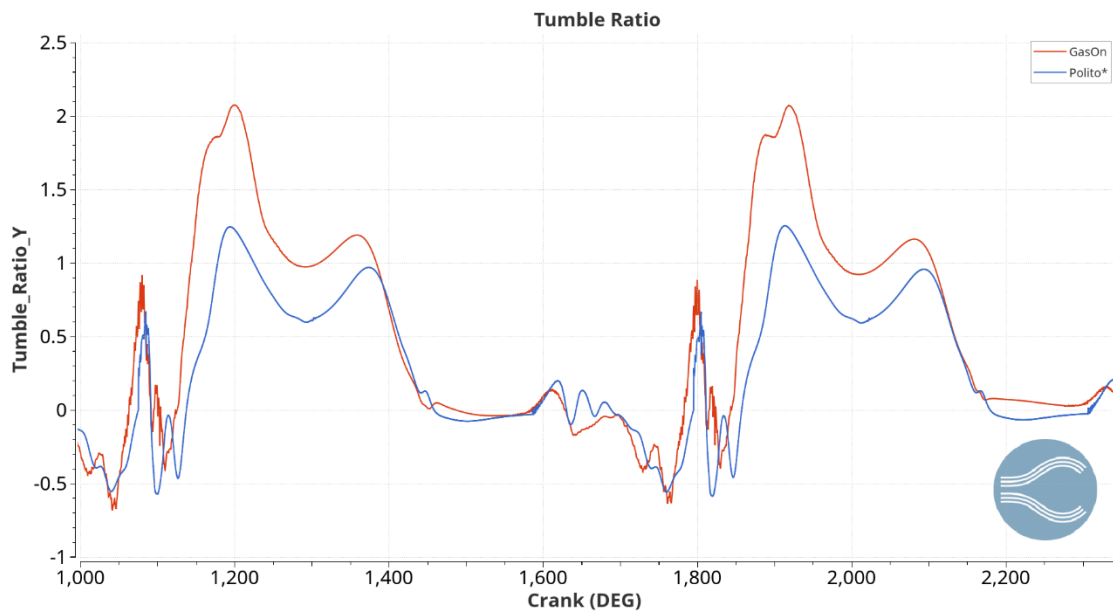


Figure 31- Tumble Ratio comparison- GasOn vs Polito

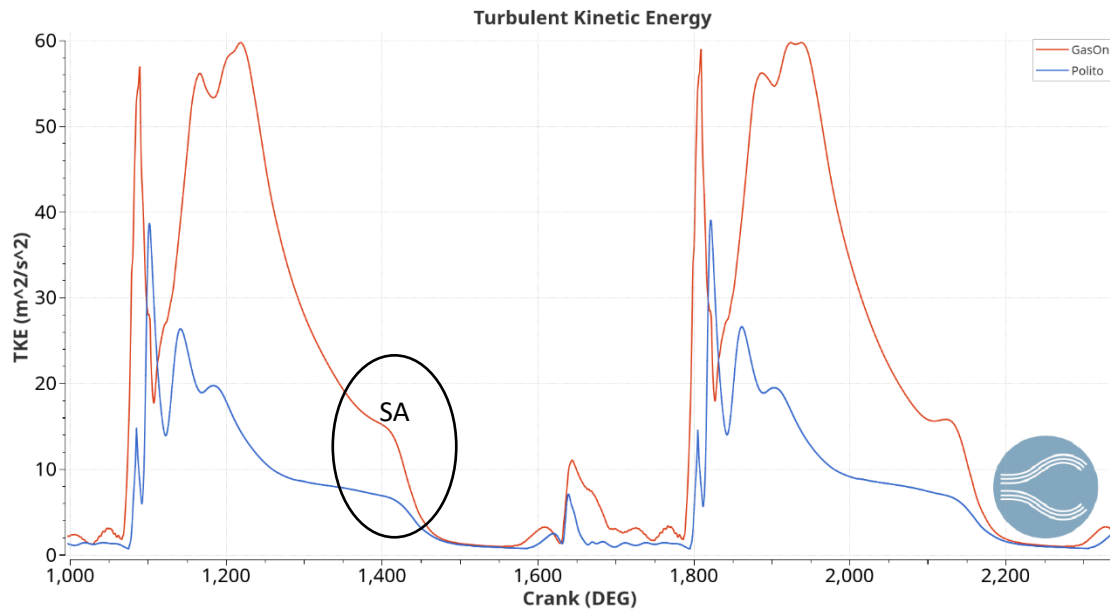


Figure 32- Turbulent Kinetic Energy

Indication of the difference in turbulence between the two engines. As ignition starts, a great difference in TKE is visible

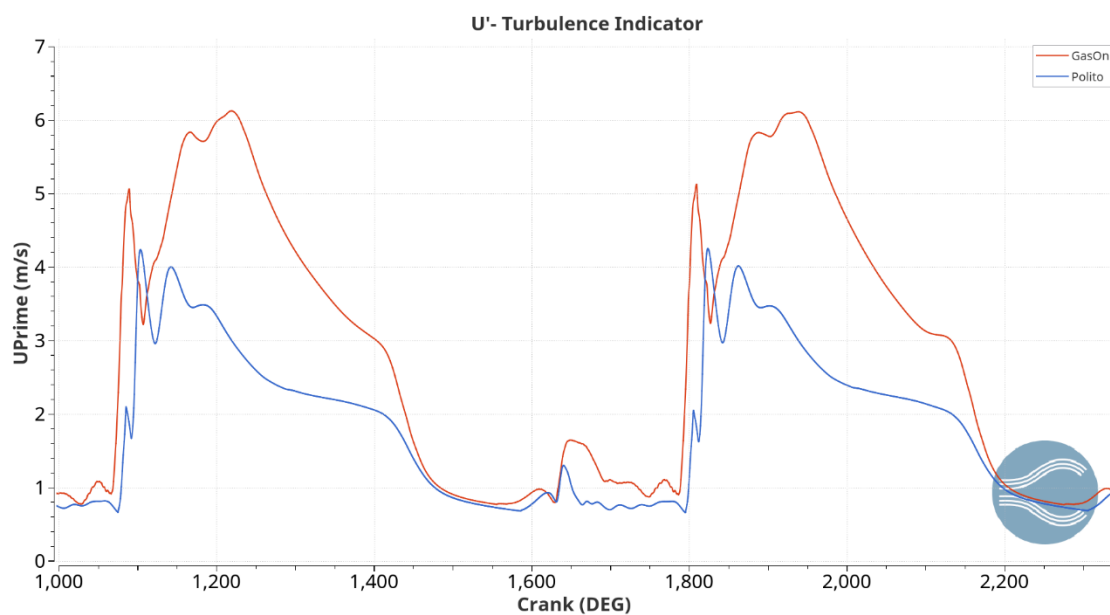


Figure 33. Uprime

U' has the same shape of TKE. It is the fluctuation around the velocity and it is derived from TKE.

Besides the differences between the two engine turbulence intensities, which is in absolute value, they also have different types of flow motion inside the chamber.

This is due to the fact that they were originally developed for different purposes:

- GasOn engine was purposely designed to work as a Direct Injection engine, so it is preferred to have a high tumble motion.
- Polito engine was designed to work with a homogeneous charge. For this purpose, a high swirl movement was chosen.

In the Figure 34 it can be seen that both swirl ratio and angular momentum around the Z axis are higher for Polito engine.

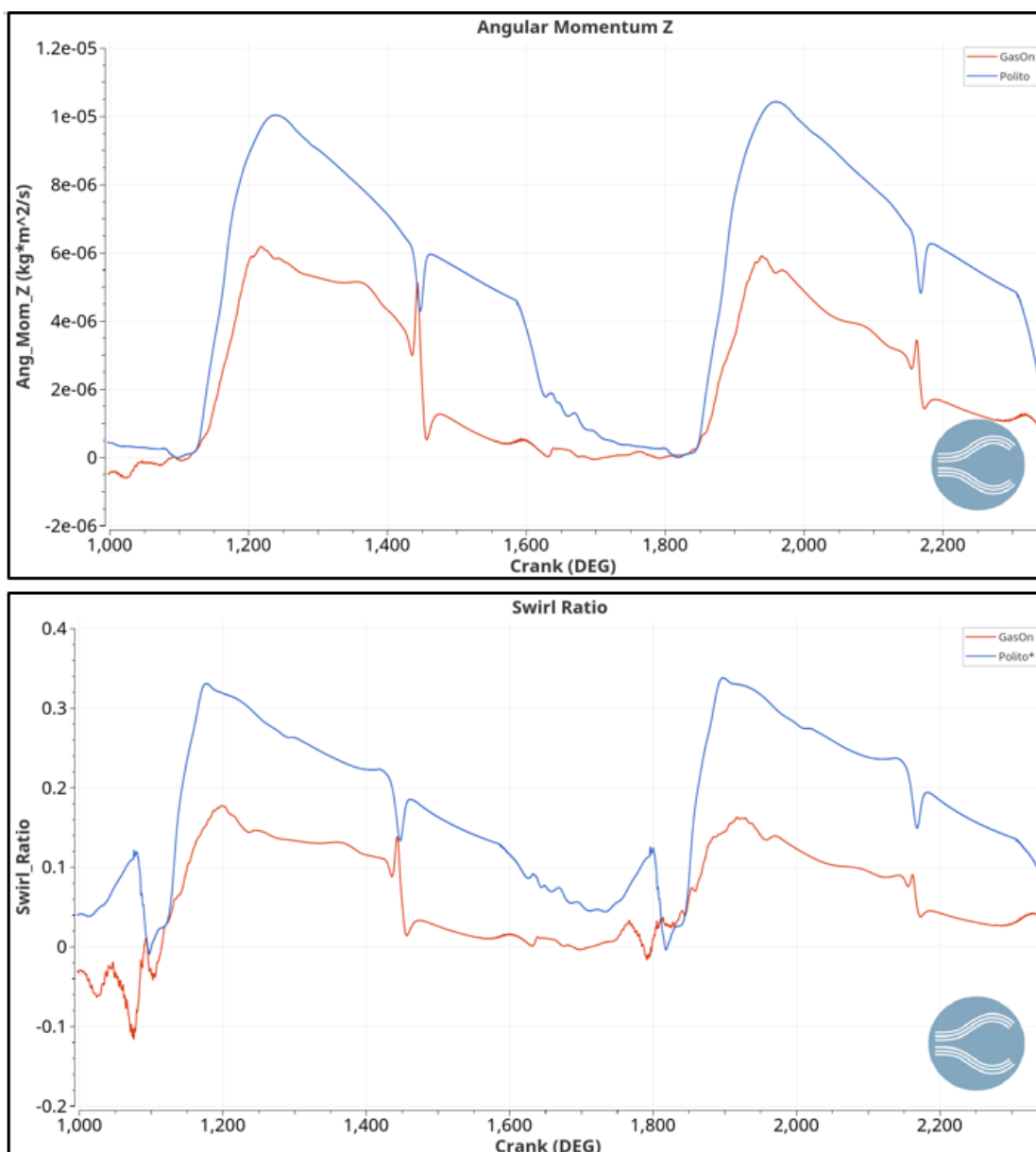


Figure 34- Swirl ratio and Angular Momentum around Z-axis

Main difference in flow motion between the two engines is pointed out

The differences in the turbulence between the two engines result in a difference in combustion. In the next figures, results from the combustion are shown:

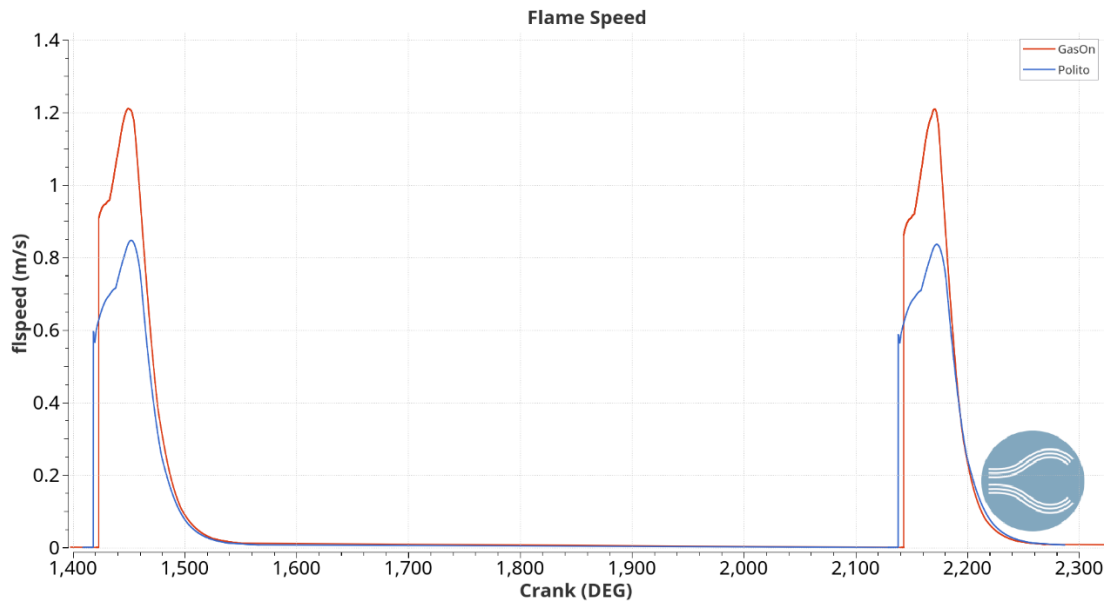


Figure 35- Flame speed

Differences during the combustion periods for both engines

It is clear how flame speed is higher in the case of GasOn engine. It can be directly related to a higher value of Turbulent Kinetic Energy (TKE). In the Figure 32 of TKE, in the area of peak values for flame speed, TKE is bigger in the case of GasOn engine.

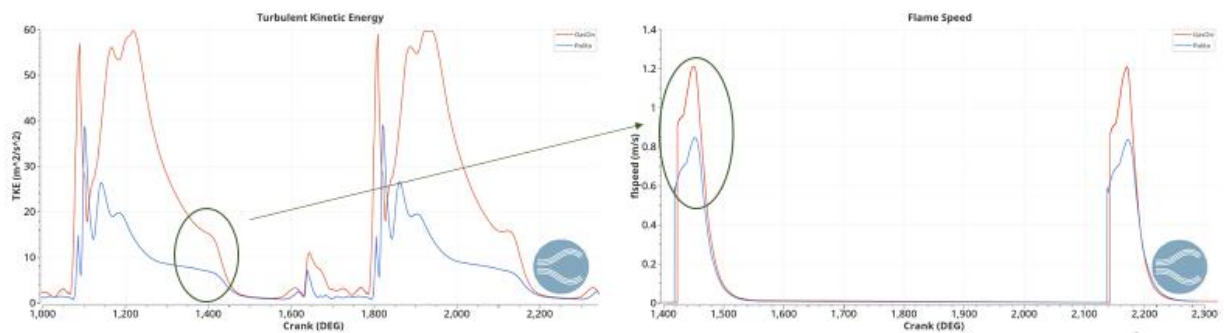


Figure 36- Effect of higher turbulence on flame speed

As burning happens at a faster rate, energy is released from the engine faster, thus resulting in a faster pressure increment and eventually in higher pressures and also temperatures inside the cylinder (Figure 37 and Figure 38).

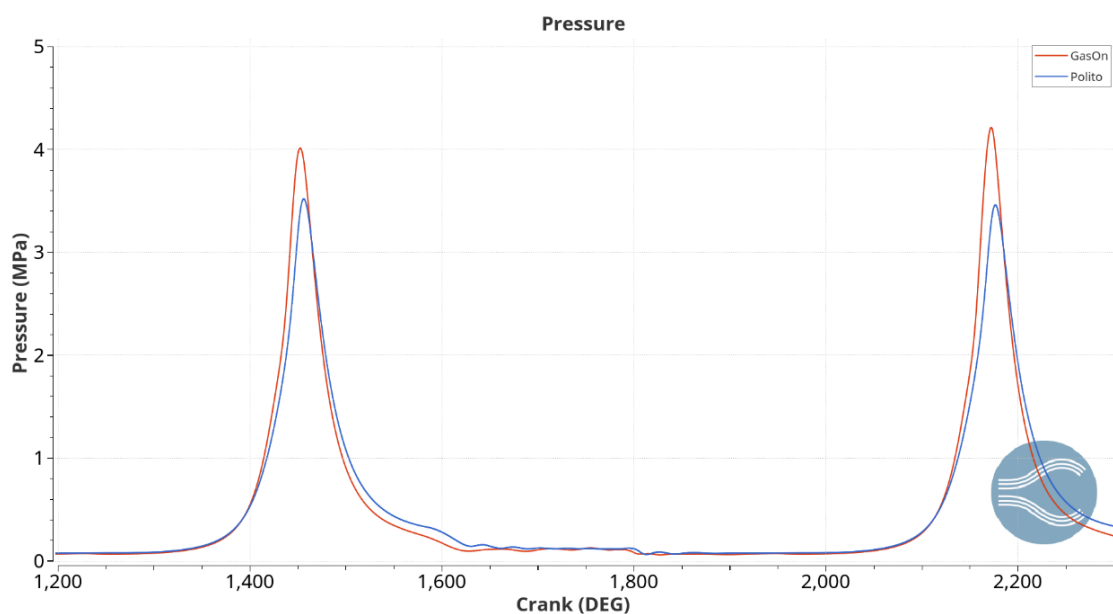


Figure 37- Pressure Comparison

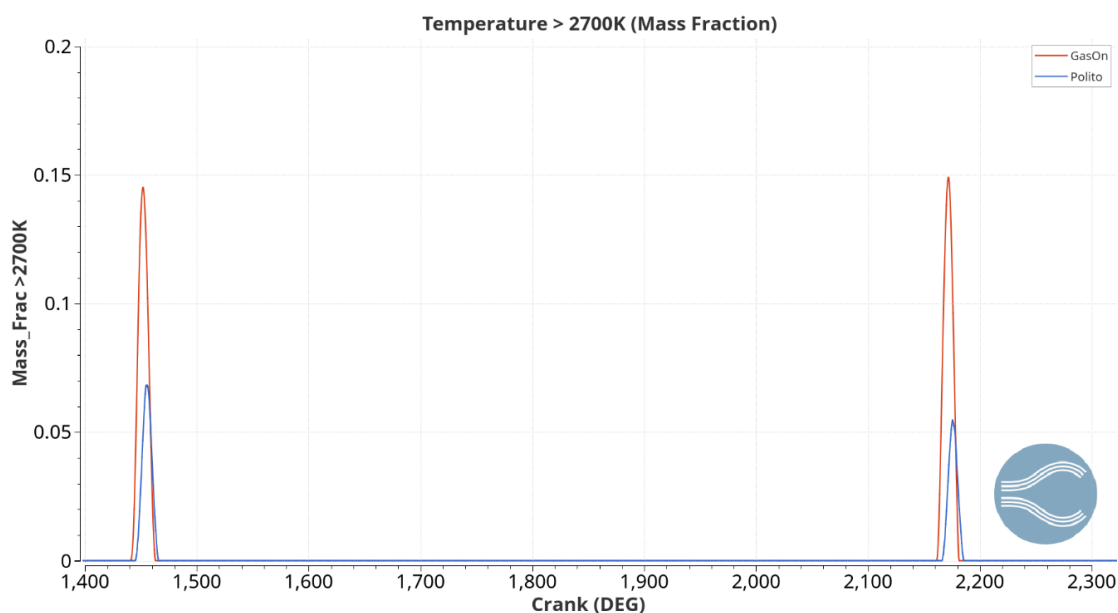


Figure 38- Mass fractions temperature

Fraction of mixture that has a temperature higher than 2700 K due to faster combustion and higher pressures

An even better understanding of the flame advance characteristics can be seen in 3D post processing of the two engines.

8.1.1 Tumble Analysis

3D post processing was used in order to see how the tumble changes between the two engines and how it changes during the strokes of the engines.

Only the intake and compression strokes are analyzed, as they are the main phases that have a great influence on the flow until before the ignition. For these phases, TKE was analyzed.

In fluid dynamics, TKE can be defined as the mean kinetic energy per mass unit. It is associated with the eddies present in every turbulent flow. A way to characterize the TKE is to physically measure the root-mean-square velocity fluctuations.

In the case of RANS equations, the TKE can be calculated from the turbulence method which is applied.

Generally, turbulent kinetic energy is produced by:

- Fluid shear
- External forcing at low-frequency eddy scales (integral scales)
- Friction
- Buoyancy

Once it is formed, TKE can be then transferred down the turbulence energy cascade and then further down until it is dissipated by the viscous forces at the smallest scales (Kolmogorov scales).

How the TKE is resolved in RANS simulations depends on the turbulence (closure) method used. For the simulations in this thesis, K-epsilon model was used. This method assumes an isotropy of turbulence where stresses in all the three directions are equal.

This assumption makes modelling of turbulence quantities (k and ϵ) simpler, but will not be accurate in scenarios where anisotropic behaviour of turbulence stresses dominates, and the implications of this in the production of turbulence also leads to over-prediction.

In the next figures (Figure 39 –Figure 42) the Turbulent Kinetic Energy is analyzed.

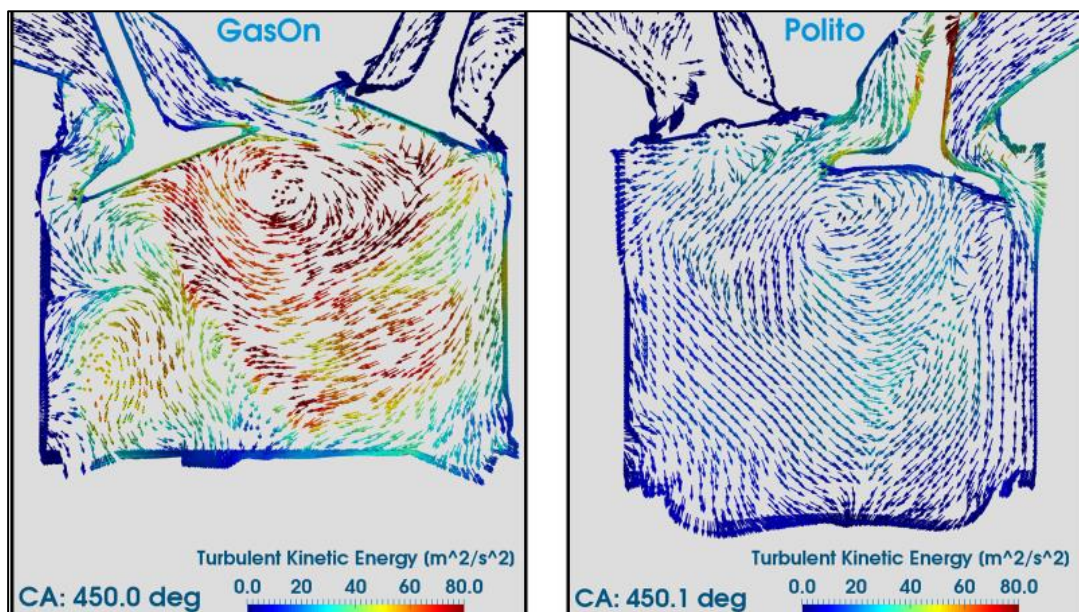


Figure 39- Comparison of TKE

Intake valve fully opened. The difference in TKE intensity is very clear

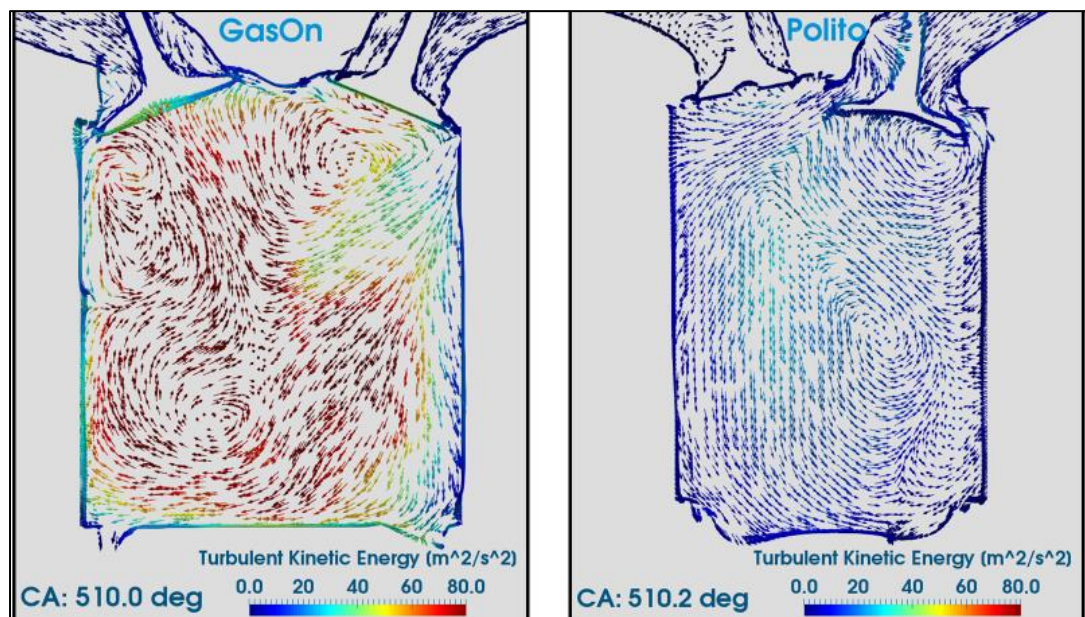


Figure 40- The piston is in the proximity of BDC
30° before the start of compression

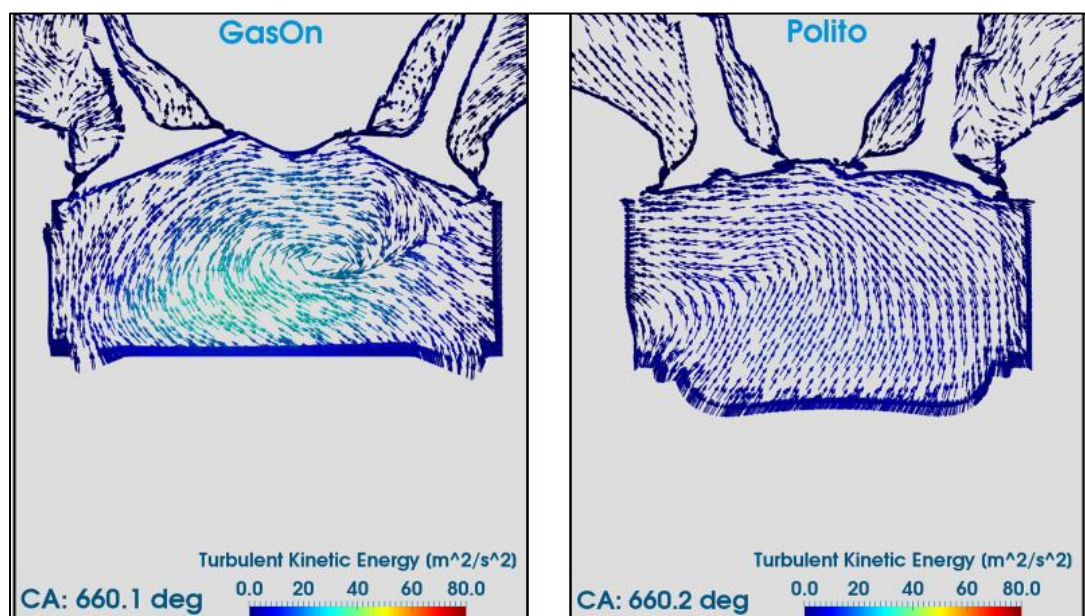


Figure 41- TKE intensity during compression phase

Decrease of TKE intensity; however, in the GasOn engine the tumble motion is still well visible

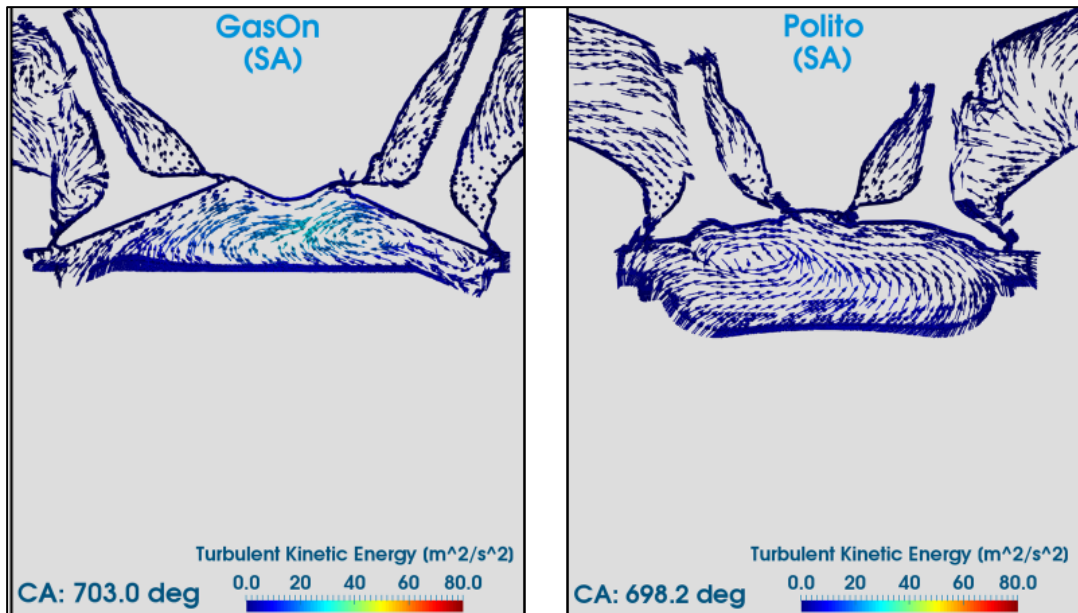


Figure 42- Turbulence at Spark Advance

TKE has decreased with GasOn which still has visible higher intensity

The figures show the simple case of pure methane without the EGR dilution.

The effect of TKE, U' and Tumble Ratio, thus the effect of combined turbulence can be seen in the next figures, where temperature and γCH_4 were analyzed.

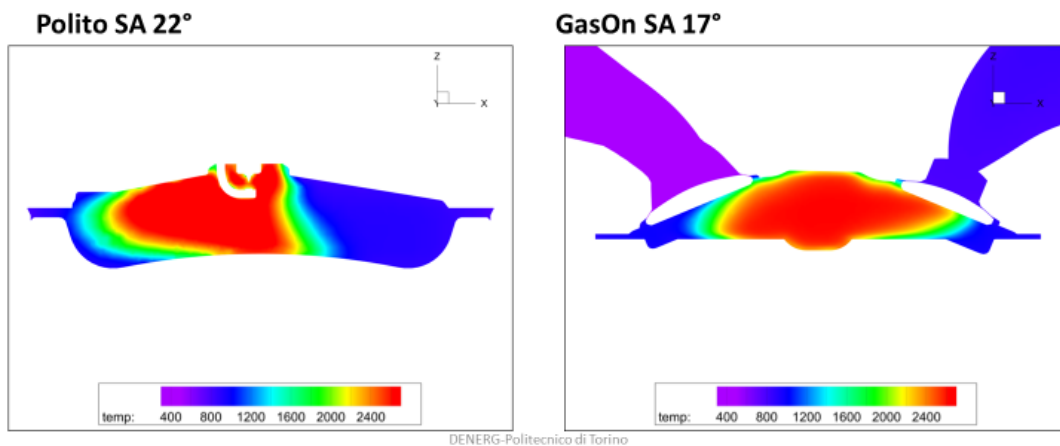


Figure 43- Temperature Distribution at TDC

CNG EGR0%

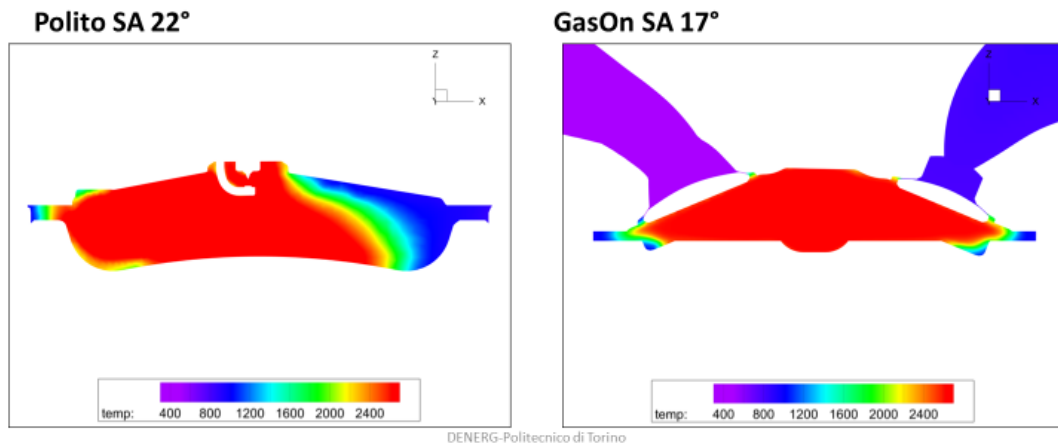


Figure 44- Temperature Distribution at TDC+10°

Theoretically it is around the point of MFB50

In the previous figure it is important to note how the flame front differs in the two cases. Maximum temperatures at the center of the cylinder have similar values, around 2400 K. However, the flamefront, which is the yellow region has different values for the two cases. In the GasOn engine it is around 2200 K while for the Polito engine it is around 2000 K.

Also, flamefront plus reaction zone have different sizes. For Polito engine, this zone is thicker, thus, at a lower temperature. This is visible in the Figure 44 at TDC.

For a better understanding of the burning advance, the next figures will be of help.

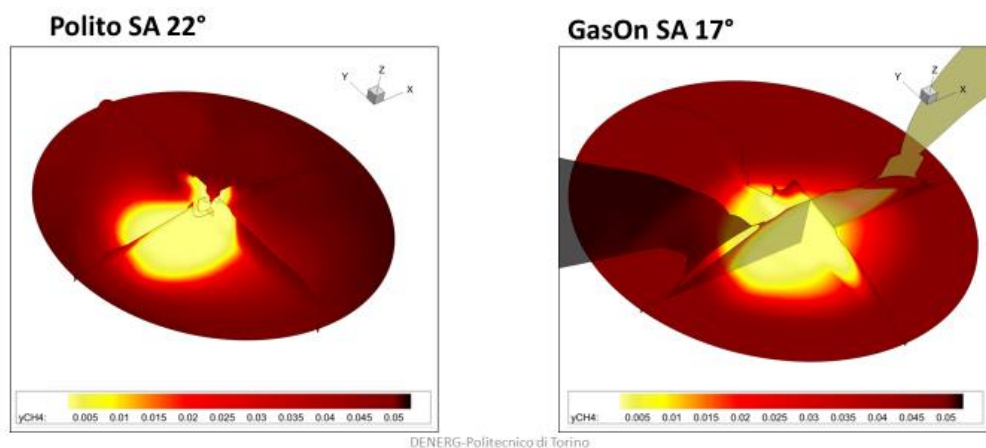


Figure 45-Consumed methane at TDC

Indication of the flame advance

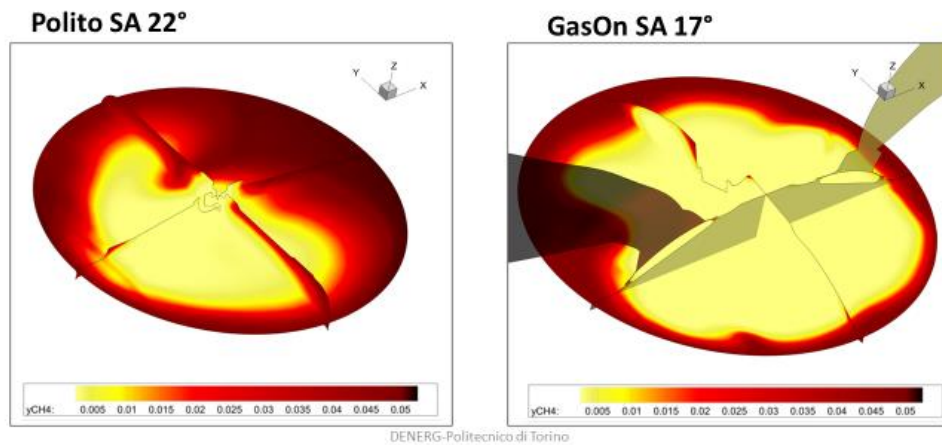


Figure 46-Consumed methane at TDC+10°

Indication of the flame advance ~MFB50

The two previous figures show the fraction of methane that has been consumed in the cylinder. The expansion of the yellow area indicates how better the combustion is happening in the GasOn engine. Particularly, as a period of 10° is shown for both engines, and even if at TDC the yellow area was quite similar, after just 10°, in the GasOn engine, flame has expanded much faster. This is an even clearer proof that, for the same case, same fuel, same operating point, slightly different spark advance and slightly different mass of methane, the engine with higher Compression Ratio and higher turbulence is able to develop and maintain a faster combustion.

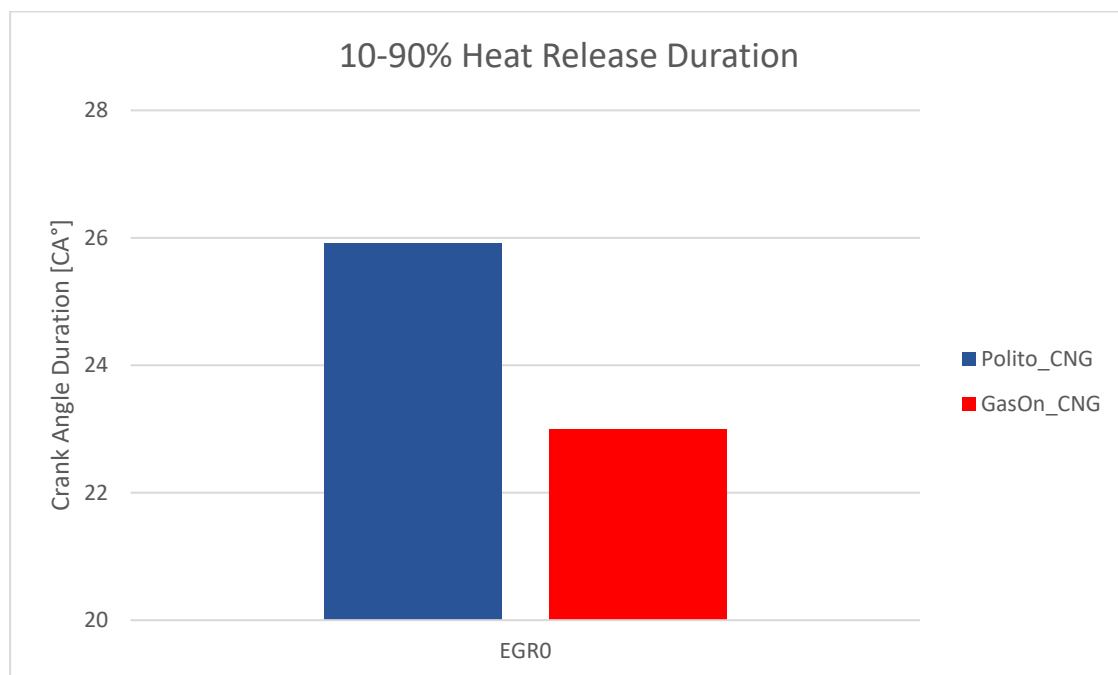


Figure 47- Main Heat Release duration

Another useful tool that can help with the understanding of premixed combustion is the Borghi plot.

This diagram is of great help when combustion regimes are discussed for a turbulent premixed combustion. The comparison between the two cases is plotted on this graph, and interesting remarks can be extracted.

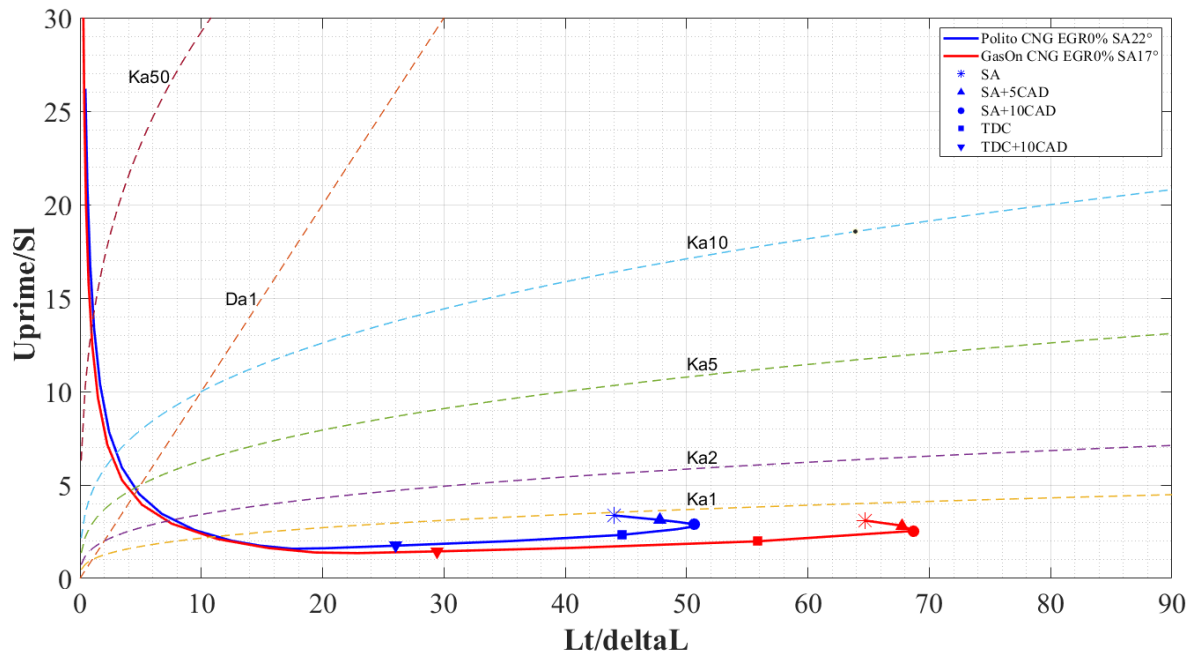


Figure 48- Borghi plot- Combustion curves CNG EGR 0%

Polito vs GasOn

In red, there is the GasOn combustion curve, starting from its spark advance; in blue it's the Polito combustion curve. The key remarks to be extracted from this curve can be:

- Due to higher turbulence in GasOn engine, the value on x-axis for this engine increases. L_t , which is the turbulent length scale is higher. Also, due to a higher compression ratio, higher temperatures are developed at the end of compression resulting in an overall higher temperature of the mixture. This, along with other causes, result in a thinner flame front, which is the value of δ_f ; it means that the ratio between these two has a higher value for GasOn engine, thus moving the curve to the right on the x-axis.
- On the y-axis, there is the ratio between U_{prime} (turbulent velocity) and SI (laminar flame speed). This ratio depends on two factors:
 1. U_{prime} , which depends on the engine characteristics
 2. SI , which depends on the fuel, turbulence, temperature, fuel composition and other factors.

On the graph, it can be seen that similar point of the two engines (SA, TDC, SA+5 etc.) are nearly at the same values on the y-axis. The reason for this could be the fact that the effect of the increase in turbulence in the GasOn engine and the increase in SI are such that their ratio is close to Polito's. This theory still has to be confirmed; to do so, simulations from other engines are needed.

- Another important fact is that both curves, at least until after they reach MFB50 (TDC+10), are found underneath the Karlovitz=1 curve. If $Ka < 1$ then the flame thickness is smaller than the Kolmogorov scale, thus the flame burning velocity is not affected by the turbulence field; It means a stable combustion.

8.2 2000x6 bar CNG EGR20%- EGR Effect

This simulation was made with the attempt to prove that for the same operating point, the engine with higher turbulence was able to complete the combustion and reach the targets of MFB50 and IMEP.

The low turbulence engine, Polito, in its simulation, was not able to have a complete combustion, thus, did not reach the required conditions of IMEP and MFB50.

On the contrary, for the GasOn engine, combustion was complete, targets were reached, thanks mainly to the higher turbulence and higher compression ratio, both of which positively influence the combustion.

<u>CNG EGR20%</u>	<u>GasOn</u>	<u>Polito</u>
SA [cad]	27°	40°
IMEP [bar]	5.7	4.1
MFB50 [cad]	728.6	738.6
10% Heat Release [cad]	716.1	717.7
90% Heat Release [cad]	745.6	762.5

Table 6- Combustion Parameters CNG EGR20 %

Again, it would be of help to have a confirmation of this phenomena on the Borghi plot.

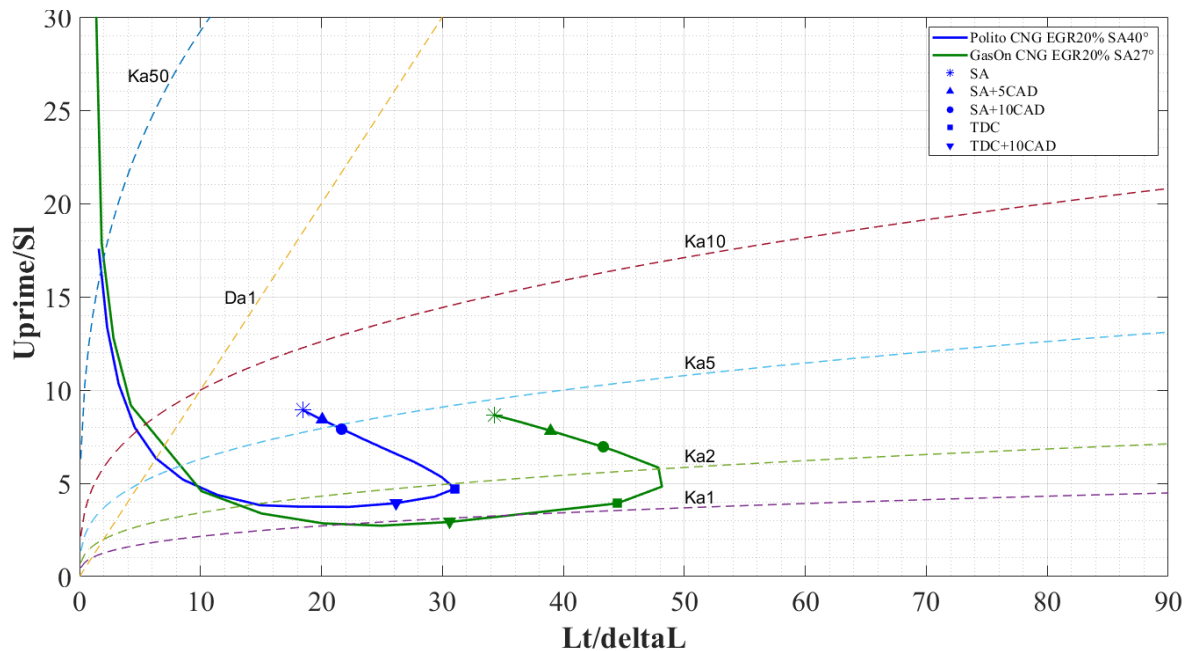


Figure 49- Borghi plot- Combustion curves CNG EGR 20%

Polito vs GasOn

The green curve refers to the GasOn engine. Even if the combustion starts in an unstable regime, above Ka2, as the combustions advances, it reaches Ka1 in a critical moment, such as TDC. It is

important that Ka_1 is reached around TDC because is a critical point during the combustion. In fact, most part of the reactions happen in this region and, being in a stable region assures a good combustion.

Also, in the point of TDC+10°, which is roughly the crank angle of MFB50, the reactions are happening in the area of $Ka < 1$. This is proof that, even if a considerable amount of EGR is present (20%), reactions manage to take place in an acceptable manner.

Completely different is the case of Polito engine. For its combustion curve in the Borghi plot, even if it starts approximately at the same height as the GasOn curve, it does not manage to go further down, thus remaining in the unstable combustion area of $Ka > 1$. TDC and TDC+10° points both are in the thin reaction zone, where it is not possible to have a complete combustion.

The next figure takes into consideration and compares, for both engines, the cases with or without EGR, and also the COV of IMEP. It has been chosen, as a limit between stable and unstable combustion, a COV of 3%.

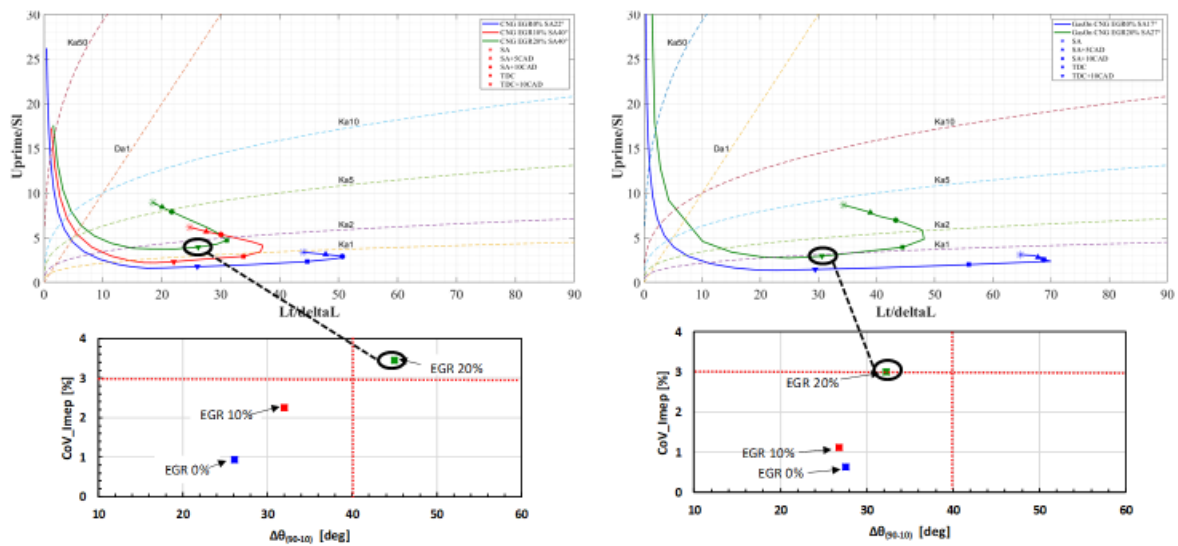


Figure 50- Effect of EGR on Borghi plots and on COV

An even clearer result can be seen from the 3D data in the next figures:

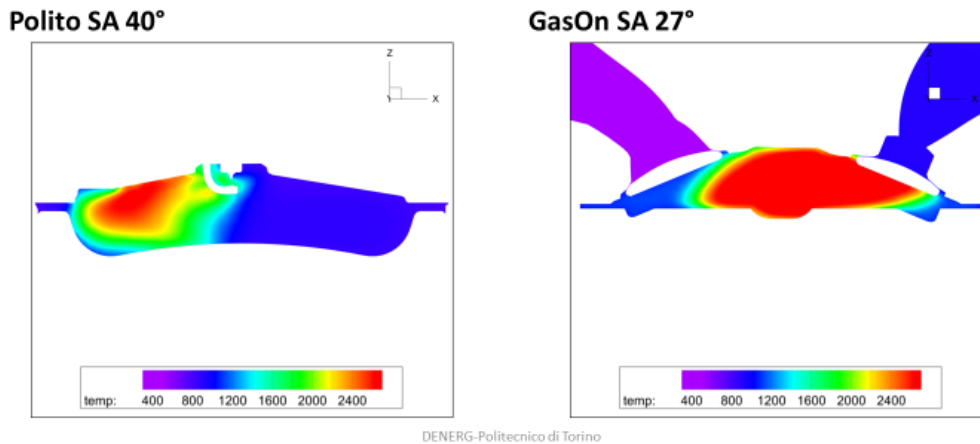


Figure 51- Temperature distribution at TDC

CNG EGR 20% Polito vs GasOn: the difference in flame distribution and thickness is accentuated at TDC

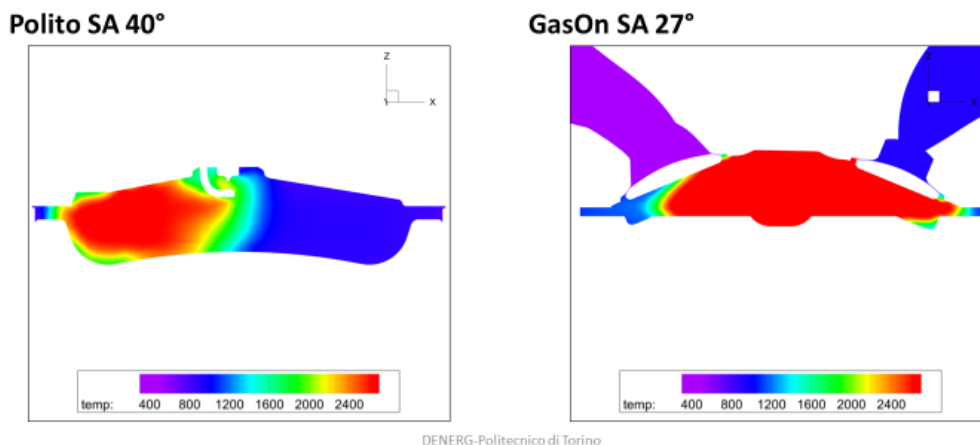


Figure 52- Temperature distribution at TDC + 10°

For CNG EGR20% at ~MFB50 Polito Engine has a temperature distribution very different with respect to the GasOn engine

From these two figures, at these particular crank angle, important features can be extrapolated:

- In Polito engine, a much thicker reaction zone is present, reason why on Borghi plot its curve is moved to the left. Also, it means lower temperatures
- There is a big difference in temperature distribution in the two engines, especially in the reaction zone, due to the presence of EGR. EGR means that in the cylinder a certain quantity of CO₂ and H₂O will be present. Both of these species have a higher heat capacitance with respect to combustion reactants. The consequence is that they take longer to heat and thus a drop of temperature in the reaction zone and consequently in the flame and flame products.

- This difference in the temperature is cause for a slow burning rate in Polito engine and, eventually, a flame extinction.

In the next figures it will be clear how the flame front is advancing in the two engines:

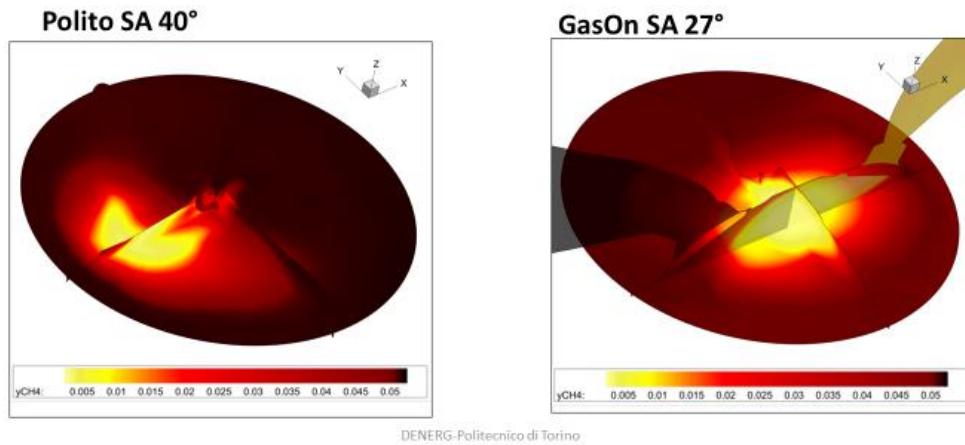


Figure 53-Consumed methane at TDC

Indication of flame advance

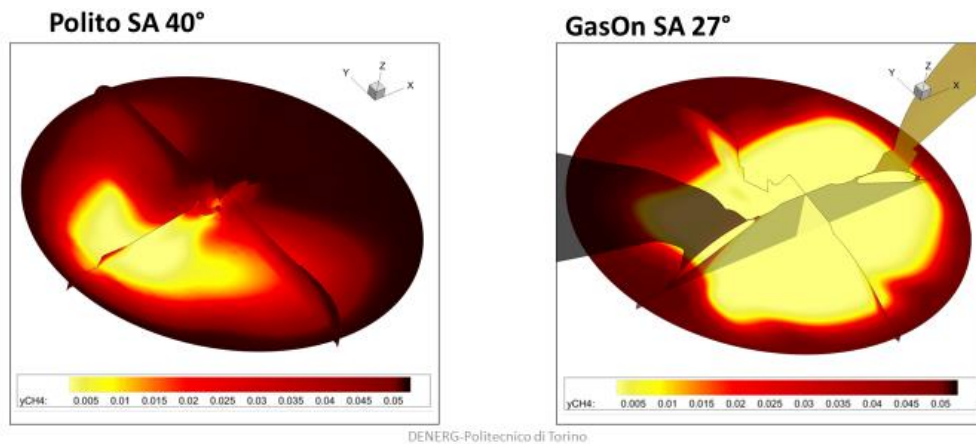


Figure 54-Consumed methane at TDC+10° (~MFB50)

In conclusion, making a comparison between different engines, with different characteristics, lead to completely different results. In particular:

- Higher turbulence and higher Compression Ratio lead to a faster combustion when no EGR is involved, leading to a more stable combustion.
- If EGR is involved, in this case 20%, the engine with low turbulence isn't able to complete the combustion leading to a failure in the reaching of IMEP and MFB50. For the high turbulence engine, combustion is complete and all the targets are reached along with all the benefits that come with an EGR diluted combustion.

8.3 HCNG- Effect of Hydrogen Addition

Before comparing the effects that H₂ has on the two engines when adding EGR, it is useful to have a general view upon the effect that only H₂ has on an engine, without considering the EGR addition.

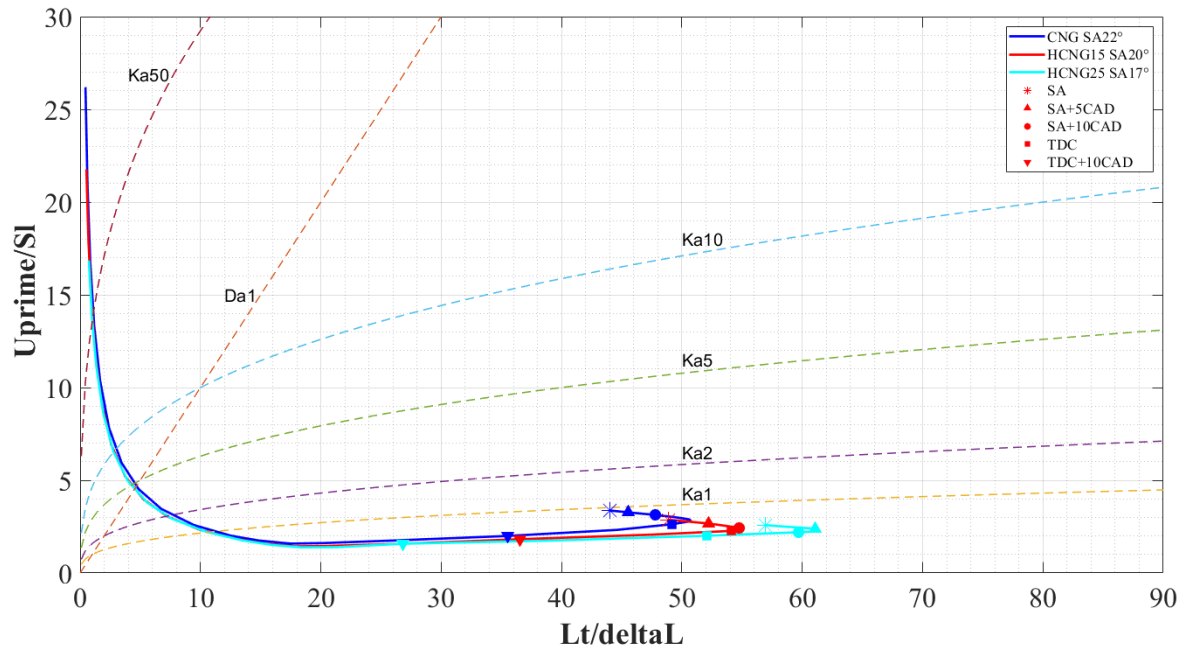


Figure 55- Borghi plot: effect of hydrogen addition

Comparison between CNG, HCNG15 and HCNG25

In the Figure 55 the curves of Polito engine are presented. No EGR is added, nor the turbulence is modified, only H₂ addition is taken into consideration. It is a useful comparison in order to have in mind what will happen to the combustion when H₂ is added. As the turbulence inside the cylinder remains constant (the engine is the same and the operating point is the same), the effect that H₂ will only affect the combustion parameters such as δ_L (flame thickness) and S_L (laminar flame speed). This work is based on the results of [8].

The main results that can be resumed as follows:

- As H₂ addition affects the S_L , increasing it, all the main combustion points (SA+5°, TDC, TDC+10°) will move downwards in the plot when H₂ % increases.
- Also, as combustion becomes faster, temperature increase more rapidly causing a thinning in the flame front (δ_L), reason why the main points also move more to the right in the Borghi plot.
- Another reason can be that, by increasing the combustion speed, flame front is able to increase its surface, thus modifying the unburnt gasses, pushing them while advancing, creating more turbulence. This could increment the turbulence length scale thus moving the points more to the right. It is a theory which still has to be verified, maybe with the help of more sophisticated tools, such as LES simulations.

Other studies are carried in Politecnico di Torino regarding the effect of hydrogen addition in CNG engines at a more molecular scale, in order to understand more clearly what can be achieved by using this method.

8.4 2000x6 bar HCNG15 EGR0%- Effect of Hydrogen Addition

This case is a relatively simple case, not so different from the simple comparison between CNG GasOn vs Polito. To see the slight differences between these two cases, Borghi plot is the best tool.

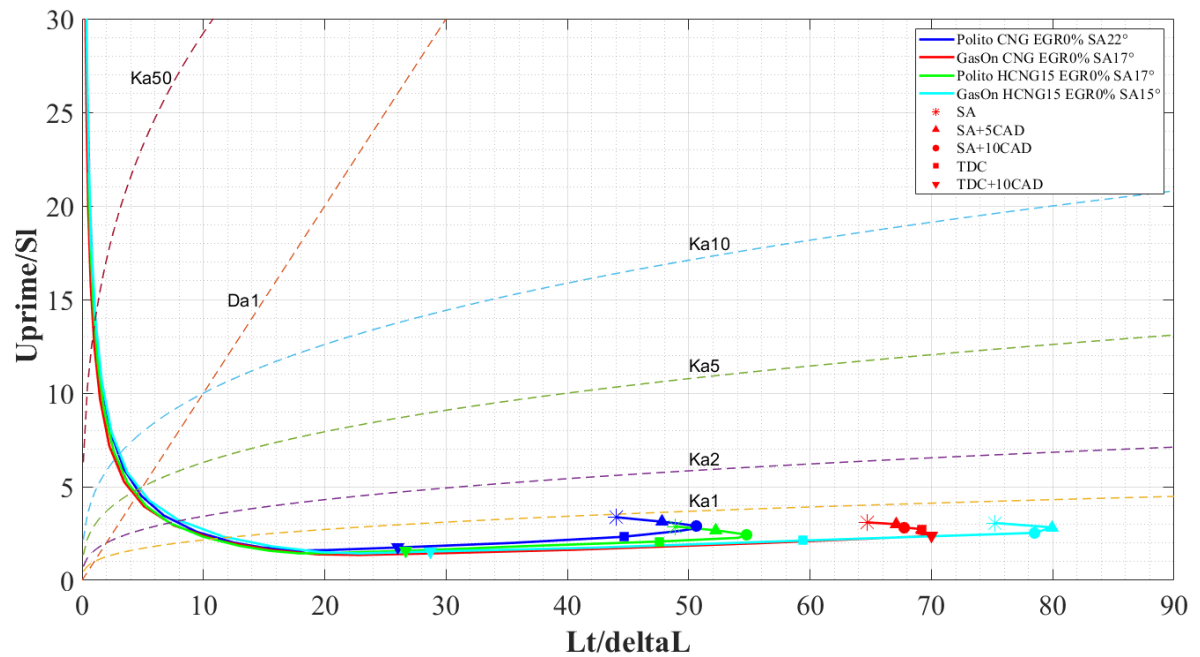


Figure 56-Borghi plot: combined effect of turbulence and Hydrogen addition

Polito vs GasOn engine for CNG and HCNG15

Borghi plot clearly shows how hydrogen addition, for both cases, has a greater influence on the flame thickness. The points, with respect to pure methane move towards the right of the graph, meaning that in the ratio of L_t/δ_L , the factor that is changing more is δ_L for each case.

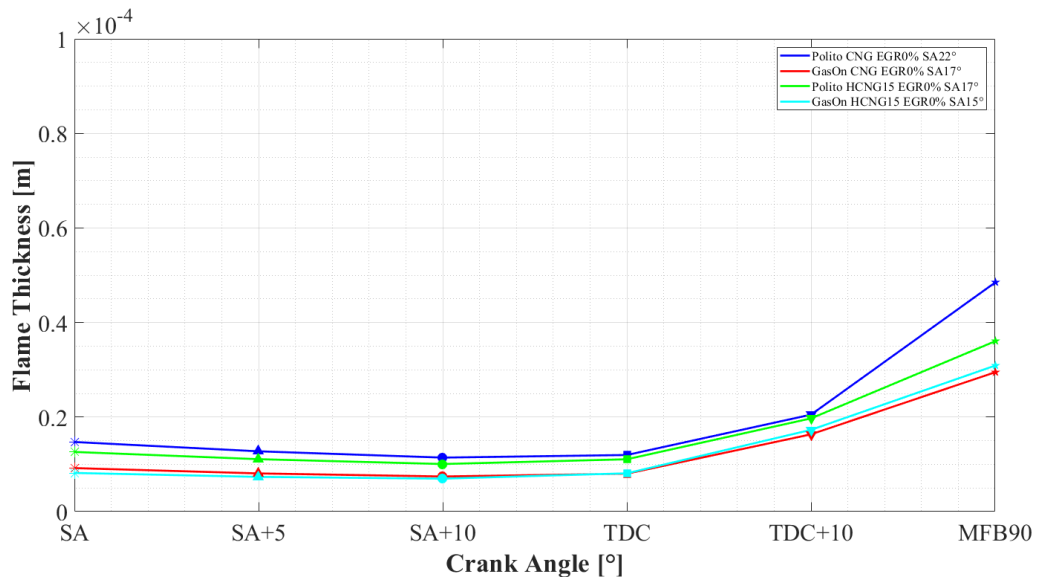


Figure 57- Effect of Turbulence and hydrogen addition on flame thickness

Flame thickness also gives an important insight. It confirms the theory which says that adding hydrogen to the mixture will thicken the flame.

8.5 2000x6 bar HCNG15 EGR10%

8.5.1 Combined effects of Hydrogen and EGR

In this section, the combined effect of H₂ addition and EGR is taken into consideration. The overall effect should only be positive for the combustion, in both engines.

The combustion is complete, the targets are reached for both cases. This confirms the hypothesis that EGR dilution can be overruled by the hydrogen addition while still maintaining the positive effect of EGR addition and without having to exaggerate the SA.

The main targets can be seen in the next table:

<u>HCNG15 EGR10%</u>	<u>GasOn</u>	<u>Polito</u>
SA [cad]	17°	25°
IMEP [bar]	5.6	5.4
MFB50 [cad]	730°	733°
10% Heat Release [cad]	718.5°	718.7°
90% Heat Release[cad]	746.6°	749.6°

Table 7- Combustion parameters, GasOn vs Polito, HCNG15 EGR 10%

In order to understand clearly the combined effect of EGR and hydrogen addition, it could be useful to plot the total duration of the combustion in both engines compared with the cases of EGR=0%.

From the works of [33] it is confirmed that an improvement in flame development speed is present (characterized as the duration between the spark and 10% mass fraction burned) and propagation speed (characterized as the duration between 10% and 90% mass fraction burned) in experimental setups. The same result was obtained also in the 3D CFD simulations as seen in the next figures, where two different results are shown. The duration from Spark Advance to 10% Heat Release (considered as an empirical point from where combustion is stable and the flame begins to propagate properly); also, the duration from Spark Advance to 90% Heat Release (which empirically is the end of the main part of flame propagation).

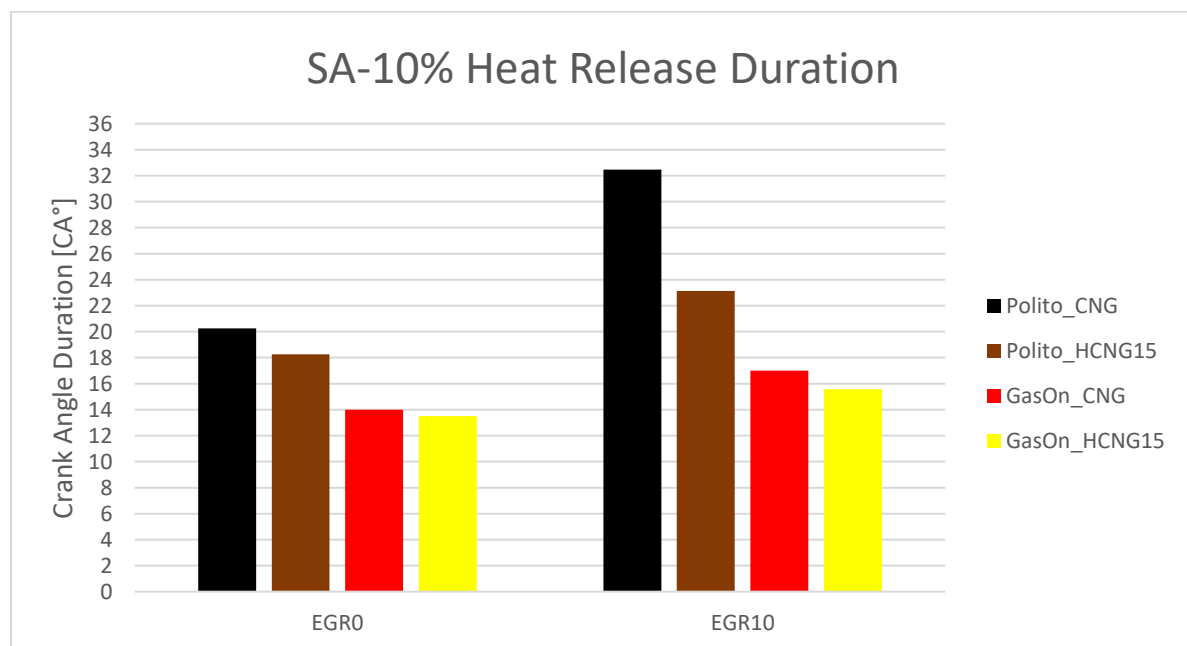


Figure 58- Duration from Spark Advance to 10% of burned fuel

The trend is for the duration to decrease when hydrogen is added. If EGR is also added the duration increases; the increase is less accentuated for the HCNG cases

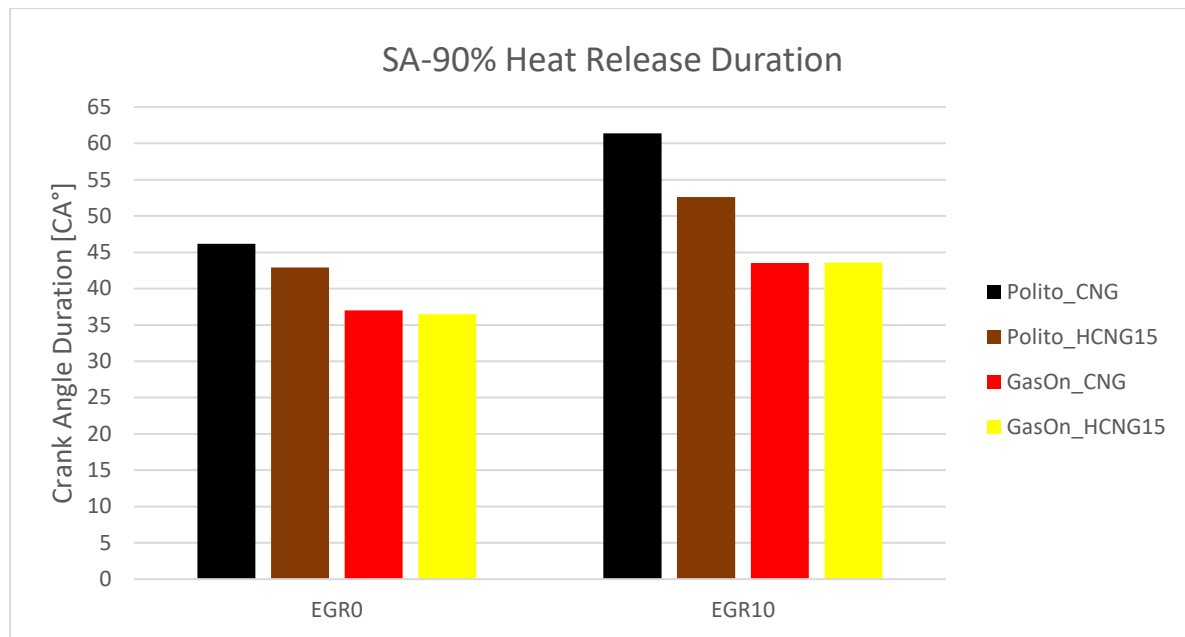


Figure 59-Duration from Spark Advance to 90% of burned fuel

The trend is for the duration to decrease when hydrogen is added. If EGR is also added, the duration increases; the increase is less important for the HCNG cases

- The general trend is an increase in the duration of combustion (or Heat Release) for both engines when EGR is added.
- For the Polito engine, the increase in the duration of combustion is more accentuated with respect to the GasOn case when EGR is added.

8.6 2000x6 bar HCNG25- Limit of Hydrogen addition

Studies were made in order to understand the effect that hydrogen addition to methane would have on the overall performances and emissions of an engine [34].

Experimentally it has been proven that adding hydrogen can extend the lean limit of combustion, reduce CO (carbon monoxide) and HCs (unburned hydrocarbons), increase thermal efficiency, increase the power output but eventually increase NOx emissions.

It is clear that continuing to increase the H2 percentage, eventually, the benefits would become smaller with respect to the drawbacks. In fact, increasing the H2 can lead to an excessive increase in NOx and even a loss in power output due to an overall lower volumetric heating value.

In Politecnico di Torino it was chosen as a limit the value of 25% in volume of H2. Some simulations were run with this particular value, also with EGR addition.

8.6.1 CNG vs HCNG25 EGR20% Polito Engine

It can be useful to see the combined effect of hydrogen addition and EGR for the same low-turbulence engine.

As already explained for the CNG EGR20%, Polito engine, it does not complete the combustion due to excessive quantity of EGR. As a solution to this problem, hydrogen addition seems like a perfect fit. A table of the main burning characteristics will show some of the differences:

EGR 20%	Polito HCNG25	Polito CNG
SA [cad]	40°	40°
IMEP [bar]	5.86	4.1
MFB50 [cad]	731.1°	738.6°
10% Heat Release [cad]	714.46°	717.7
90% Heat Release[cad]	748.35°	762.5

Table 8- Polito Engine: Combustion characteristics for CNG and HCNG25

Clearly, in the case of HCNG25, combustion is complete and the targets are reached effortlessly. The Spark Advance is quite high, but it was necessary in order to meet the requirements.

On the Borghi plot, more interesting results can be seen.

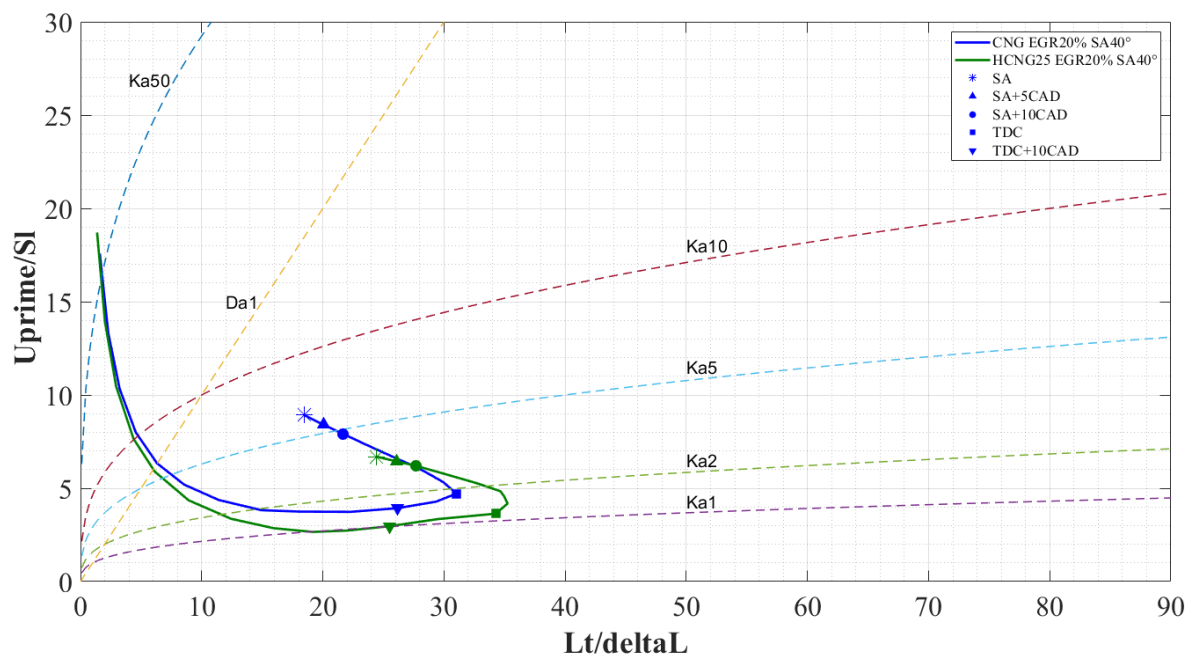


Figure 60- Borghi plot: Polito CNG vs HCNG25 EGR 20%

The graph indicates the effect of the hydrogen addition in the form of:

- Higher laminar flame speed, meaning the points are lower on the graph

- Thinner flame, meaning that the points are more to the right

Even so, a big part of the curve is still moved in a region of nearly unstable combustion; this is the effect of the EGR addition. Nevertheless, the key points of the combustion (TDC, TDC +10°) are found on the $Ka=1$ curve, which means a good enough zone for combustion.

This means that, even for a low turbulence engine, EGR addition which normally would stop the combustion, is contrasted by the addition of hydrogen; the latter, stabilizes the combustion, allowing the engine to take full advantage of the EGR, even in this low load conditions.

8.6.2 HCNG25 EGR0% & EGR25% GasOn vs Polito

This comparison is important in order to see the combined effect of:

- Differences in turbulence
- Hydrogen addition
- EGR dilution

On the Borghi plot the differences are very clear:

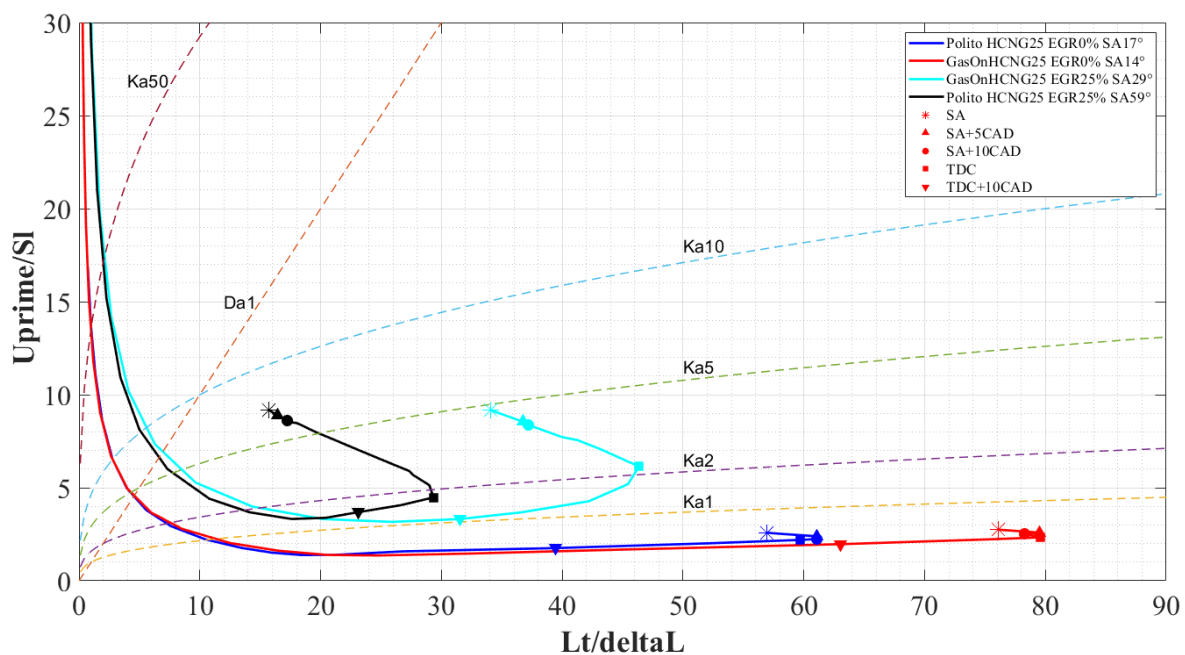


Figure 61- Borghi Plot: combined effects of turbulence, hydrogen addition and EGR dilution

Combustion cases of HCNG25 EGR 0% and HCNG25 EGR 25% on both Polito and GasOn engines

An important point to be noted is that in the case of Polito EGR25% combustion was not complete, due to excessive quantity of EGR; an extreme attempt was made in order to reach a complete combustion by increasing the spark advance up to 59°. Even so, combustion resulted in being very instable, thus incomplete.

<u>HCNG25 EGR0%</u>	<u>GasOn</u>	<u>Polito</u>
SA [cad]	14°	17°
IMEP [bar]	5.6	6
MFB50 [cad]	729°	729.9°
10% Heat Release [cad]	719°	718.85°
90% Heat Release[cad]	744.5°	742.2°
<u>HCNG25 EGR25%</u>	<u>GasOn</u>	<u>Polito</u>
SA [cad]	29°	59°
IMEP [bar]	5.56	5.1
MFB50 [cad]	728.6°	729.9°
10% Heat Release [cad]	715°	711.6°
90% Heat Release[cad]	747°	746.3°

Table 9- Combustion Parameters of HCNG25 EGR0 and HCNG25 EGR 25%

From both Figure 61 and Table 6 the following conclusions can be drawn:

- For EGR0% no difficulties occur in the combustion for both cases
- For EGR25% both Polito and GasOn have their combustion curves in the area of $Ka > 1$, meaning an instable combustion; nevertheless, GasOn engine has the points of TDC and TDC+10° in the area very near to $Ka = 1$, meaning that the most critical points of the combustion are next to the stable region of combustion. That's the reason why, with an adequate spark advance, for the GasOn engine, a complete combustion is reached.
- Also, in Polito engine, due to its very anticipated ignition, the whole combustion process is very long, meaning that it starts when the piston is still in the compression phase, which can cause a slowing in the combustion reactions that should be happening. In the few cycles that have been run this didn't cause much of a problem, but in a real engine, in real operating conditions this can cause a flame extinction or even a misfire.

The difference between the whole combustion process can be seen in the next figure:

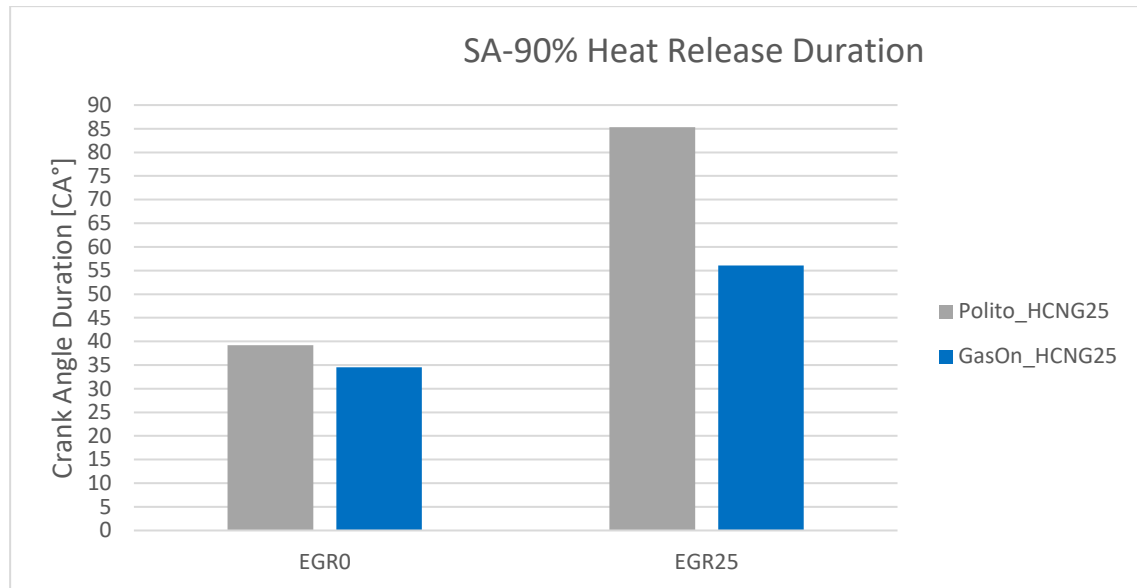


Figure 62- Differences in terms of Combustion duration

Other important characteristics of the combustion for the critical operating point with EGR25% are visible in the next figures:

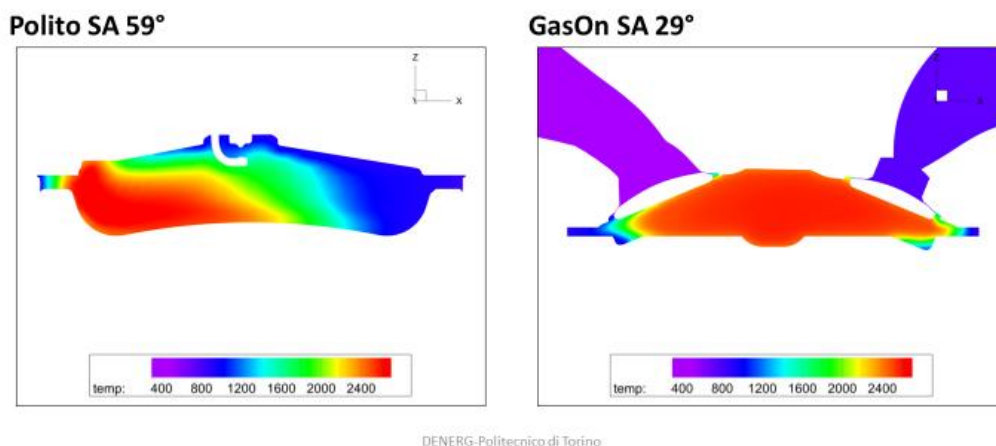


Figure 63- Temperature distributions at TDC+10°

Incomplete combustion of Polito and complete combustion of GasOn (HCNG25 EGR 25%)

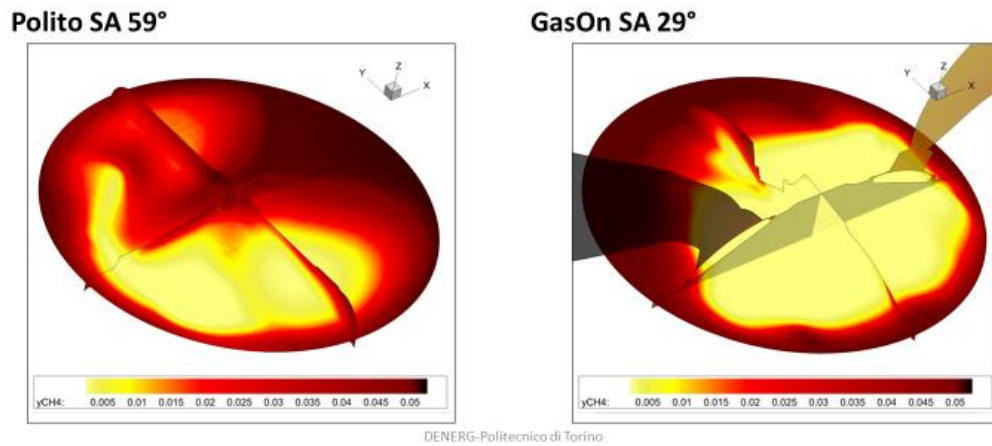


Figure 64- Consumed methane at TDC +10°

Incomplete combustion of Polito and complete combustion of GasOn (HCNG25 EGR 25%)

From these two figures two very important aspects of the combustion can be extrapolated:

- For Polito case, as the combustion is happening in the zone of $Ka > 1$, a break in the flame front is very probable to occur; in fact, in the flame advance figure it is clear how, for the CA which represents cca MFB50, there are three areas of combustion, separated. It means that the assumption of flame front breaking is correct. As for the GasOn engine, combustion is much more homogeneous.
- Another important feature is the flame front. In the temperature figure it is very clear how for Polito engine the area of reactions is much wider with respect to the GasOn case. This feature can be seen in the next figure.

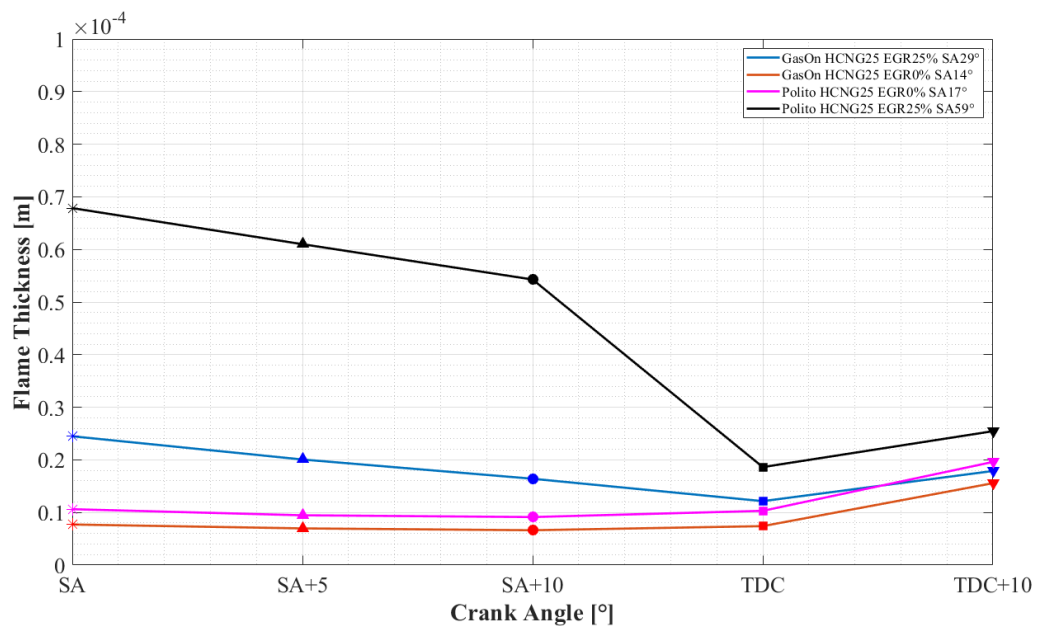


Figure 65- Flame Thickness- Effect of EGR and Hydrogen on flame thickness

HCNG25 EGR0% and EGR25% Polito vs GasOn

In this figure, it is important to note the difference in flame thickness between the cases. The effects are due to hydrogen addition and EGR dilution. As expected, the following results are confirmed:

- Hydrogen addition thins the flame
- EGR dilution thickens the flame
- A theory that needs even more confirmation, nevertheless, increase in turbulence seems to thin the flame due to a faster combustion (burnt gasses have a greater pressure and temperature and, expanding, push the flame front, thinning it).

8.7 Conclusion

The work of this thesis was aimed to show what the effects of turbulence, hydrogen addition and EGR dilution were on combustion stability.

In order to do that, two different engines were used. Simulation were performed in such a way the effects were tested both separately and combined. The two engines were necessary in order to have different levels of turbulence, as a single engine with variable turbulence levels was not available. Because the same operating point was simulated with the same conditions and same models, the comparison is assumed to be representative.

The main conclusions that can be extrapolated from this thesis are:

- Higher turbulence levels in an engine is responsible for faster burning velocities;
- Higher turbulence levels allow for higher tolerance in terms of EGR percentage allowed in an engine while still having a stable combustion;
- Due to its higher diffusivity and better burning qualities, hydrogen, when added in the mix enhances the burning velocity and also reduces CO₂, CO, HC levels but, due to the higher temperatures developed during the combustion, it may be responsible for higher NO_x formation thus, its quantity cannot be excessive;
- Hydrogen addition allows a higher EGR tolerance, thus helping combustion in conditions that weren't good enough for a pure CH₄ air and EGR mix;
- The combined effect of higher turbulence and hydrogen addition allows for the combustion to occur in a more effortless manner (lower SA are needed for reaching MBT);
- The combined effect of higher turbulence, hydrogen addition and EGR dilution benefits the combustion especially in terms of emissions as it is known that hydrogen and EGR are both accountable for emission reduction.

8.8 Future works

In DENERG, after a careful analytical post-processing process, a direct relation between burning velocity and hydrogen addition was found. It took into consideration the 2000x6 bar operating point for the two engines; a nearly linear trend was found between hydrogen addition and burning velocity:

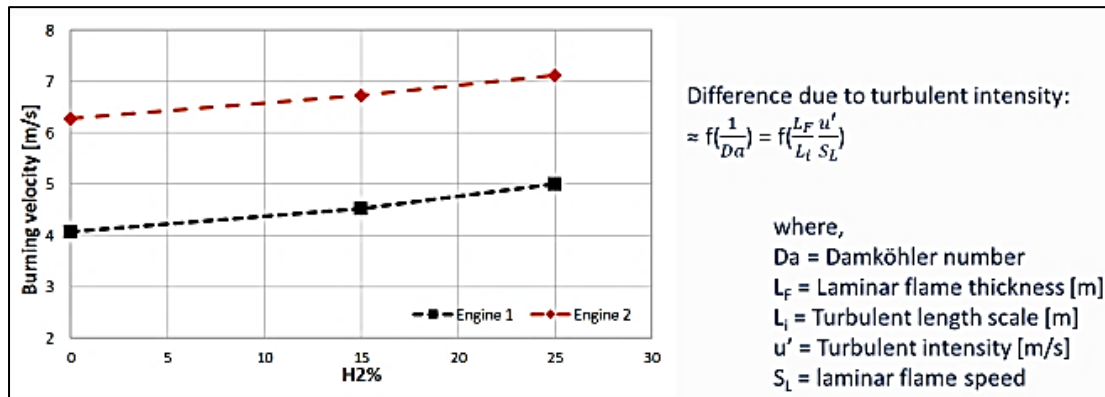


Figure 66- Burning velocity

Hypothesis on the trend of burning velocity with increasing hydrogen addition percentage

The drawback is that this trend was found only on two engines, for one operating point. A useful future work would be to check this function's validity with EGR cases and different load points.

9 LES Simulation setup, procedure and results

The initial objective for the LES simulation in this thesis was to try to develop a model able to perform full sized simulations of combustion of multiple cycles for the GasOn engine (simulations already available that were performed with the RANS turbulence model). Once those were completed, the idea was to confirm the hypothesis that a LES simulation was able to capture cycle-to-cycle variations that are probable to occur during the normal cycles of an engine, especially if EGR and high turbo-charging levels are present.

Once the results would have been available, a comparison was to be made between LES simulations results and RANS simulation results; more importantly, a comparison was to be made between LES simulations and experimental data. That way, we would have been able to confirm that LES simulations were realistically a good tool to be used in order to find possible solutions for the cycle-to-cycle-variation problem.

Studies were made in the context of this thesis on how to approach this kind of LES simulations, how to do a correct setup and how to deal with the possible problems.

It is important to remember that the work that was done for this thesis on LES simulations is just a preliminary approach, with results that need to be validated. It is probable that more attempts will be made in the future, in order to eventually reach a good model, able to produce reliable results.

9.1 Case setup

A LES simulation requires more attention with respect to RANS. Because it is a simulation able to resolve a smaller length-scale eddies, roughly said, more turbulence, it requires a more special treatment especially in the most critical areas such as: boundaries, moving boundaries, near the walls, high flow-speed areas, high heat areas, high heat exchange areas etc.

Some of the most critical points that needed particular attention when switching from RANS simulations to LES simulations were:

- Wall models
- Mesh refinement
- Sub-grid scale models

9.1.1.1 Wall models

Engine wall heat transfer is one of the important issues in the study of internal combustion engines. Analysis of engine wall heat transfer is among the most complex engineering topics because even experimentally, many of the parameters cannot be directly measured.

Problems arise because during the different cycle phases, different phenomena are happening, such as the turbulent motion, combustion process in the cylinder and thermal boundary layer near the cylinder walls. During the engine operating cycles, the flow has a highly unsteady behaviour, with many transient regimes in the cylinder volume, which creates great variations in the heat fluxes between fluids and walls.

These factors are responsible for disturbing and continuingly altering the heat transfer from the fluid to the walls.

Keeping all these facts in mind, in order to obtain and provide accurate results, accurate boundary conditions are needed. LES based wall models are used when the turbulence model is changed from RANS to LES.

New wall shear stress and wall heat transfer models are used; these rely on the information from LES turbulence modeling of the flow. By doing so, more accurate results of the wall shear stress and wall heat flux are obtained. Based on the works of [35], the wall model used for this simulation is the Werner-Wengle (WW) wall shear stress model.

9.1.1.2 Mesh refinement

It is known that a LES simulation requires a finer grid with respect to a RANS simulation. The drawback of this requirement is an increase in the request of resources and consequently an increase of computational time.

In the laboratories of DENERG, resources were available in a limited quantity, so, it was necessary to make the best use of them. Particular attention was required by the meshing of the engine, especially during the critical phases such as injection and intake/exhaust.

The mesh had the following characteristics:

- Base grid size= 4 mm;
- Fixed embedding active during intake, exhaust and especially injection which was able to modify the grid size up to 0.25 mm
- AMR (adaptive mesh refinement) which was able to modify the mesh even more with dimensions up to 0.125 mm, in particular during the injection phase. To be able to do so, special parameters were imposed during the case setup such as: increments of flow velocity inside each cell; increase in temperature inside each cell; species concentration. If those parameters would reach the limits imposed, then AMR would start and refine the mesh in the cells where those events happen (and in the immediate adjacent cells).

For even more accurate results from LES simulations, it would better to refine the mesh even more; for this thesis, with the resources available, 0.125 mm was the best compromise that could be reached.

9.1.1.3 Sub-grid scale models

Sub grid scales (also known as SGS) are models used to approximate SGS Reynolds-stress.

The important thing about the subgrid-scale Reynolds stress is that it contains local averages of the small-scale field. Ergo, models need to contain informations about local velocity field or local averages based on the local history of the fluid.

The choice was between multiple SGSs but, for a more accurate result, the best choice for this application was the Dynamic Smagorinsky SGS.

Nevertheless, it is debatable that, given the limited amount of resources available, this work could have been done with the simplest, thus less expensive methods (in terms of computational resources).

9.2 Procedure

The main purpose of this simulation was to have a comparison between a LES and RANS simulation of the same case. It has been chosen as a comparative point the case of GasOn engine, 1500 rpm, full load, injection event. The reason for the choice of simulating only the injection event and not the full cycle is due to the limited resources and limited amount of time. Combustion requests high mesh scaling, meaning very reduce cell dimensions thus it requests q great quantity of computational power, which at the moment was not available. Injection also demands for a lot of computational power but in the lab was manageable; moreover, injection has been chosen because in a DI SI engine it is a critical event and needs to be monitored.

Early injection means that methane is injected while the intake valve is still open. This is one of the solutions possible and it comes with the advantage of excellent mixing of methane and air.

	Injection timing	Injected mass [mg]
LES	Early	52
RANS	Early	52

Table 10- Injection parameters for LES and RANS cases

The objective was to match the injected mass in the cylinder with the experimental data available. In order to validate the model, for the LES case, multiple attempts were made in order to reach the desired total mass of methane injected in the chamber.

The approaches that were chosen in order to set up the model were based on some 3D post processing that were made for some previous, preliminary simulations.

Once the model was satisfying, a simulation of the injection was completed and results were analysed and compared.

9.3 Results and discussion

The purpose of the LES simulation was aimed at showing why, using this turbulent model, better results could be obtained in terms of accuracy and therefore prediction of multiple parameters.

If, like in the case of an injection simulation, the goal is to study the effects of mixing, penetration, backflow and heat exchange, LES gives a more realistic insight on what occurs in the cylinder during this event.

More importantly, using LES simulations, they can be an important tool to predict what could happen when certain conditions are changed.

In the next figures, differences between RANS and LES results are shown in order to understand how different the two models are.

A sequence of 10 degrees of injection is shown; the case is of early injection, meaning that the intake valve is still open during the injection event and air is entering.

At first, the flow kinematic aspect was studied:

- RANS turbulence model is based on averaged quantities, which means that small scales of the turbulence are included as a part of the large scales.
- On the other hand, for LES models, smaller scales are calculated, which means that a difference will be seen when dealing with flow kinematic characteristics.

A comparison was made for a period of 10° during both intake and injection (the injector was fully open). Velocity vectors were extrapolated and plotted.

In the next figure the difference in the velocity vectors between LES and RANS are shown. Although the LES case may seem irregular and with a casual distribution of the vectors, it is actually a more realistic description of the flow inside the cylinder.

The injected flow opens in a cone shaped flow as soon as it enters the cylinder, meaning that the pressure distribution is different with respect to the RANS case (the methane follows the less restrictive path inside the cylinder).

Because the methane flow has a cone shape, it means that inside the cone there will be a low-pressure zone; this allows the methane to expand not only outwards, towards the cylinder walls but also inwards as it advances to the piston head.

Also, for the LES simulation, velocity vectors clearly show how a flow movement is advancing towards and into the intake duct (phenomena much less seen with the RANS simulation). This will be better seen in other figures from the comparison of the two simulations.

In contrast, for the RANS case, the flow seems not to encounter any obstacles and goes straight to the piston head. The velocity vectors are more ordinate, moving as a unity; only very large eddies are visible and the flow doesn't seem to be affected by the inlet valve which is open and air is entering.

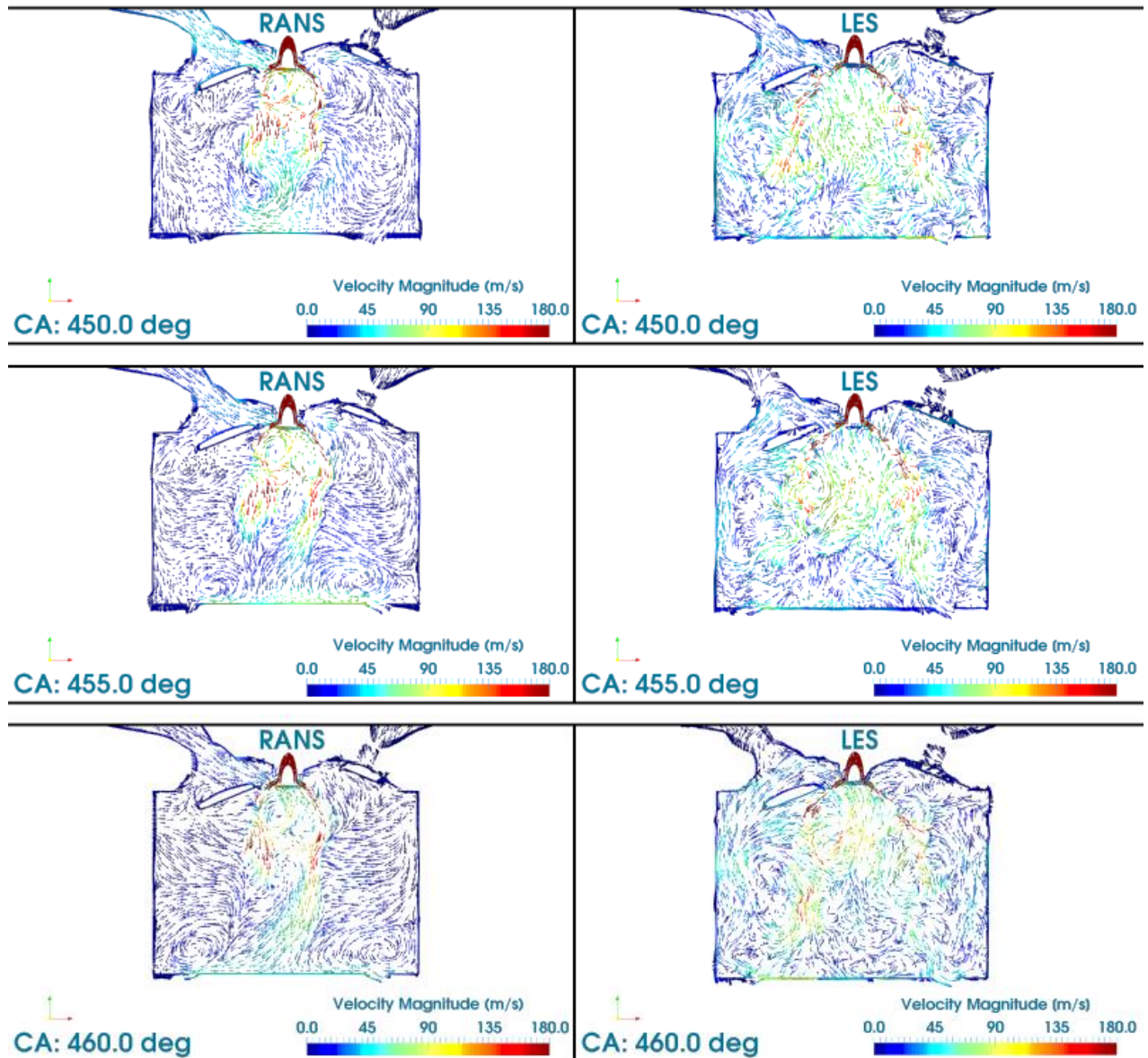


Figure 67- Velocity vectors evolution during injection

Comparison between LES and RANS

Other variables can be important when studying the effects of injection in an engine. The fact that the LES simulation is able to capture in a better way more of the turbulence, thus more of the flow properties, is an upside if the goal is, as in this case, to show why LES is an optimal tool for engine applications.

Very similarly to the description of the velocity field vectors is the Mach number. The next figure shows the distribution of Mach number inside the cylinder for the two cases:

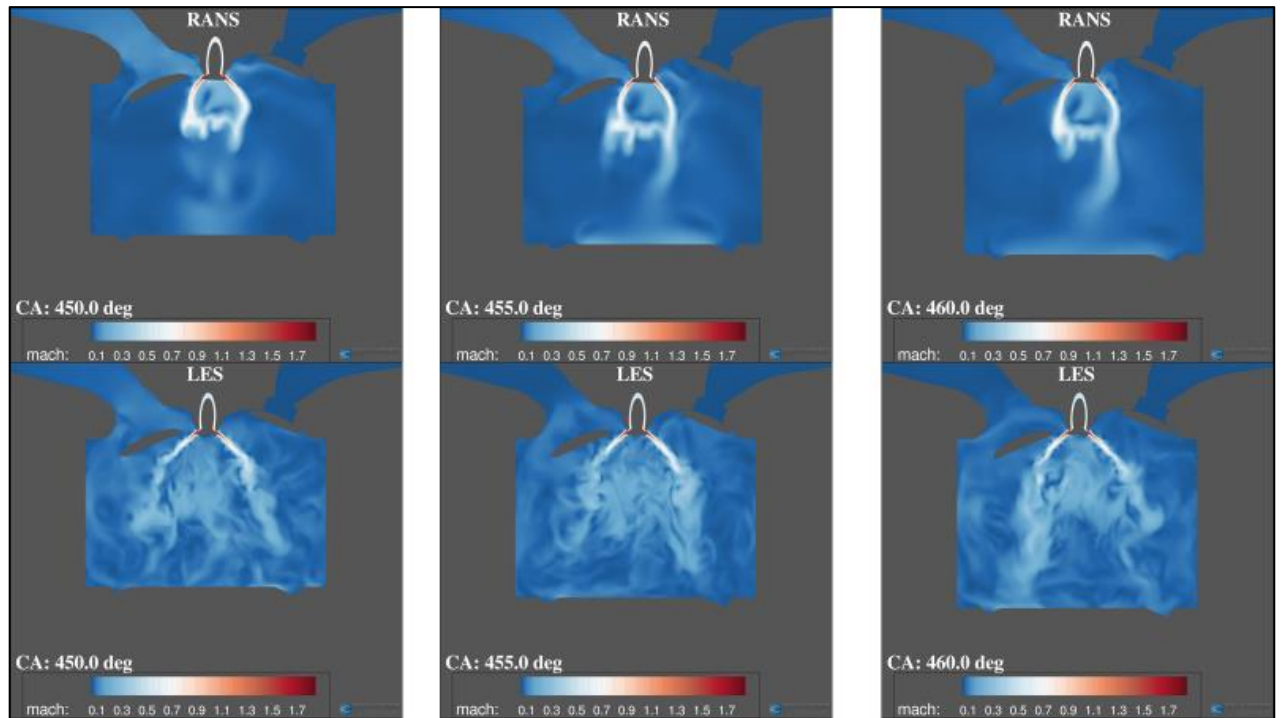


Figure 68- Differences in Mach number evolution

Comparison between LES and Rans simulations of the injection

The cone shaped flow of methane is much more visible in this figure. Also, in the LES case is much more visible how the expansion affects the flow of methane.

Also, in the RANS case, this figure shows a strong impingement of methane on the top of the piston, which doesn't seem to be the case (in the same way) for the LES case.

If the flow is resolved with accuracy, it means that also the consequences of the flow effects are captured and can be studied with attention. An important effect of high turbulence resolution is the mixing of the species inside the cylinder.

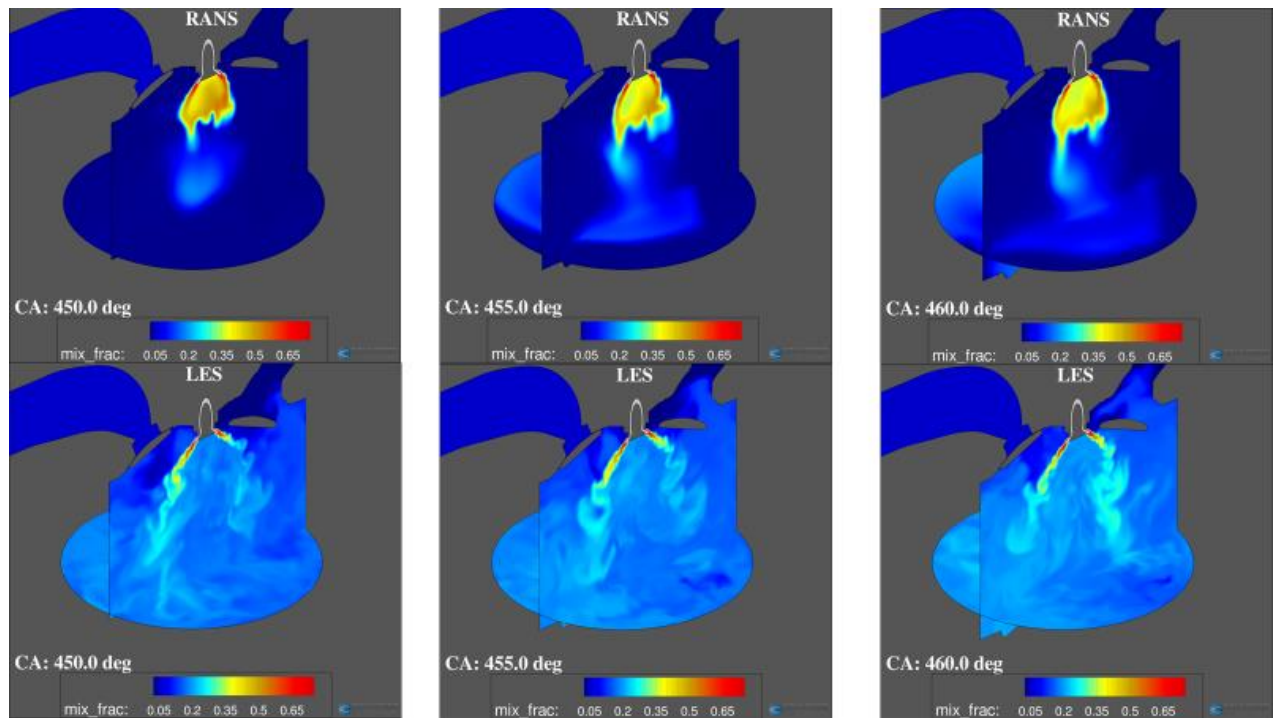


Figure 69-Mixing fraction details

Comparison between LES and RANS simulations

Figures like the previous ones can be used to study the areas where mixing doesn't occur as it should.

As this thesis is being written, the LES simulation is ongoing, with the objective towards observing what will happen after multiple cycles of the engine, even if combustion is not taken into consideration. Future works will probably confirm if a LES simulation of motored cycles is able to capture the realistic evolution of the flow.

9.4 Conclusion

Theoretically, LES simulations have a huge potential in the world of CFD simulations. They are a good trade-off between needed resources and accuracy of the results. They are less time consuming with respect to DNS simulations while still giving more than enough accurate results.

LES simulations are meant to be applied in cases in which more complex phenomena is needed to be studied, such as cycle-to-cycle variation, knock, misfire and other stochastic events; these are likely to occur in modern engines which are designed to perform in more critical conditions such as: with high EGR dilution, high turbo-charging levels, high compression ratio.

LES simulation can be used, as in the case of this thesis, to simulate critical events during the engine cycles, such as injection. In this case, it was possible to study and to visualize the effect of injection timing and injection conditions on:

- Mixing
- Velocities distributions
- Jet penetration

- Wall impingement
- Backflow
- Pressure distribution and consequently jet distribution

In the case of this thesis, these simulations do not find a clear application, but in the real world, with the right resources, LES could be the perfect tool for predicting situations that otherwise, (for example with RANS turbulence model) could not be predicted.

10 Figures Index

Figure 1- Turbulent premixed combustion regimes.....	5
Figure 2- Logarithmic Borghi plot [10]	6
Figure 3- Finite volume method- Mass Conservation	9
Figure 4- Finite volume scheme [14].....	13
Figure 5- Solution procedure + PISO algorithm [15]	15
Figure 6- Eddy formation from a jet [10]	18
Figure 7- Schematization and differences between LES and DNS simulations [12].....	19
Figure 8- Time averaging of a flow	24
Figure 9- Flame structure, chemical reactants and products of combustion [10].....	28
Figure 10- Burning velocities.....	30
Figure 11- Bunsen Burner scheme [10].....	31
Figure 12- Velocity vectors.....	32
Figure 13- ATKIM inductive scheme.....	34
Figure 14- Flame Front description	37
Figure 15- Length scales of eddies with respect to burning velocities [10]	38
Figure 16- Destructive interaction between eddies and flame front [10]	39
Figure 17- Representation of a turbulent flame advance [29].....	40
Figure 18- Burning speeds in a laminar and turbulent combustion.....	40
Figure 19- Flame front advance in the computational domain [15].....	41
Figure 20- Flamelet regime assumption scheme [29].....	42
Figure 21- Computational cell of ECFM Combustion model [15].....	43
Figure 22- Computational cell of ECFM Combustion model [15].....	43
Figure 23- Modelling of turbulent combustion.....	43
Figure 24- AMR application in CONVERGE.....	48
Figure 25- Calibration methodologies for both Polito (Engine 1) and GasOn (engine 2)	49
Figure 26- Polito Engine	50
Figure 27- Polito Engine Calibration.....	51
Figure 28- GasOn engine	52
Figure 29- GasOn Engine Calibration Results.....	53
Figure 30- Normalized heat release rate for Polito engine: Validation of MFB50 with respect to experimental data	54
Figure 31- Tumble Ratio comparison- GasOn vs Polito.....	55
Figure 32- Turbulent Kinetic Energy.....	56
Figure 33. Uprime.....	56
Figure 34- Swirl ratio and Angular Momentum around Z-axis.....	57
Figure 35- Flame speed	58
Figure 36- Effect of higher turbulence on flame speed	58
Figure 37- Pressure Comparison	59
Figure 38- Mass fractions temperature	59
Figure 39- Comparison of TKE	60
Figure 40- The piston is in the proximity of BDC.....	61
Figure 41- TKE intensity during compression phase	61
Figure 42- Turbulence at Spark Advance	62
Figure 43- Temperature Distribution at TDC.....	62

Figure 44- Temperature Distribution at TDC+10°	63
Figure 45-Consumed methane at TDC	63
Figure 46-Consumed methane at TDC+10°	64
Figure 47- Main Heat Release duration	64
Figure 48- Borghi plot- Combustion curves CNG EGR 0%	65
Figure 49- Borghi plot- Combustion curves CNG EGR 20%	66
Figure 50- Effect of EGR on Borghi plots and on COV	67
Figure 51- Temperature distribution at TDC	68
Figure 52- Temperature distribution at TDC + 10°	68
Figure 53-Consumed methane at TDC	69
Figure 54-Consumed methane at TDC+10° (~MFB50)	69
Figure 55- Borghi plot: effect of hydrogen addition	70
Figure 56-Borghi plot: combined effect of turbulence and Hydrogen addition	71
Figure 57- Effect of Turbulence and hydrogen addition on flame thickness	72
Figure 58- Duration from Spark Advance to 10% of burned fuel	73
Figure 59-Duration from Spark Advance to 90% of burned fuel	74
Figure 60- Borghi plot: Polito CNG vs HCNG25 EGR 20%	75
Figure 61- Borghi Plot: combined effects of turbulence, hydrogen addition and EGR dilution	76
Figure 62- Differences in terms of Combustion duration	78
Figure 63- Temperature distributions at TDC+10°	78
Figure 64- Consumed methane at TDC +10°	79
Figure 65- Flame Thickness- Effect of EGR and Hydrogen on flame thickness	79
Figure 66- Burning velocity	81
Figure 67- Velocity vectors evolution during injection	86
Figure 68- Differences in Mach number evolution	87
Figure 69-Mixing fraction details	88

11 Tables Index

Table 1- Hydrogen properties as a fuel with respect to Methane and gasoline [8]	4
Table 2- Gulder Method- Constants.....	33
Table 3- Polito Engine characteristics	51
Table 4- GasOn Engine Characteristics.....	53
Table 5- Details on GasOn simulations.....	54
Table 6- Combustion Parameters CNG EGR20 %	66
Table 7- Combustion parameters, GasOn vs Polito, HCNG15 EGR 10%	73
Table 8- Polito Engine: Combustion characteristics for CNG and HCNG25	75
Table 9- Combustion Parameters of HCNG25 EGR0 and HCNG25 EGR 25%	77
Table 10- Injection parameters for LES and RANS cases.....	84

12 Bibliography

- [1] M. Baratta, S. d'Ambrosio, D. Misul, and E. Spessa, "Effects of H₂ Addition to Compressed Natural Gas Blends on Cycle-to-Cycle and Cylinder-to-Cylinder Combustion Variation in a Spark-Ignition Engine," *J. Eng. Gas Turbines Power*, vol. 136, no. 5, p. 051502, 2013.
- [2] D. van Bebbler *et al.*, "Numerical Investigation of Direct Gas Injection in an Optical Internal Combustion Engine," *SAE Tech. Pap. Ser.*, vol. 1, pp. 1–27, 2018.
- [3] H. S. Tira, "Impact of Alternative Fuels and Hydrogen – Enriched Gaseous Fuel on Combustion and Emissions in Diesel," no. March, p. 167, 2013.
- [4] S. S. Srinivasan, S. A. Sherif, F. Barbir, T. N. Veziroglu, M. Mahishi, and R. Pratt, "Hydrogen energy technologies," *Energy Effic. Renew. Energy Handbook, Second Ed.*, no. December, pp. 1669–1702, 2015.
- [5] M. A. DeLuchi, "Hydrogen vehicles: an evaluation of fuel storage, performance, safety, environmental impacts, and cost," *Int. J. Hydrogen Energy*, vol. 14, no. 2, pp. 81–130, 1989.
- [6] G. A. Karim, "Hydrogen As an Engine Fuel Some Pros and Cons," vol. 14, no. 4, 2007.
- [7] S. O. Akansu, Z. Dulger, N. Kahraman, and T. N. Veziroğlu, "Internal combustion engines fueled by natural gas - Hydrogen mixtures," *Int. J. Hydrogen Energy*, vol. 29, no. 14, pp. 1527–1539, 2004.
- [8] C. G. Bauer and T. W. Forest, "Effect of hydrogen addition on the performance of methane-fueled vehicles. Part I: effect on S.I. engine performance," *Int. J. Hydrogen Energy*, vol. 26, no. 1, pp. 55–70, 2001.
- [9] R. Borghi and M. Destriau, *Combustion and flames*. Paris: Editions Technip, 1998.
- [10] N. Peters, *Turbulent Combustion*. Press syndicate of the University of Cambridge, 2004.
- [11] L. Vervisch and D. Veynante, "Turbulent combustion modeling," *Prog. Energy Combust. Sci.*, vol. 28, no. 3, pp. 193–266, 2002.
- [12] J. Ferziger and M. Peric, *Computational methods for fluid dynamics*, 3rd ed. Springer, 2002.
- [13] S. B. Pope, *Turbulent Flows*, vol. 12, no. 11. 2001.
- [14] M. Baratta, "Metodologie di simulazione numerica multidimensionale e modelli di turbolenza applicati allo studio del moto della carica nel cilindro di un motore alternativo."
- [15] M. S. CONVERGECFD and M. Series, "CONVERGE Manual, CONVERGE CFD 2.3," no. May, 2016.
- [16] J. BARDINA, J. FERZIGER, and W. REYNOLDS, "Improved subgrid-scale models for large-eddy simulation," 2013.
- [17] A. Leonard, "Energy cascade in large-eddy simulations of turbulent fluid flows," *Adv. Geophys.*, vol. 18, no. PA, pp. 237–248, 1975.
- [18] S. J., "General circulation experiments with the primitive equations," *Mon. Weather Rev.*, vol. 91, no. 3, pp. 99–164, 1963.
- [19] J. Mcmillan and R. S. Rogallo, "Tests of New Subgrid-Scale Models in Strained Turbulence," pp. 0–10, 1980.
- [20] V. Yakhot and S. A. Orszag, "Renormalization group analysis of turbulence," *J. Sci. Comput.*,

vol. 1, no. 1, pp. 3–51, 1986.

- [21] D. C. Wilcox, *Turbulence modeling for CFD*. 1993.
- [22] C. G. Speziale, S. Thangam, T. B. Gatski, V. Yakhot, and S. A. Orszag, “Development of turbulence models for shear flows by a double expansion technique,” *Phys. Fluids A Fluid Dyn.*, vol. 4, no. 7, pp. 1510–1520, 2002.
- [23] M. Metghalchi and J. C. Keck, “Burning velocities of mixtures of air with methanol, isooctane, and indolene at high pressure and temperature,” *Combust. Flame*, vol. 48, no. C, pp. 191–210, 1982.
- [24] L. O. Gulder, “Omer L. Gulder,” *SAE Int. J. Engines*, 1984.
- [25] E. Hu *et al.*, “Laminar flame speeds and ignition delay times of methane-air mixtures at elevated temperatures and pressures,” *Fuel*, vol. 158, pp. 1–10, 2015.
- [26] P. Goel, “3D-CFD Simulation of the Combustion Process in a NG Engine by Adopting a LFS Submodel from Detailed Kinetic Mechanism,” 2017.
- [27] O. Colin and K. Truffin, “A spark ignition model for large eddy simulation based on an FSD transport equation (ISSIM-LES),” *Proc. Combust. Inst.*, vol. 33, no. 2, pp. 3097–3104, 2011.
- [28] N. Peters and J. Göttgens, “Scaling of buoyant turbulent jet diffusion flames,” *Combust. Flame*, vol. 85, no. 1–2, pp. 206–214, 1991.
- [29] T. Poinso and D. Veynante, “Theoretical and Numerical Combustion.” 2001.
- [30] P. Lafitte, *La propagation des flammes dans les mélanges gazeux*. Paris, Hermann, 1939.
- [31] F. E. Marble, “The Coherent Flame Model of the Turbulent Chemical Reactions,” *Acta Astronaut.*, vol. 4, pp. 291–391, 1977.
- [32] M. Baratta, D. Misul, E. Spessa, L. Viglione, G. Carpegna, and F. Perna, “Experimental and numerical approaches for the quantification of tumble intensity in high-performance SI engines,” *Energy Convers. Manag.*, vol. 138, pp. 435–451, 2017.
- [33] E. Conte and K. Boulouchos, “Influence of Hydrogen-Rich-Gas Addition on Combustion, Pollutant Formation and Efficiency of an IC-SI Engine,” *SAE Tech. Pap. Ser.*, vol. 1, no. 724, 2010.
- [34] A. Cattelan and J. Wallace, “Exhaust Emission and Energy Consumption Effects from Hydrogen Supplementation of Natural Gas,” *SAE Tech. Pap. Ser.*, vol. 1, no. 412, 2010.
- [35] C. Plengsaard and C. Rutland, “Improved Engine Wall Models for Large Eddy Simulation (LES),” *SAE Tech. Pap. Ser.*, vol. 1, 2013.